Light-Based Additive Manufacturing of Porous Polymers

Dissertation submitted to the University of Sheffield in partial fulfilment of the requirements for the degree of Master of Science

Nihan SENGOKMEN OZSOZ

Supervisor: Dr Frederik Claeyssens

The University of Sheffield

Faculty of Engineering

Department of Materials Science and Engineering

August 2019

ACKNOWLEDGEMENTS

There are several people that I would like to say thank you for role in my dissertation. I am sincerely appreciated for my supervisor, Dr Frederik Claeyssens. His help and patience as opposed to my all questions made everything understandable over the duration of the project. Additionally, guidance of my lab mentor, Dr Colin Sherborne, is significant. He always helped me deal with obstacles in every single step of during my project, which includes planning of experiments and my project schedule, use of equipment, solving of problems about devices, and revising my dissertation draft.

Support of my husband, Ilkin, is prominent during the writing period of my dissertation. Whenever I encountered any issue especially computer-related problems, he always helped me. Apart from this, he always listened to me without bored when my stress level was high. Without him every issue that I encountered would be more challenging. Thank you Kitir, my cat. Even if she does not know her importance, she always motivated me by the presence.

I am appreciated efforts of encouragement of my extended family members and especially my father, Turhan, my mother, Huriye, and my brother, Cihan. Also, thanks, my friends and my best friends, Ulfida and Cagri, for their support.

Last but not the least, I immensely say thank you Republic of Turkey Ministry of National Education, my sponsor, for their financial support. If Republic of Turkey did not give this opportunity to me, I would not be here. Thanks for your foundation, again.

ABSTRACT

Additive manufacturing techniques that have popularity in various applications have different methods such as fused deposition modelling, direct ink writing, selective laser sintering, and stereolithography. Additionally, various printing inks or materials can be used in these techniques. This project focuses on light-based additive manufacturing of porous polymers which is significant for the following applications; tissue engineering, sound absorption, thermal insulation, energy absorption, and catalytic applications. In order to fabricate porous polymers, the best way to combine emulsion templating with stereolithography. The former provides microporosity whilst the letter allows the occurrence of macroporosity. By emulsion templating, high internal phase emulsions (HIPEs) are produced and then, this emulsion is used as ink for stereolithography. The photocurable emulsions contain an internal phase that is mainly water and a continuous phase which includes monomers, a crosslinker, a surfactant, and a photoinitiator. If the internal phase is higher than 74% it is named as HIPE. When the polymerisation of HIPEs via stereolithography polyHIPEs occur; and so highly interconnected porous scaffolds are obtained through the removal of water in HIPE. This study examines the 3D printing of HIPEs on commercial stereolithography set-up to investigate the utility of this technique to make multiscale porous structures for the mentioned applications. Additionally, parameters affecting the properties of the final product is analysed for microstereolithography set-up products. The porosity was retained during the printing layer-by-layer via the commercial 3D printer. Moreover, porosity depends on the amount of light absorber. It was observed that interconnectivity is related to internal phase volume, increasing water ratio enhances the occurrence of more interconnected structures. Finally, high printing speeds and powers caused a reduction in pore quality.

LIST OF ABBREVIATIONS

2D	Two dimensional
3D	Three dimensional
CAD	Computer-aided design
DIW	Direct ink writing
DMD	Digital mirror devices
EHA	2-ethylhexyl acrylate
FDM	Fused deposition modelling
HIPE	High internal phase emulsion
IBOA	Isobornyl acrylate
LCD	Liquid crystal display
SEM	Scanning electron microscopy
SLA	Stereolithography
SLS	Selective laser sintering
TMTPA	Trimethylolpropane triacrylate
UV	Ultraviolet

TABLE OF CONTENTS

Word Count: 13,435

LIST OF FIGURES

LIST OF TABLES

CHAPTER 1: INTRODUCTION

Additive manufacturing technologies have extensive usage area in various applications, and there are several kinds of methods such as fused deposition modelling (FDM), direct ink writing (DIW), selective laser sintering (SLS), and stereolithography (SLA) [1]–[3]. Additionally, different materials such as metallic powders, ceramic powders or slurries, polymer powders can be used as printing inks or materials for additive manufacturing techniques [3]–[5].

Polymers, which has numerous different applications in developing technologies such as automotive, aerospace, housing materials, building structures, and medical, play a major role in people's daily life [6], [7]. Furthermore, polymers are more advantageous when compared to conventional materials in these areas [6]. As they have the adaptability to various demands; controllable qualities for usage area-specific and the ability to readily duplicate, they have become a superior option in biomedical sciences [8]. Polymeric materials are used in following sub-areas in biomedical sciences; tissue engineering, medical devices, regenerative medicine, etc. [9]. Besides, there has been huge progress in polymer sciences affecting cosmetic surgery, tissue engineering, and drug delivery [8].

In addition to these, porous structures have popularity on applications, and their design has been inspired by nature. [10]. Everything started by investigating natural porous materials with exquisite and complicated structures such as wood, bone, and coral [10], [11]. Researchers noticed that nature has already optimized mechanical properties, and they have spent a great effort to imitate natural architectures in order to make synthetic materials [10], [11]. Porous materials have been utilized gradually in engineering applications such as tissue engineering, insulators, acoustic applications, and catalytic applications thanks to their unique structure that improves practical and mechanical properties [5], [10].

Numerous traditional techniques are taken place in the literature in order to manufacture porous structures, such as supercritical carbon dioxide foaming, direct foaming, sacrificial template, and gel casting [12]–[14]. Nevertheless, these traditional techniques face

difficulties in terms of accuracy, multi-functionality, and multi-scale production; for this reason, additive manufacturing technology has been used for the printing of cellular structures [10]. Additive manufacturing has the capability to fabricate products that are not possible to manufacture by using traditional methods, gives a chance in order to pattern innovative materials for different applications [15].

To conclude, when focused on porous polymers' applications, there are various more types of applications such as tissue engineering, sound absorption, thermal insulation, energy absorption, and catalytic applications. Furthermore, this project will focus on stereolithography of porous polymers as an additive manufacturing technology.

In this project, light-based three-dimensional production methods of porous polymer materials will be examined, and to investigate these methods, polyHIPEs will be used and parameters affecting the properties of the final product will be analysed. Then, the optimum values will be determined for related parameters.

To summarize, the aim of the project is the investigation of 3D printing of porous polymer s. Moreover, how to use of polyHIPEs as ink for stereolithography will be researched.

CHAPTER 2: LITERATURE REVIEW

2.1. Additive Manufacturing

An emerging idea originated to generate three-dimensional objects layer by layer utilizing computer-aided design (CAD) in the early 1980s, which was rapid prototyping that is named additive manufacturing or 3D printing at present [16]. Additive manufacturing technologies are utilized to manufacture, model, and prototype parts via 3D printer or laser set-up [16]. It was generated to aid and encourage engineers, and there is a rising demand for this technology since the 1990s[16]. In addition to these, additive manufacturing is a highly appropriate technique in order to maintain the reproduction of the objects or the repairing of the model [16].

Additive manufacturing, which is used for different areas such as tissue engineering, aerospace industry, energy applications, is a beneficial technique to obtain products with complex shapes [17]. This is the three-dimensional production technique based on layer-by-layer manufacturing [18]. The basic principle of additive manufacturing is to use computer-aided design (CAD) programs to fabricate the product directly from the files [19]. Additive manufacturing techniques are also greatly suitable to fabricate complex shapes. Even though these are slow methods, these provide highly interconnected porous, homogeneous structure and superior mechanical properties [17], [20]. In order to create three-dimensional shapes, there are several types of additive manufacturing techniques such as fused deposition modelling, direct ink writing, selective laser sintering, and stereolithography [3], [17], [21]. Each method has some benefits and drawbacks concerning speed, resolution limit, and accuracy [1]. Among these methods, stereolithography ensures maximum accuracy and sensitivity [20]. The ability to produce sensitive interior and exterior constructions of stereolithography makes it a precious manufacturing method in especially tissue engineering [22]. It is the best technique as it ensures higher resolution using light to polymerise the material. For this reason, stereolithography is the most suitable production technique for the parts used in tissue engineering that are complex and require high precision and accuracy.

2.1.1. Fused Deposition Modelling (FDM)

Fused deposition modelling, which is a solid-based additive manufacturing technique, was improved by Scott Crump in the late 1980s and was commercialised in 1990 by Stratasys [2], [3]. Basically, this method includes support and building materials, and they are melted in a plasticizing unit, then, extrusion is done via a die; therefore, 2D cross-section is obtained onto the platform [3]. Afterwards, the platform is moved down, and the process is repeated for the next layer until the product is completed [3]. After the completion of the product, support materials are detached [3].

2.1.2. Direct Ink Writing (DIW)

Direct ink writing is the other extrusion based additive manufacturing technique [2]. In this method, the extrusion of material is done directly with no melting or solidification in contrast to FDM method [2]. For this reason, the viscosity of the printing material should be low to be able to become fluid; on the other hand, in order to provide the net shape of the object on the printing platform, high viscosity is necessity [2]. As a consequence, pseudoplastic fluid materials such as polymers are favoured for this technique [2].

2.1.3. Selective Laser Sintering (SLS)

Selective laser sintering that enables to produce objects with high mechanical strength was invented by Carl Decker and commercialized by DTM/3D Systems in 1992 [3]. In this process, first of all, the temperature of the polymer powder is increased to process temperature, and then, a laser beam scans the object contour [3]. Afterwards, when the first layer finished, the platform is moved down, and the process is repeated by supplying new polymer powder until the object is created layer-by-layer [3].

2.1.4. Stereolithography

Stereolithography (SLA), which is one of the most used additive manufacturing techniques, was patented by Hull in 1986 [2], [23]. Stereolithography, also known as vat polymerization, is one type of three-dimensional manufacturing technique that works on the basis of the selective curing of a photosensitive resin [18], [19], [24]. This method enables a cross-linking of the liquid polymer by using ultraviolet (UV) light [19], [20], [24].

Since stereolithography contains computer and spatially-controlled irradiation, this provides production of objects from a computer-based design directly [19], [22]. While an object that is determined by CAD files is produced via stereolithography, the photocurable resin is exposed to UV light [22]. This causes the occurrence of free radicals and the other reagents, and the resin is polymerised thanks to these radicals and reagents [22]. When the first layer is polymerised, it is cohered to building table in order to assist for being next layers and the final structure [22]. After completing the first layer, the building stage is adjusted to print the next layer, and these continue until the 3D architecture is finished [22].

In addition to these, there are two different methods, digital light projection and scanning (laser-based) in order to combine stereolithography with emulsion templating [22], [24]. The scanning method that uses computer-driven laser beams is a direct write technique, and it fabricates the object layer-by-layer from bottom to up [22]. In digital light projection, the photocurable resin is kept in a vat, and then, UV light is reflected on a clear surface at the lowest part of the vat; therefore, when the light comes to the resin, the whole layer is polymerised at the same time [22]. Using these two methods with a computer-controlled building stage, the 3D matter is able to be created layer-by-layer [20]. A physical mask was utilized to specify the exact design to be manufactured during the process of digital light projection in the first enterprises of SLA, and then, resolution and flexible designing were improved by applying liquid crystal display (LCD) in order to make specific patterns [25], [26]. Afterwards, the projection system developed by utilizing digital mirror devices (DMD) as a dynamic design creator, and it became to allow giving high resolution [22]. Digital mirror devices are numerous micro-scale mirrors that have the ability of rotation separately, and they are settled in alignment [22]. Furthermore, DMD devices can have top-down or bottom-up projection systems. While the main benefits of bottom-up projection systems are

the better resolution, material preservation, and faster process time; the major limitation is the interaction between material and basement [27].

When compared to other additive manufacturing techniques, stereolithography is superior about designing and manufacturing of microscale pieces [20], [22]. It, therefore, allows the fabrication of scaffolds with high resolution, suitable mechanical and physical properties, appropriate porous structure in terms of size, degree, distribution, and interconnection [19], [22].

Furthermore, two-photon polymerisation (2PP) is another form of photopolymerisation which is used to fabricate smaller scaffolds [22], [28]. Two-photon polymerisation is also recognised as direct laser writing (DLW) or multiphoton processing (MPP) [29]. 2PP is a stereolithography technique, and femtosecond laser is used to cure the photocurable resin in this technique [28], [30]. Also, the building stage is immobile and the monomer is only polymerised at the focal point of the objective as it requires the absorption of two photons of light to initiate the polymerisation reaction as opposed to one photon of light that the other stereolithography techniques use. Therefore, it provides very high micron and sub-micron resolution and nanoscale scaffolds can be manufactured by using this technique [30]. Alternatively, the laser focus moves to create 2D scanning pattern, and beam spot translation in the Z-axis creates 3D architecture [30].

In addition to all this information about additive manufacturing, there is an interesting application that is the combination of 3D polymer material with metal as making a coating. In this process, firstly 3D polymer structure is produced through curing photomonomer via UV light [31]. Then, nickel-phosphorous thin films are stored on this polymer architecture via electroless plating, and therefore, the polymer is etched out [31]. This plating allows the deposit of films inside the pores and complicated forms without any significant weight increase [31]. Therefore, lightweight metallic micro-lattices are obtained.

2.2. Applications of Porous Polymers

2.2.1. Tissue Engineering

Tissue engineering covers exchange and/or mending of injured tissues via generating surroundings that encourage cells to multiply [9]. A scaffold is needed in order to repair damaged tissues since it behaves as a short-lived template to be able to multiply cells [32]. Moreover, polymeric scaffolds that are used to restore bone, skin, neural tissues, cartilage belong to the tissue engineering working area as one type of biomaterials [9], [32]. Polymeric scaffolds have more controllable properties such as their porous structure, forms, dimensions, and microstructures than the other types of scaffolds, ceramics or metals [32]. Generally, scaffolds are identified as three-dimensional porous, open-cell biomaterials permitting cells distributed in the scaffold to interact with each other [32], [33]. They should have the following roles due to being exposed to in-vivo environments: to encourage cell adhesion, cell-biomaterial interactions and allow carrying adequate gases and nutrients being necessary for cells, appropriate microstructure to integrate tissues and display mechanical and structural wholeness [8], [32], [34].

The most essential point is the 3D structure of scaffold in terms of using it in tissue engineering since a three-dimensional cell build needs to be combined into three-dimensional tissue [33]. According to the intended use, scaffolds should be designed. Designing and creating scaffolds are main working fields in tissue engineering as scaffolds have an incomparable function in that area [32]. Mechanical, chemical, and physical requirements must be taken into attention to design the most suitable scaffold for the survival of cells and creation of tissues [33]. For instance, if the tissue is stiff as a bone, the scaffold must be hard; on the other hand, if it is soft such as skin, a ductile scaffold is necessity [33]. This means that related tissue determines the necessary properties of the scaffolds. Moreover, a porous structure is needed in scaffolds to improve cell penetration and creation of three-dimensional tissue [33].

3D printing technologies are preferred methods for biomedical applications, especially for tissue engineering in order to manufacture highly porous scaffolds [35]. Additionally, the

printing ink materials used to manufacture scaffolds are as important as their target properties. They can be synthetic or natural polymers whose properties depend on the composition, organization of their molecules, and structure [32]. There are different methods to produce printing ink by using various types of polymers and their compositions. For example, one of the production methods is emulsion templating which will be explained in the next sections.

2.2.2. Sound Absorption

Acoustic design of means of transport and constructions needs porous materials that are used for sound control to ensure sound absorption [36], [37]. Porous materials' popularity arises from easy to use, suitable for a variety of combinations, the sort of feasible designs, and also, the case that not need any additional energy input [36]. Additionally, the acoustic characteristic mainly depends on the geometric structure, and micro-perforated panel absorbers (MPPAs), narrow tube periodic structures, or passive destructive interference absorbers can be used to improve noise control [37]–[39].

First of all, MPPAs are thin panels with sub-millimeter diameter perforations [37]. Although the geometric design of micro-perforated panel absorbers is comparatively simple, the manufacturing of sub-millimeter perforations is tough and expensive by utilizing laser technology, jetting, or etching [37], [38]. For this reason, additive manufacturing is used to produce perforated layers with various perforation ratios [37]. Secondly, narrow tube periodic structures can be either single or multi-periodic structures and also, multi-periodic structures are periodically organised units of tubes [38]. When the tubes are narrow instead of large, visco-thermal effects have a crucial function in the absorption of sound, and this absorption mechanism includes thermal conduction and viscosity losses at the boundaries of the narrow tube [38]. The fabrication of impeccable shape narrow tubes in millimeter size is hard and costly by traditional methods such as corrugation, and therefore, additive manufacturing is a preferable method at this point [37], [38]. Moreover, additive manufacturing is a better choice to produce complex shape acoustic absorbers as it eliminates one of the main restrictions of passive destructive interference absorbers, which necessitates the use of large absorbing devices to absorb low frequencies [39].

Furthermore, the other significant point is that the utilization of porous materials is essential instead of traditional porous materials in order to decrease people's health related and environmental problems [40], [41]. Various studies have taken place in literature for the purpose of investigation of innovative porous materials having remarkable acoustic performance. For instance, glass fiber and mineral wool were examined to produce porous fibrous materials [42]. The other example is that an industrial tea-leaf-fiber and bio-luffa-fiber were investigated in terms of acoustic properties [43], [44].

2.2.3. Catalytic Applications

Porous materials are a necessity for the fabrication of catalyst supports as well as the other beneficial applications such as sound absorption and insulating materials. Catalyst supports need open-cell and highly porous structures with notable interconnectivity to ensure mass and heat transfer [11].

Stereolithography (SLA) is an additive manufacturing technique that enables to produce catalytic supports, mixers, and reactors by optimizing their geometries from photosensitive materials [2], [45]. In spite of the fact that the use of only photosensitive materials for SLA is an enormous challenge due to the difficulty of the usage of photosensitive materials in the catalytic industry, coating with active constituents of the surface of printed objects might be a solution of that problem [2]. The reason to prefer the SLA method despite this big shortcoming is that it provides to fabricate printed structures with high resolution, and this is significant for catalytic applications [2]. Furthermore, polymers are frequently utilized for additive manufacturing, and even though they are highly suitable to make mechanical parts and models, their low surface areas, inadequate surface properties, and thermal stabilities are not appropriate for catalytic applications [2], [3], [46]. The solution for this limitation can be the manufacturing of organic-inorganic hybrid materials which are the incorporation of active components into printable polymers, therefore; the dispersion of inorganic particles in the polymer makes to obtain printing ink [2]. Recently, 3D printing technologies have disadvantages mentioned above for catalytic applications; however, they have great potential applications such as the preparation of microreactors and monolithic catalysts in the future [2].

2.2.4. Thermal Insulation

Thermal insulation applications need low thermal conductivity, and polyurethane foams provide this significant requirement as well as their low density [15], [47]. The low thermal conductivity depends on cell morphology such as the size distribution of pore sizes, the amount of close and open cells, and the wall thickness of pores [48]. While open cells ensure sound absorption, close pores make the materials suitable for thermal insulation [47]. Basically, thermal insulation arises from the combination of pore size and structure, which trap gas that has low thermal conductivity inside [47]. Moreover, different additives that are low thermal conductive materials and heat storage materials can be used to improve their thermal performances [15], [49]. For instance, one of the additives might be cork that ensures the reduction in the thermal conductivity of polyurethane foams [15].

Additive manufacturing is an emerging technology to manufacture polyurethane foams in order to allow fabricating new shapes and dimensions, even though they can produce via well- structured technology [47]. As additive manufacturing is commonly utilized to manufacture quite complicated shapes, the polyurethane foam industry must consider this method [47]. In addition, additive manufacturing gives an opportunity to design new thermal insulator materials and also, produced insulation layers are used on roofs, spherical tanks, pipes, and buildings in order to provide thermal insulation [47].

2.2.5. Energy Absorption

Providing energy absorption materials that are widely utilized in vehicles, aerospace, marine, and building sectors are lightweight sandwich structures [50]. These sandwich structures comprise of two thin solid face-sheets at the bottom and top surfaces and thick lightweight core that is between solid sheets and the core link them without almost no weight rise [51]. Therefore, lightweight sandwich structures ensure highly bending and buckling resistance and energy absorption capability [51]. The efficiency of energy absorption is related to porous sandwich structure, geometric parameters, and component materials [51].

Additive manufacturing allows producing porous lightweight sandwich structures with geometrical more complex shapes and pore sizes [52]. Furthermore, when compared to

traditional methods, 3D printing technology gives clearly-defined size, shape, and density [52]. Also, new materials can be tried for 3D printing such as polyurethane as mentioned previous part. For example, 3D printing of polyurethane foams was tried, and their properties were investigated, and while they were similar to bulk rubber in terms of resilience properties, their density was four times lower than that of rubber [52]. For this reason, additive manufacturing technologies are promising methods in order to manufacture porous materials by using various kind of materials; especially polymers to utilize in many applications.

2.3. Emulsion Templating

Numerous technologies have been used to build scaffolds with the porous structure to restore tissues [32]. One of these is emulsion templating that has significance to form the porous structure of scaffold [53]. Emulsion templating is a popular method as it gives a chance to control pore size and interconnectivity [54].

In this method high internal phase emulsions (HIPEs) which involve two different phases as internal and continuous phases are used [53]. The main aim of using emulsions, especially HIPEs, is to generate microporosity [53], [55]. Meanwhile, the internal phase that is mostly water is a major part of the total emulsion whereas continuous phase includes hydrophobic monomers and crosslinker [53]. For instance, isobornyl acrylate (IBOA), 2-ethylhexyl acrylate (EHA) as monomers can be used to prepare these emulsions which have easily tunable mechanical properties [24], [55]. Additionally, HIPE can be seen in Figure 3. 1-F.

The emulsion is created by mixing monomers, water, and proper surfactant through slowly dropping of the internal phase into the continuous phase [24], [56]. When the internal phase exceeds 0.74 of the total volume it is categorized as HIPE [24], [57], [58]. Polymerization of the continuous phase creates polyHIPE that stands for polymerised high internal phase emulsion; during polymerization, water droplets are removed from the emulsion, thus, the highly interlinked porous structure is obtained [24], [55], [57]. The characteristics of this

porous structure such as the degree of porosity and the pore size can be controlled easily via control of the production procedure [56]. Nonetheless, when the pore is bigger than 50 μm, it is challenging to produce polyHIPEs with interconnected pores [59]. To prevent this difficulty, porogen additives can be used or emulsion stabilizers might be alternated, but these cause poor mechanical properties and close-pore morphology at this time [54]. On the other hand, three-dimensional printing technologies have the capability to optimize mechanical properties and pore structure [60].

In addition to these, altering the composition of HIPE controls the mechanical properties of the polyHIPE scaffold [53], [56], [61]. Thanks to this great porous structure, polyHIPEs have an expanding usage in tissue engineering applications, especially as a scaffold [56]. In order to control both microporosity and macroporosity in the scaffold, the combination of emulsion templating with additive manufacturing techniques is the right choice since microporosity is controlled by the emulsion templating while macroporosity is directed by the additive manufacturing [24], [57].

In this study we will investigate 3D printing of HIPEs on commercial stereolithography set-up to investigate the utility of this technique to make multiscale porous structures for the mentioned applications. Additionally, 3D printing of HIPEs on microstereolithography set-up will be examined to analyse the parameters affecting the properties of the final product.

Subset of objectives:

- Making a stable polyHIPE based ink
- Investigation of direct write with the inks
- Investigation of the properties of produced structures

CHAPTER 3: MATERIALS AND METHOD

3.1. Materials

In this project, 2-ethylhexyl acrylate (EHA) and isobornyl acrylate (IBOA) as monomers, trimethylolpropane triacrylate (TMPTA) as a crosslinker were used to synthesise HIPE. In addition to these, a surfactant that is Hypermer B246-SO-(MV) and a photoinitiator ((2,4,6-trimethylbenzoyl)-phosphine oxide/2-hydroxy-2-methylpropiophenone, 50/50) were also utilized. Furthermore, the light-absorber, 2-(2H-Benzotriazol-2-yl)-4,6-bis(1-methyl-1-phenylethyl) phenol which is UV-234, also commercially known as Tinuvin®234 were added in some steps of the project. All materials used to synthesise HIPE are demonstrated in Figure 3. 1-(A). Besides, acetone and methanol were used as solvents.

The monomers, the surfactant, the photoinitiator, the light-absorber, acetone, and methanol are from Sigma-Aldrich (Poole, UK), while the surfactant is from Croda, UK.

3.2. HIPE Synthesis

Firstly, HIPEs should be synthesised in order to be able to fabricate PolyHIPEs. For this purpose, acrylate based HIPEs were created by mixing two monomers, 2-ethylhexyl acrylate (EHA), isobornyl acrylate (IBOA) and a crosslinker, trimethylolpropane triacrylate (TMPTA), in which EHA and IBOA were used in 50 wt% each and then, TMTPA was added at 22wt% of the mixture of monomers (Figure 3. 1-B). Afterwards, the surfactant was added at 10 wt% of the mixture of all three acrylates and left to dissolve on the magnetic stirrer by putting magnetic stirrer bar inside it (Figure 3. 1-C). The magnetic stirrer is adjusted to 400 rpm, and it took approximately 3 hours for 34.8 grams stock solution that shows in Figure 3. 1-(D).

Before making HIPEs, the stock solution was prepared from the chemicals that are mentioned above. Different amounts of chemicals were used at the same ratio, it means that

amounts of the solution changed based on grams but the ratio between the chemicals did not change, it was the same for all preparation process (Table 3. 1).

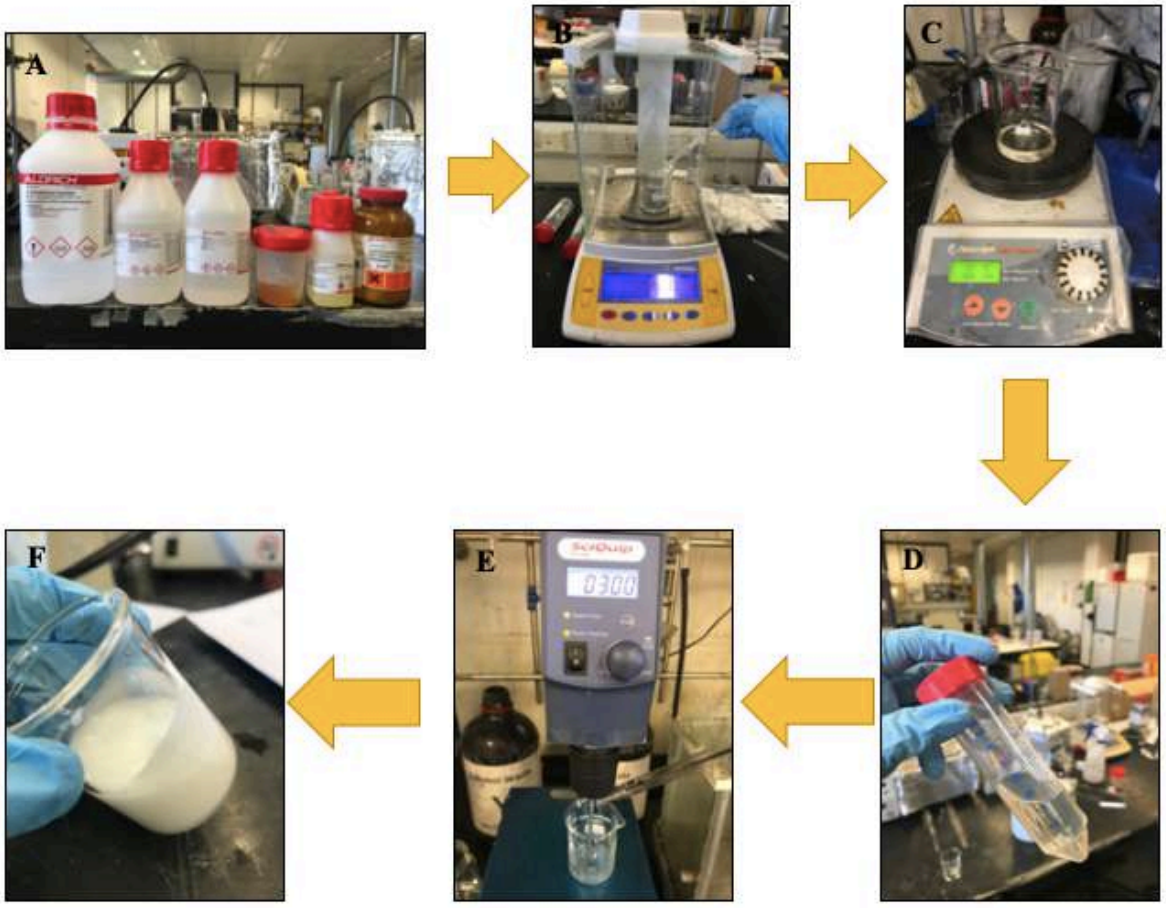

Figure 3. 1. *Schematic diagram of HIPE Synthesis; A: Chemicals used to prepare stock solution and to synthesise HIPEs, B: The scaling of chemicals to prepare stock solution, C: Dissolving of the surfactant via the magnetic stirrer, D: Stock solution, E: The preparation of HIPEs by adding water and stirring, and F: HIPE (high internal phase emulsion)*

After the preparation of the stock solution, distilled water as an internal phase was added to a continuous phase that is a small amount of the stock solution through the dropwise, while stirring at different speeds of mixing (Figure 3. 1-E). To stir the internal phase and the continuous phase SciQuip-Pro 40 was used; therefore, HIPEs were produced (Figure 3. 1-F).

Table 3. 1. *Chemicals used to synthesise HIPEs*

EHA (50%) (g)	**IBOA (50%) (g)**	**TMTPA (cross-linker-22 wt%) (g)**	**Hypermer (surfactant-10 wt%) (g)**
2.96	2.96	1.28	0.72
14.8	14.8	6.4	3.6
29.6	29.6	12.8	7.2

This project focused on the effects of different parameters on the final product in terms of the pore structure and producibility quality. For this aim, HIPEs was manufactured at different speeds of mixing and various continuous phase / internal phase ratios were tried. The ratios of continuous phase / internal phase were 1:4, 1:8, and 1:12 and the speeds of mixing were 100 rpm, 300 rpm, and 500 rpm for every continuous phase / internal phase ratio (Table 3. 2). While the speeds of mixing and the amount of internal phase increase, polyHIPE becomes more viscous. As viscosity affects the printing or the curing quality, the investigation of the different speeds of mixing and various continuous phase / internal phase ratios is highly important to determine optimum conditions to print or cure materials. Moreover, the other reason for the addition of a large amount of distilled water is that water is quite cheap compared to the cost of monomer and the electricity to operate the stirring device. Total volume includes more water and less monomer, water is cheaper than monomer. If a polymer block is printed, it will be 74% water and 26% polymer as opposed to 100% polymer. If we can obtain the same quality product with a higher than 74% amount of distilled water and a low speed of mixing, it will be much more cost-effective. Furthermore, high water ratio enables to fabricate more porous structures.

The addition of the photoinitiator and the light absorber was done before the addition of distilled water into the continuous phase. The light absorber was not used in every HIPE preparation process; however, the photoinitiator was added to every continuous phase in order to be able to the curing process. The amount of the photoinitiator was 5 wt% of the

solution, while the light absorber was added at different amounts; 1 wt%, 2 wt%, and 4 wt% to investigate the effects of it onto curing regime and the pore morphology of products.

Table 3. 2. *Different continuous phase / internal phase ratios and speeds of mixing used in this project*

Continuous Phase / Internal Phase	**Speed of Mixing (rpm)**
1:4	100-300-500
1:8	100-300-500
1:12	100-300-500

3.3. Stability Test

HIPEs are known as highly stable emulsions. To determine the stability, 10 samples were prepared and left for 37 days. Prepared compositions were 1:4 and 1:12 for every different speed of mixing; 100 rpm, 200 rpm, 300 rpm, 400 rpm, 500 rpm. Then, a photograph was taken from day 1 to day 5 in every day. Afterwards, the last two photographs were taken on day 7 and day 37 to observe whether there is any alteration on the appearance of samples.

The stability of HIPEs is especially significant for large scale productions to be able to store them in bottles. Even though they are greatly stable, the continuous phase and the internal phase will start to separate from each other after a while. For this reason, people should be careful about storing HIPEs.

The photographs taken will be served in the results section with comments.

3.4. Porous PolyHIPE Materials Fabrication

Three devices were used to fabricate porous polyHIPE materials, which are UV-Curing machine, microstereolithography set-up, and Kudo 3D Titan2 printer. Each method was used for different purposes.

3.4.1. UV-Curing Machine

HIPEs were prepared of 1:4, 1:8, and 1:12 continuous phase / internal phase ratios at 300 rpm speed of mixing, and then, they were placed into a commercial benchtop UV curing instrument in a glass beaker. Afterwards, the machine was set, and polyHIPEs were obtained through photopolymerisation for 5 minutes. After the curing, the polyHIPEs were removed from the UV curing instrument and washed with acetone. The dimensions of the polyHIPEs were 3.8 cm diameter and 0.5 cm thickness. Figure 3. 2 presents the UV-curing machine (A) and the sample created via UV-curing (B).

Additionally, this method was used for HIPEs that were left for 7 days. After leaving them 7 days, they were cured by commercial benchtop UV curing instrument on the same conditions; power and processing time and washed with acetone in the same way. The purpose of this, to compare the porosity of HIPEs that were directly cured after preparing and HIPEs that were left for 7 days.

Numerous polyHIPEs were formed by using the microstereolithography set-up. HIPEs were prepared of 1:4, 1:8, and 1:12 continuous phase / internal phase ratios at 300 rpm speed of mixing to observe the effect of the amount of water on printing quality. So, the same speed of mixing was preferred for different amounts of distilled water. Furthermore, to observe the effect of the speed of mixing, the same continuous phase / internal phase ratio was utilized and the speed of mixing was altered. For this purpose, HIPEs were prepared of 1:8 continuous phase / internal phase ratio at 100 rpm, 300 rpm, and 500 rpm speeds of mixing. Table 3. 3 demonstrates various continuous phase / internal phase ratios and speeds of mixing used for microstereolithography set-up.

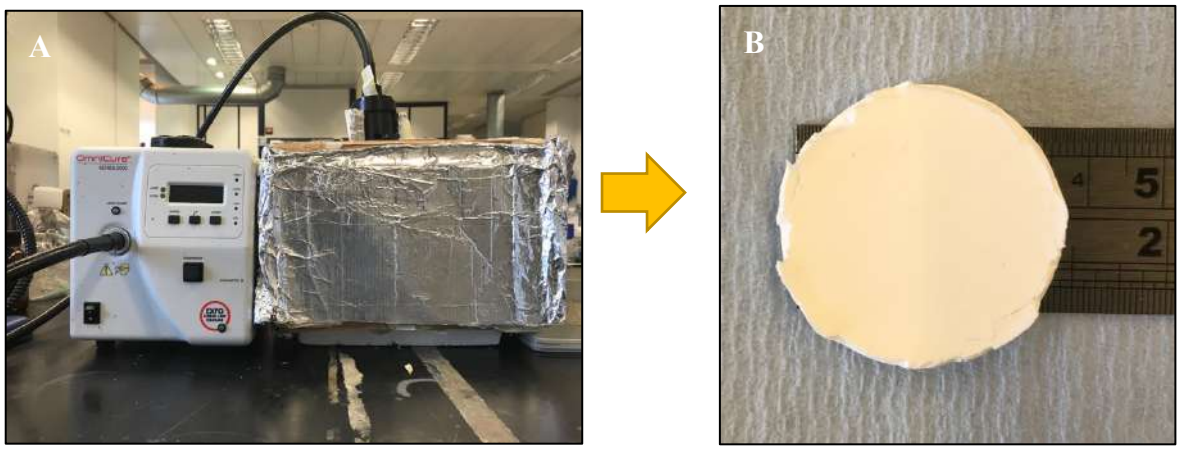

Figure 3. 2. *UV-Curing Machine (A) and the sample created via UV-curing (B)*

3.4.2. Microstereolithography Set-up

The other variables are printing power (mW) and printing speed (mm/s) for microstereolithography set-up. For instance, if the power is not enough, the object is not produced since the resin does not stick to the production platform of the stereolithography set-up; on the other hand, if the power is excessively high, HIPEs cure but the exact shape cannot be created, bad-shaped objects occur. In addition to these, the effect of printing speed is similar with printing power; If the printing speed is too high, there will not be enough time to be bale occur the specific object. For these reasons, printing power and printing speed need to be optimized as well. In this project, 40 mW, 50 mW, 60 mW, 70 mW, and 80 mW powers were used for each printing speed; 0.01 mm/s, 0.02 mm/s, and 0.04 mm/s (Table 3. 4).

Additionally, the beginning time can be another variable, which influences whether the object sticks the plate. Beginning time is the time given to HIPEs in order to stick the plate before the plate is moved down. Standard beginning time used was 1 minute. For some samples that did not stick the plate, different beginning times were tried as 30 seconds, 45 seconds,1.5 minutes, and 2 minutes, and totally, 16 samples were fabricated to have an idea about the effect of beginning time on the final product. The findings will be explained in the results section.

Table 3. 3. *Different continuous phase / internal phase ratios and speeds of mixing used for microstereolithography set-up*

Continuous Phase / Internal Phase	Speed of Mixing (rpm)
1:4	100-300
1:8	100-300-500
1:12	100-300

By using the microstereolithography set-up (Figure 3. 3.-A and B), small tubes were fabricated on the dimensions of 0.5 cm diameter and 0.6 cm height (Figure 3. 3.-C) for every variable, and 105 samples were manufactured. Thereafter, the porosity of these small tubes will be compared among each other by choosing the best quality printed samples in order to determine the optimum conditions.

Table 3. 4. *Printing speed and printing power used in microstereolithography set-up*

Printing Speed (mm/s)	Printing Power (mW)
0.01	40-50-60-70-80
0.02	40-50-60-70-80
0.04	40-50-60-70-80

The other experiment done in microstereolithography set-up was the determination of resolution. To observe resolution, two small tubes were formed by starting from the maximum distance between them and getting closer until two tubes were merged step by step. The resolution of microstereolithography set-up samples will be compared to Kudo 3D printer resolution.

All samples were washed with methanol after removing from the plate and dried in air.

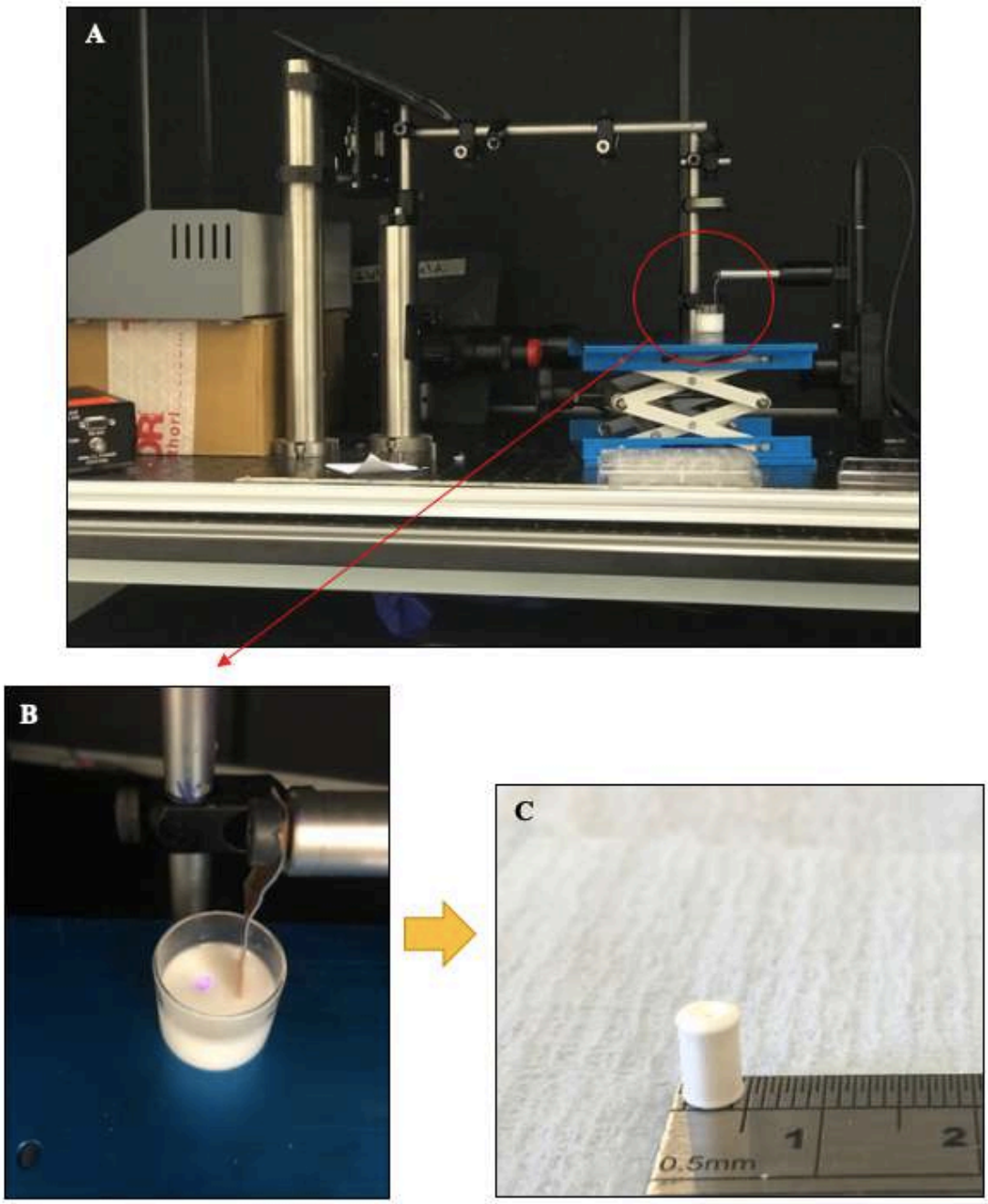

Figure 3. 3. *Microstereolithography set-up (A), while laser is on (B), and the sample created through microstereolithography set-up(C)*

3.4.3. Kudo 3D Titan2 Printer

Kudo 3D Titan2 Printer enables to produce objects with high resolution. In this method, firstly, Kudo 3D Spot-e elastic resin was used to calibrate the printer and to observe the working principles of it.

In Kudo 3D printer, exposure time is adjusted for each layer or from one layer to another layer. This feature is the main variable in this method. By using the printer, totally 37 samples were created, and different exposure time combinations were utilized for 27 samples to determine the best quality conditions. The other variables are lift height, lift speed, down speed, and delay time. These were changed for number of samples to observe the effects of them on printing quality. Details will be presented in the results section.

HIPEs were prepared of 1:4 continuous phase / internal phase ratios at 300 rpm speed of mixing. The reason for choosing 1:4 continuous phase / internal phase ratios at 300 rpm speed of mixing for this method is that these conditions gave the best quality samples in microstereolithography set-up.

As a beginning, calibration file (Figure 3. 4-C) that was produced with resin was manufactured with HIPEs this time, and then, PolyHIPE scaffolds were fabricated by using Kudo 3D printer. Two different structures were tried to form; the first one is simple bone structure (Figure 3. 4-A) and the second one is more complex bone structure (Figure 3. 4-B). Generally, the simple bone structure was used in experiments that are done for porosity observation. The aim of the usage of more complex bone structure is to try the fabrication of more complex shapes via Kudo 3D printer. Figure 3. 5 illustrates the Kudo 3D printer (A), while printing (B), after finishing printing (C), and the sample formed by Kudo 3D printer (D).

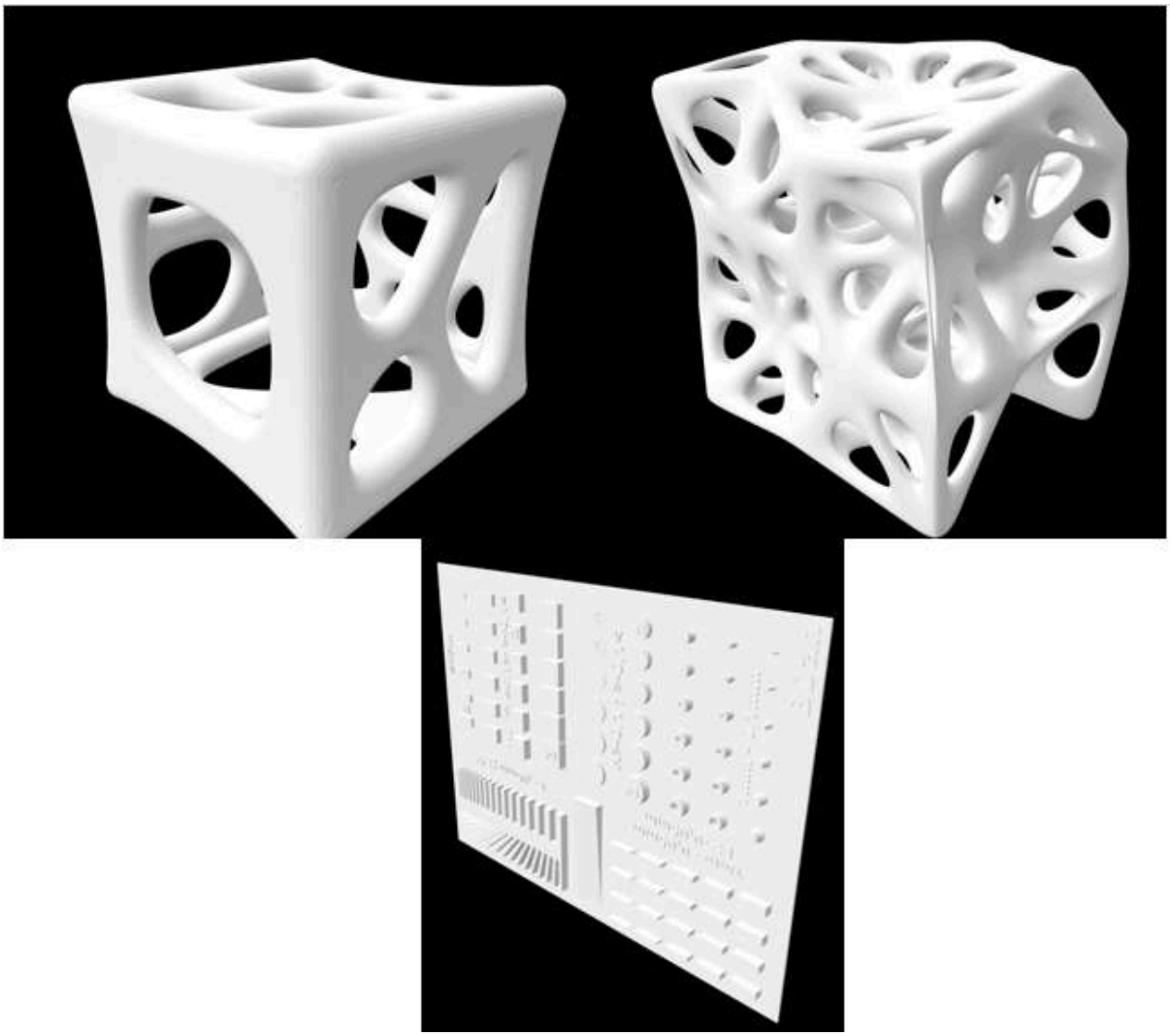

Figure 3. 4. *The files used to manufacture A: Simple bone structure, B: Complex-shaped bone structure, and C: Calibration file via Kudo 3D printer*

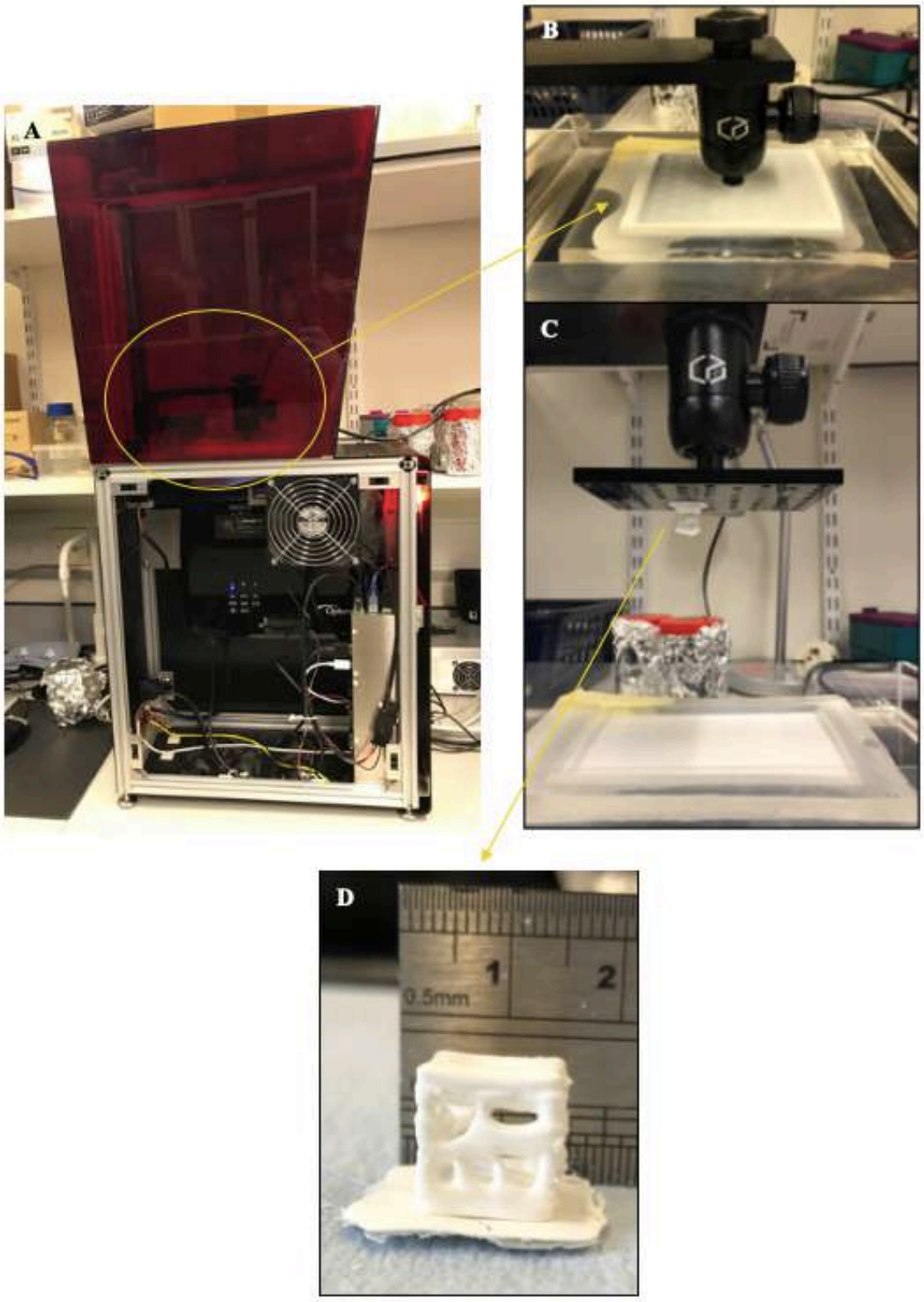

Figure 3. 5. *Kudo 3D printer (A), while printing (B), after finishing printing (C), and the polyHIPE sample formed by Kudo 3D printer (D)*

HIPEs were prepared by adding 1 wt% light absorber, Tinuvin®234. By using this HIPE, cube-shaped polyHIPE scaffolds were created in 6 different dimensions; 1.1 cm, 1.3 cm, 1.5 cm, 1.8 cm, 2 cm, and 2.2 cm. Then, their porous structures were investigated to observe whether there is any difference among different dimensions. Afterwards, 2 wt% and 4wt% light absorbers were utilized in order to compare the samples including different amounts of the light absorber in terms of the quality of the object and pore morphology. Additionally, for this aim, a scaffold was produced without light absorber. They were produced in $1.1 \times 1.1 \times 1.1$ cm dimensions, which was the smallest scaffold.

Furthermore, the other different scaffold fabricated by Kudo 3D printer was from HIPE which was left for 7 days. After leaving it 7 days, it was printed of the same size scaffold with the scaffold that does not include any light absorber. Also, the same values were used for exposure time and other variables.

The final experiment done in Kudo 3D printer was the determination of resolution. To observe resolution, two small tubes were formed by starting from the maximum distance between them and getting closer until two tubes were merged step by step. As mentioned in the previous part, the resolution of Kudo 3D printer samples will be compared to microstereolithography set-up resolution.

All products were washed with methanol after removing from the printer and dried in air.

3.5. Scanning Electron Microscopy

Hitachi TM3030 Plus benchtop scanning electron microscopy (SEM) was used to image polyHIPE samples. Small pieces were cut from the samples to image them. Then, they were placed onto SEM specimen holders (Figure 3. 6.-A). All samples were coated with gold to increase surface conductivity before SEM imaging (Figure 3. 6.-B). Totally, 38 polyHIPE samples were examined; 6 UV-Curing samples, 22 microstereolithography set-up samples, and 10 Kudo 3D printer samples. While the porosity was investigated for all samples, the surface porosity was also examined for Kudo 3D printer samples.

Figure 3. 6. *PolyHIPE samples for SEM before (A) and after (B) gold coating*

During SEM imaging, 5 kV voltage and standard backscattered electron imaging were utilized. Then, images were taken after setting the brightness and focus. There are two options to save an image, quick save and save. While the quick save option ensures low-resolution images, save option gives images with high resolution. For this project, high-resolution images were taken.

While for UV-Curing and microstereolithography set-up samples, x500 magnification was used, for Kudo 3D printer samples, x100 and x500 magnifications were used. Besides, the pore size distribution measurements were done by using x500 magnification SEM images for all samples.

CHAPTER 4: RESULTS

4.1. Stability Test

Stability test has proved that HIPEs are highly stable. Any separation between the continuous phase and the internal phase was not observed for 7 days HIPEs (Figure 4. 1 and Figure 4. 2). On the other hand, there is a thin water layer at the top on day 37 HIPEs in Figure 4. 2. This means that the continuous phase and the internal phase have started to separate from each other after a month.

Based on the different continuous phase / internal phase ratios, the HIPEs that has lower internal phase have separated earlier than higher internal phase HIPEs. Furthermore, the lower speed of mixing causes the earlier separation of continuous and internal phases. As the speed of mixing and the ratio of internal phase increase, HIPEs become more stable.

Table 4. 1. *Different continuous phase / internal phase ratios and speeds of mixing used for stability test*

Label	Continuous Phase: Internal Phase	Speed of Mixing (rpm)
a-b	1:4-1:12	100
c-d	1:4-1:12	200
e-f	1:4-1:12	300
g-h	1:4-1:12	400
i-j	1:4-1:12	500

Table 4. shows the different continuous phase / internal phase ratios and speeds of mixing used for stability test. Additionally, this refers to Figure 4. 1 and Figure 4. 2 for the determination of samples in terms of the internal phase ratios and speeds of mixing.

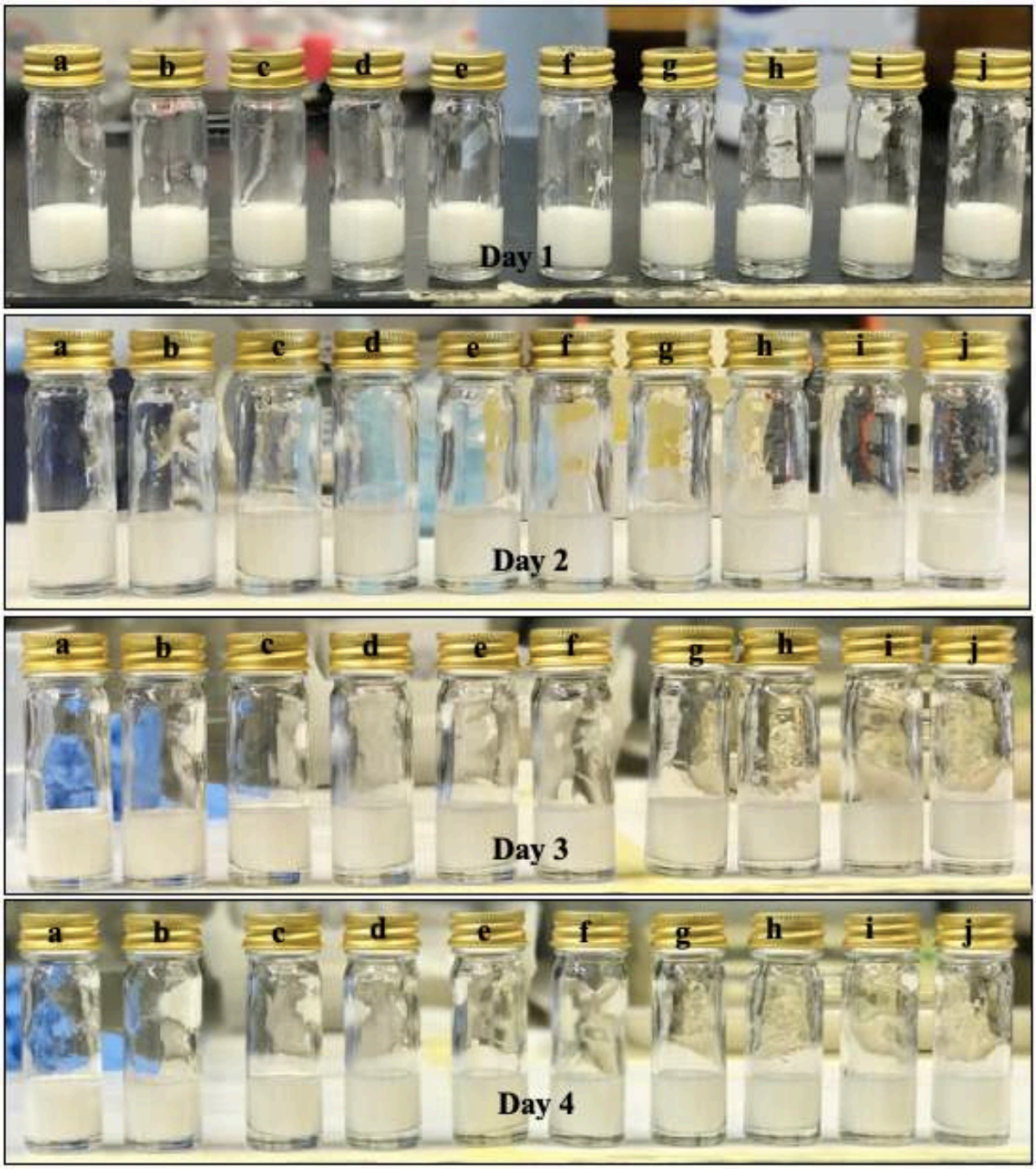

Figure 4. 1. *HIPEs after leaving 1 day, 2 days, 3 days, and 4 days*

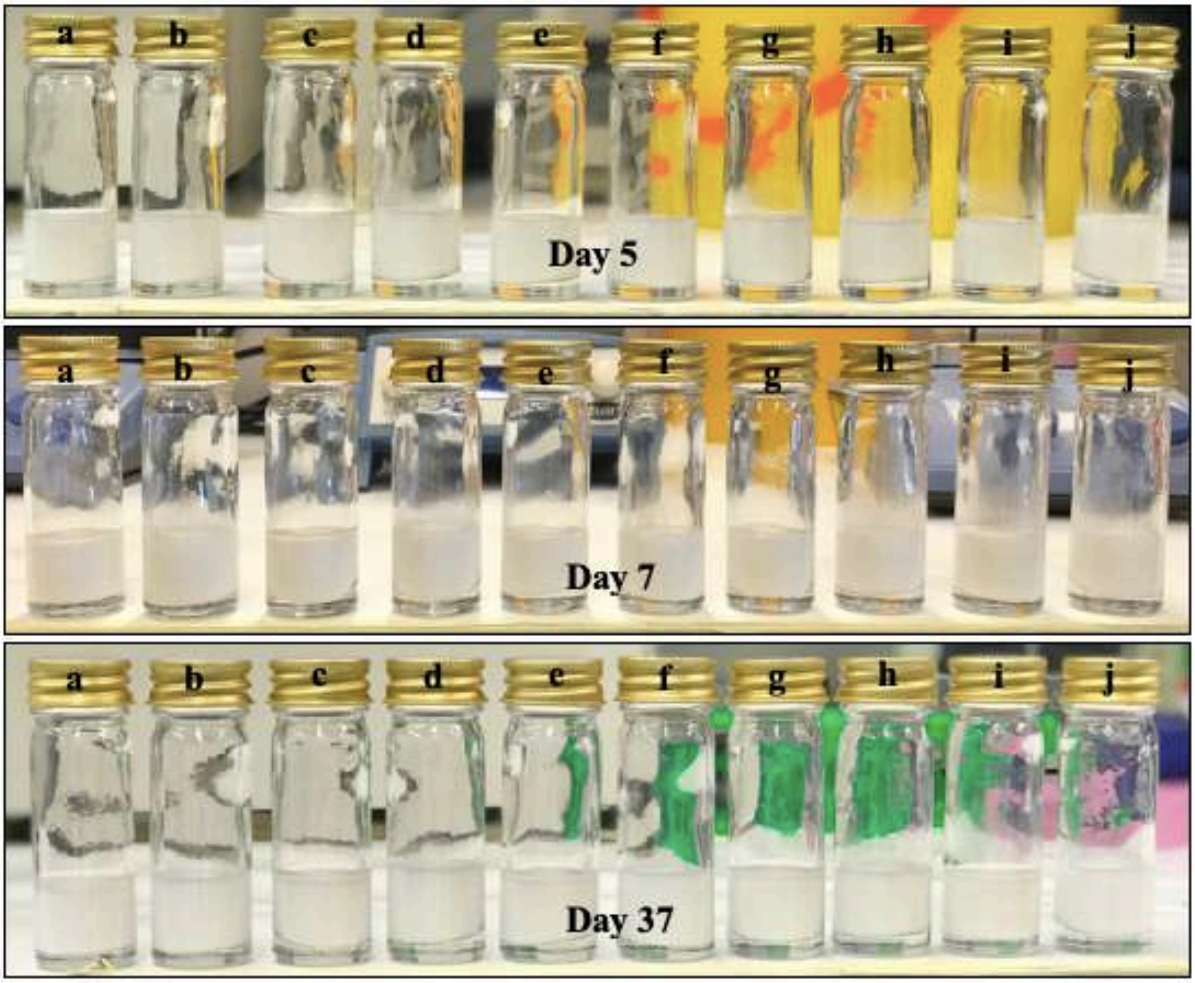

Figure 4. 2. *HIPEs after leaving 5 days, 7 days, and 37 days*

4.2. Effects of Waiting Period of the HIPEs Before UV-Curing on Porosity

Waiting period affects the pore size distribution and porous structure in terms of the amounts of pores and interconnectivity.

Figure 4. 3 demonstrates the relationship between pore diameter and the waiting period of HIPEs for different internal phase volumes. Based on this graph, the pore size distribution does not change remarkably with the altered waiting period. For 1:4 water ratio samples, the smallest pore diameter is 12.4 μm and the largest pore size is 46.7 μm for 1-day sample; on the other hand, for 7 days sample, the smallest and largest pore sizes are 15.2 μm and 43 μm,

respectively. When the 1:8 water ratio samples were examined in that graph, the minimum and maximum values of pore diameter are determined as 11.6 μm and 47.4 μm for 1-day sample and 10.6 μm and 42.2 μm for 7 days sample. Finally, for the 1:12 water ratio samples, 7.5 μm and 32.6 μm are the lowest and highest pore diameters for 1-day sample and 13 μm and 77.7 μm are the diameters of for 7 days samples.

While the smallest range of pore diameters belongs to 1:12 water ratios of 1-day samples, the largest range of pore diameters is in the same water ratio for 7 days samples. The average pore diameter value of the 1-day sample is approximately 17.76 ± 5.56 μm, whereas this average is nearly 31.52 ± 14.02 μm for 7 days sample. On the other hand, there are no significant differences between the other samples. The lowest and highest pore diameters are highly close to each other for the other four samples; the 1:4 and 1:8 water ratios for 1 day 7 days samples. Moreover, the average pore diameter of these four different samples that is almost same is roughly 25 ± 7.5 μm.

Figure 4. 4 illustrates SEM images of UV-curing polyHIPE samples magnified 500 times. A-C-E images show 1-day samples while B-D-F images demonstrate 7 days samples, and their water ratios are 1:4, 1:8, and 1:12, respectively. The water ratio affects the porosity of the samples. As the water ratio increases from A to E and from B to F, porosity rises as can be seen in Figure 4. 4.

Additionally, the small voids in the pores demonstrate the degree of the interconnectivity as these voids are the holes that connect adjacent pores. As the amount of this voids increase, the structure will become more interconnected. According to Figure 4. 4, interconnectivity rises as water ratio increases. Figure 4. 4-A has the lowest interconnectivity while Figure 4. 4-E has the highest. The same relationship is observed for Figure 4. 4-B and F. Figure 4. 4-B has the lowest and Figure 4. 4-F has the highest interconnectivity.

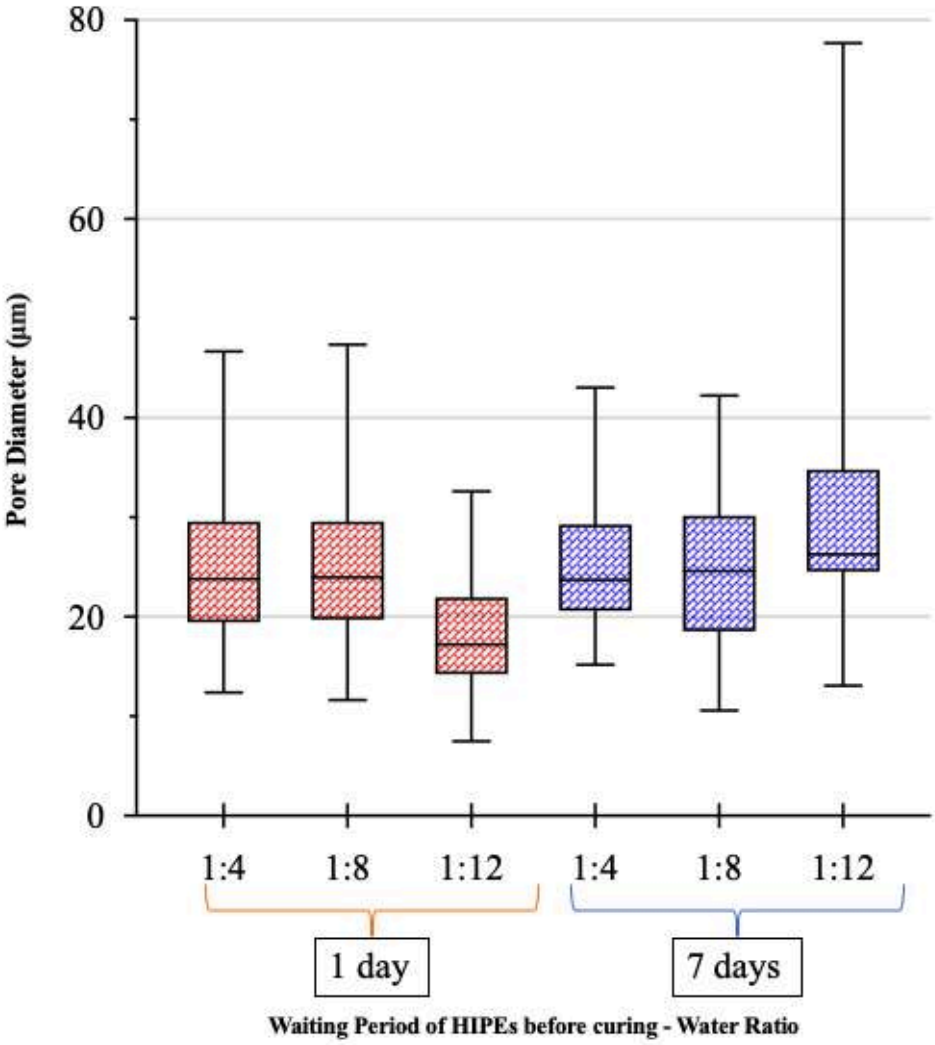

Figure 4. 3. *The graph of pore diameter (µm) and waiting period of HIPEs before curing (1 day-7 days)-water ratio (1:4-1:8-1:12)*

An alteration has been observed in the porosity and interconnectivity in terms of the comparison of the waiting period. 1-day samples are less porous and less interconnected than 7 days samples, except for 1:12 water ratio samples. The 1-day sample has more porosity and more voids ensuring the interconnectivity than 7 days sample, for 1:12 water ratio samples.

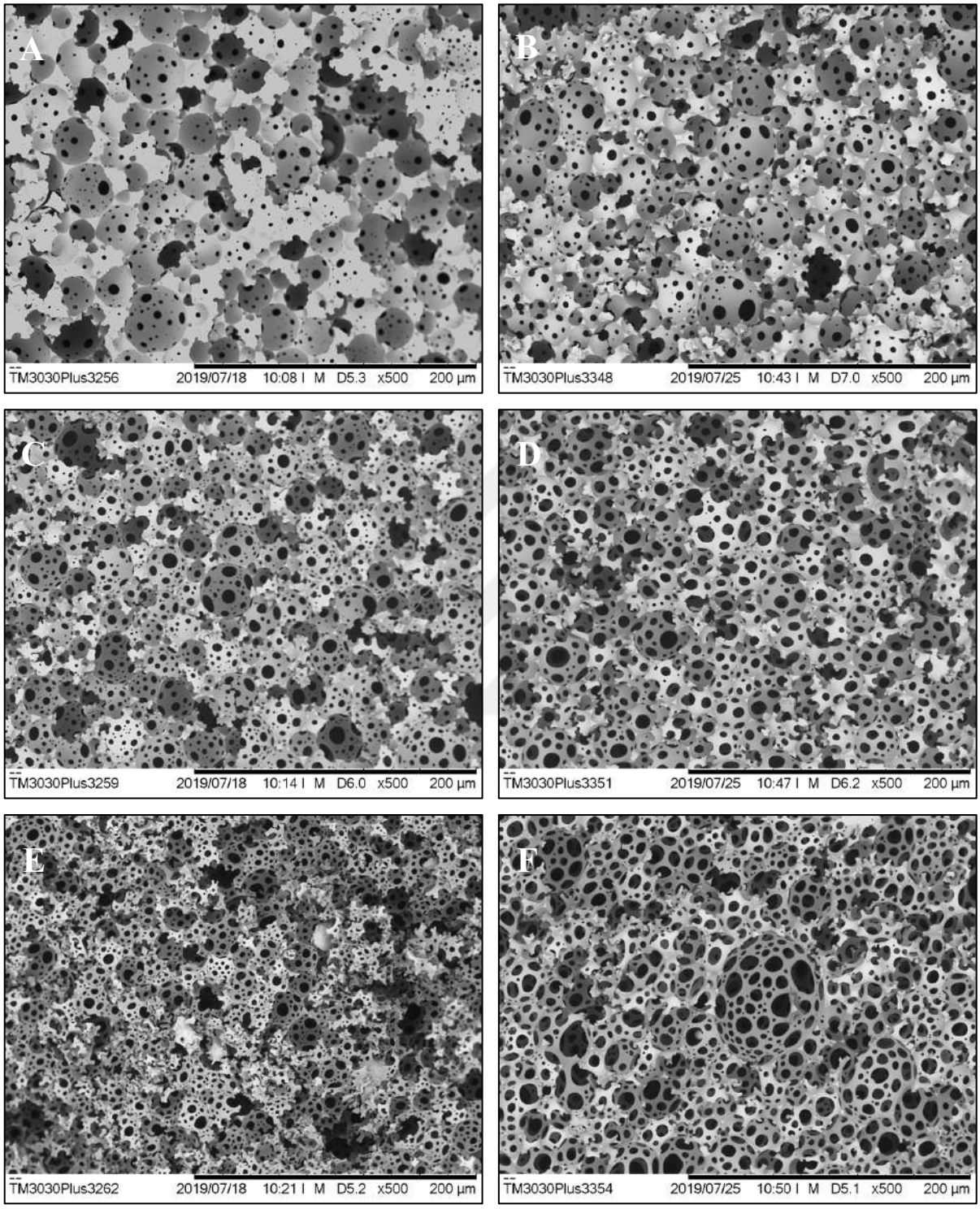

Figure 4. 4. *SEM Images of UV-Curing PolyHIPE Samples; A-C-E: 1 day (1:4-1:8-1:12 water ratio) and B-D-F: 7 days (1:4-1:8-1:12 water ratio)*

4.3. Analysis of Microstereolithography Set-up Samples

4.3.1. Effect of Printing Speed and Power on Printing Quality

The determination of the influences of printing speed and power on the printing quality is highly important as there are many various combinations of the printing speed and power. For this reason, graphs have been created for every different combination of water ratio and speed of mixing. These graphs are presented in Figure 4. 5. A-B-C-D-E-F demonstrates the 1:4 water ratio and 100 rpm speed of mixing, 1:4 water ratio and 300 rpm speed of mixing, 1:8 water ratio and 100 rpm speed of mixing, 1:8 water ratio and 300 rpm speed of mixing, 1:12 water ratio and 100 rpm speed of mixing, and 1:12 water ratio and 300 rpm speed of mixing, respectively. The parameters that objects have been created in net shape are shown in green colour while red colour illustrates the parameters that objects could not be formed. Also, yellow color shows an object was created but it is not net shape.

For the 1:4 water ratio and 100 rpm speed of mixing, the best printing conditions are 40 mW, 50 mW, 60 mW powers in 0.01 mm s^{-1} printing speed and 60 mW, 70 mW, 80 mW powers in 0.02 mm s^{-1} printing speed while the worst conditions are 70 mW, 80 mW powers in 0.01 mm s^{-1} printing speed and 40 mW, 50 mW powers in 0.02 mm s^{-1} and 0.04 mm s^{-1} printing speeds.

For the 1:4 water ratio and 300 rpm speed of mixing, every power in 0.01 mm s^{-1} printing speed and 50 mW, 60 mW, 70 mW, 80 mW powers in 0.02 mm s^{-1} printing speed ensure the best printing quality although the object could not be created in 40 mW power in 0.02 mm s^{-1} printing speed.

For the 1:8 water ratio and 100 rpm speed of mixing, the best circumstances are 40 mW, 50 mW, 60 mW powers in 0.01 mm s^{-1} printing speed and 40 mW, 50 mW powers in 0.02 mm s^{-1} printing speed whereas the object could not be formed only in 40 mW power in 0.04 mm s^{-1} printing speed.

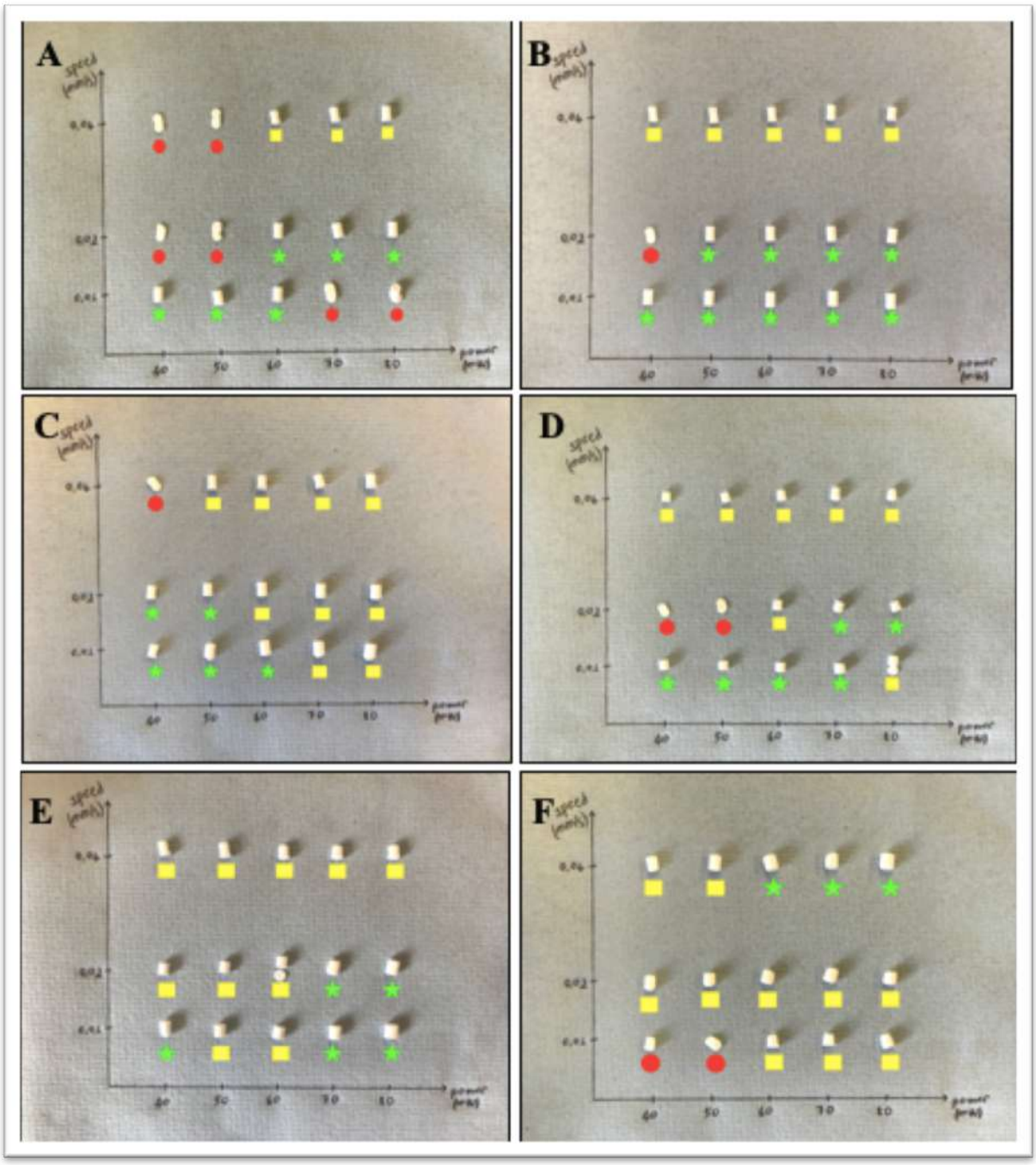

Figure 4. 5. *Microstereolithography Set-up Samples; A: 1:4 Water Ratio and 100 rpm Speed of Mixing, B: 1:4 Water Ratio and 300 rpm Speed of Mixing, C: 1:8 Water Ratio and 100 rpm Speed of Mixing, D: 1:8 Water Ratio and 300 rpm Speed of Mixing, E: 1:12 Water Ratio and 100 rpm Speed of Mixing, and F: 1:12 Water Ratio and 300 rpm Speed of Mixing*

For the 1:8 water ratio and 300 rpm speed of mixing, 40 mW, 50 mW, 60 mW, 70 mW powers in 0.01 mm s^{-1} printing speed and 70 mW, 80 mW powers in 0.02 mm s^{-1} printing speed allow producing high-quality objects. On the other hand, 40 mW, 50 mW powers in 0.02 mm s^{-1} printing speed are not suitable to manufacture the objects.

For the 1:12 water ratio and 100 rpm speed of mixing, in every power and printing speed, the tube-shaped object occurred even if it is not the well-shaped. However, 40 mW, 70 mW, 80 mW powers in 0.01 mm s^{-1} printing speed and 70 mW, 80 mW powers in 0.02 mm s^{-1} printing speed are the best conditions in order to fabricate the good quality objects.

For the 1:12 water ratio and 300 rpm speed of mixing, 60 mW, 70 mW, 80 mW powers in 0.04 mm s^{-1} printing speed provide the best printing quality while 40 mW, 50 mW powers in 0.01 mm s^{-1} printing speed are the worst circumstances.

In addition to these, any object could not be created by using 1:8 water ratio and 500 rpm speed of mixing HIPEs as it is too viscous.

4.3.2. Effect of Beginning Time on Printing Quality

The beginning of the printing process, the first layer of resin may not stick to the building platform due to very small viscosity, too low power, or insufficient beginning time. Various beginning times were tried for different samples to examine this problem. Also, all data that is the water ratio and speed of mixing of the samples, printing speed, power, and various beginning times for these three variables are shown in Table 4. 2.

At the end of this experiment, different results were obtained for low and high printing speeds. For high speeds, shorter beginning time is needed to create net shape objects. Nonetheless, if the beginning time is not enough, the object cannot stick the plate and the object cannot occur. On the other hand, for low speeds, shorter beginning time results in the nonproduction of the feature. It means if low printing speed is preferred, longer beginning times should be used compared to high printing speed.

Table 4. 1. *Different Beginning Times for Microstereolithography Set-up Samples*

Water Ratio and Speed of Mixing (rpm)	**Printing Speed (mm/s)**	**Power (mW)**	**Beginning Time (seconds)**
1:4-100	0.01	70	60
			90
			120
1:4-300	0.04	40	60
			30
		80	60
			30
1:8-300	0.01	40	60
			120
	0.02	80	30
			45
			60
			90
	0.04	70	30
			45
			60

4.3.3. Investigation of Porous Microstructures

By using microstereolithography set-up tube-shaped polyHIPE samples were created. Then, cross-sections were cut from the best quality printed samples chosen in order to image their microstructure via SEM.

Figure 4. 6 demonstrates the SEM images of the samples created with 1:4 water ratio and 100 rpm speed of mixing. A and B show 0.01 mm s^{-1} printing speed and 50 mW-60 mW powers samples while C and D illustrate 0.02 mm s^{-1} printing speed and 60 mW-70 mW powers samples. 0.02 mm s^{-1} printing speed samples have the unclear pores, they may not have formed or might have been damaged during printing because of printing speed. For 0.01 mm s^{-1} printing speed samples, the lower power sample (A) is more porous than higher power (B) sample. Additionally, 0.02 mm s^{-1} printing speed and 60 mW power sample has the highest degree of interconnectivity.

The SEM images of the samples which are formed with 1:4 water ratio and 300 rpm speed of mixing are presented in Figure 4. 7. While A and B illustrate the samples with 0.01 mm s^{-1} printing speed and 50 mW-60 mW powers, C and D indicate the 0.02 mm s^{-1} printing speed and 60 mW-70 mW powers samples. Also, E and F demonstrate the 0.04 mm s^{-1} printing speed and 60 mW-70 mW powers samples. Based on these six images, the 0.02 mm s^{-1} printing speed and 60 mW-70 mW powers samples (C and D) have more porosity than the other four samples. Moreover, the highest degree of interconnectivity belongs to the 0.02 mm s^{-1} printing speed and 60 mW-70 mW powers samples (C and D) as well. In addition to these, it has been observed that the structure is unclear in the 0.04 mm s^{-1} printing speed samples (E-F) in terms of the determination of the pores.

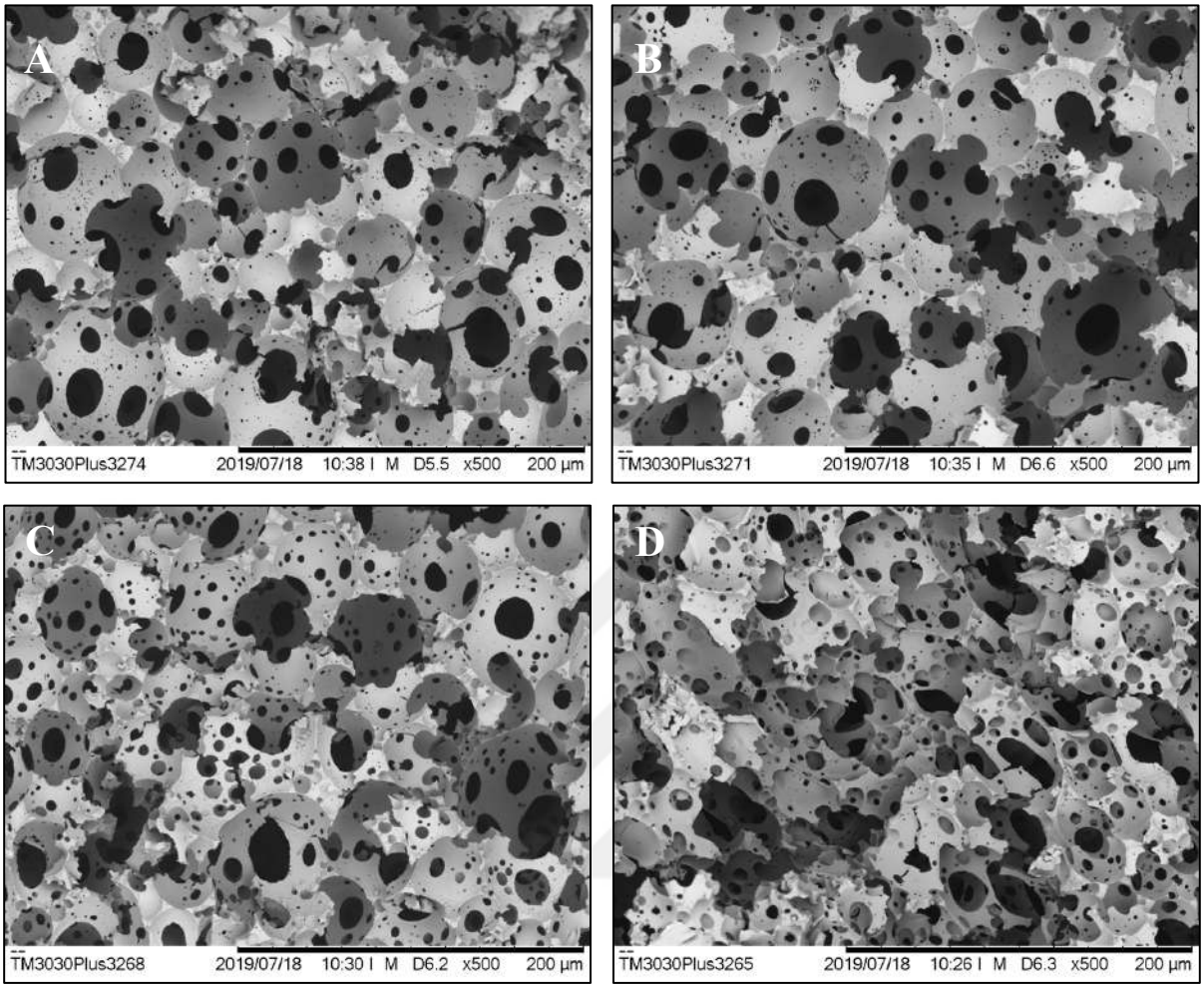

Figure 4. 6. *SEM Images of 1:4 Water Ratio and 100 rpm Speed of Mixing Microstereolithography PolyHIPE Samples; A-B: 0.01 printing speed, A: 50 mW power - B: 60 mW power and C-D: 0.02 printing speed, C: 60 mW power - C: 70 mW power*

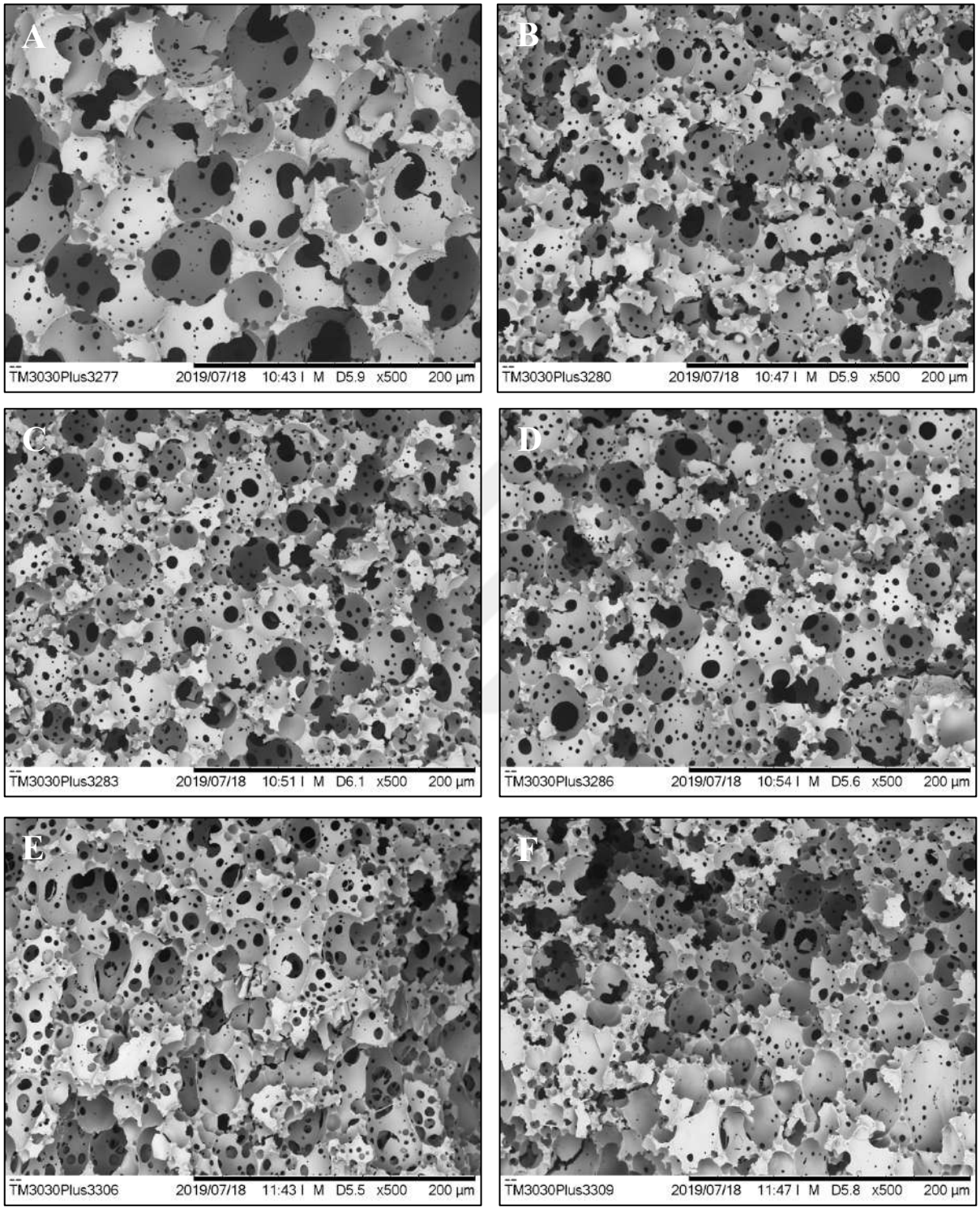

Figure 4. 7. *SEM Images of 1:4 Water Ratio and 300 rpm Speed of Mixing Microstereolithography PolyHIPE Samples; A-B: 0.01 printing speed, A: 50 mW power - B: 60 mW power, C-D: 0.02 printing speed, C: 60 mW power - D: 70 mW power and E-F: 0.04 printing speed, E: 60 mW power - F: 70 mW power*

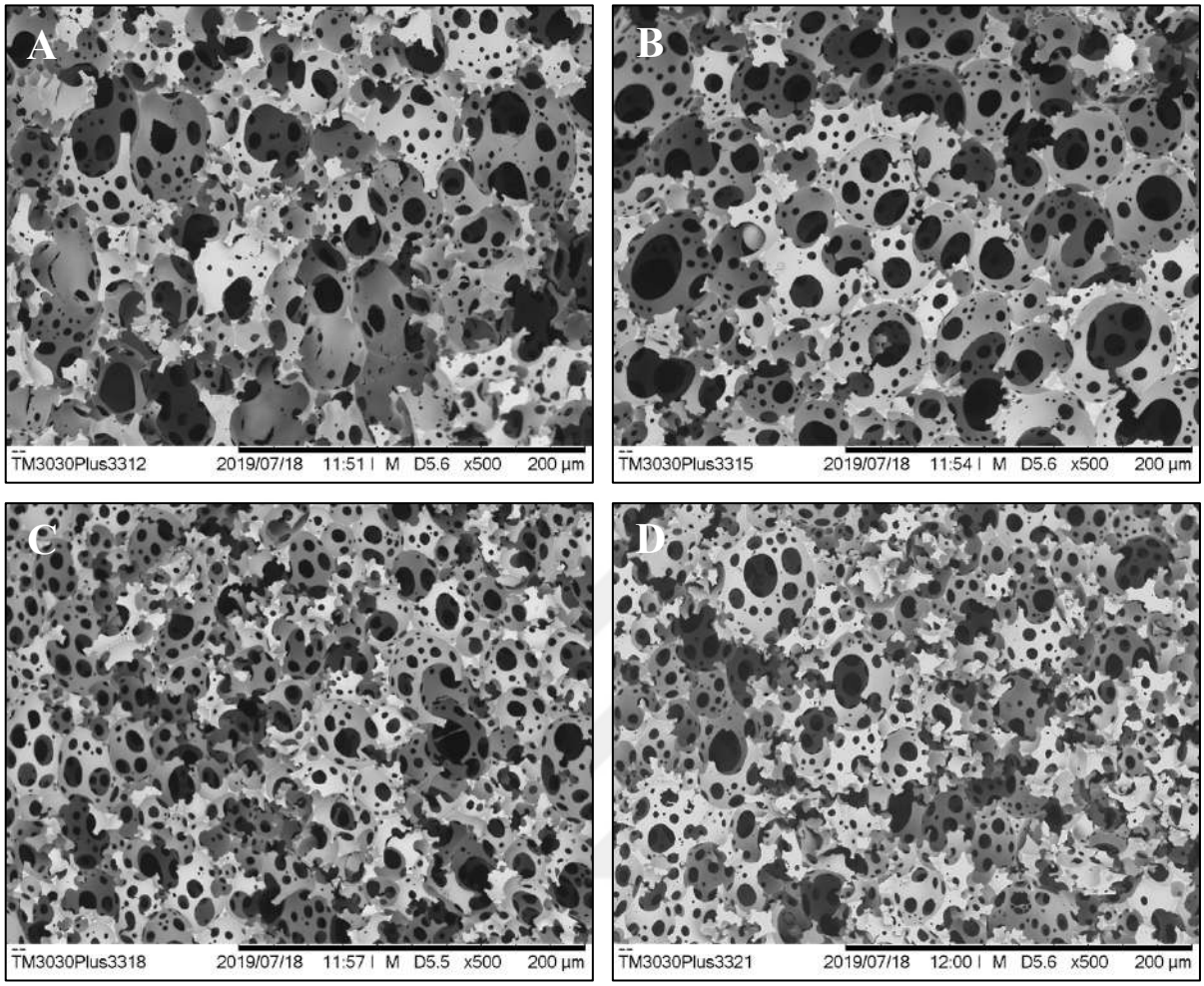

Figure 4. 8. *SEM Images of 1:8 Water Ratio and 100 rpm Speed of Mixing Microstereolithography PolyHIPE Samples; A-B: 0.01 printing speed, A: 50 mW power - B: 60 mW power and C-D: 0.02 printing speed, C: 40 mW power - C: 50 mW power*

1:8 water ratio and 100 rpm speed of mixing samples' SEM images are illustrated in Figure 4. 8. A and B present the 0.01 mm s^{-1} printing speed and 50 mW-60 mW powers samples whereas C and D show the 0.02 mm s^{-1} printing speed and 40 mW-50 mW powers samples. 0.02 mm s^{-1} printing speed and 40 mW-50 mW powers samples (C and D) are more porous and have more interconnectivity than the 0.01 mm s^{-1} printing speed and 50 mW-60 mW powers samples (A and B).

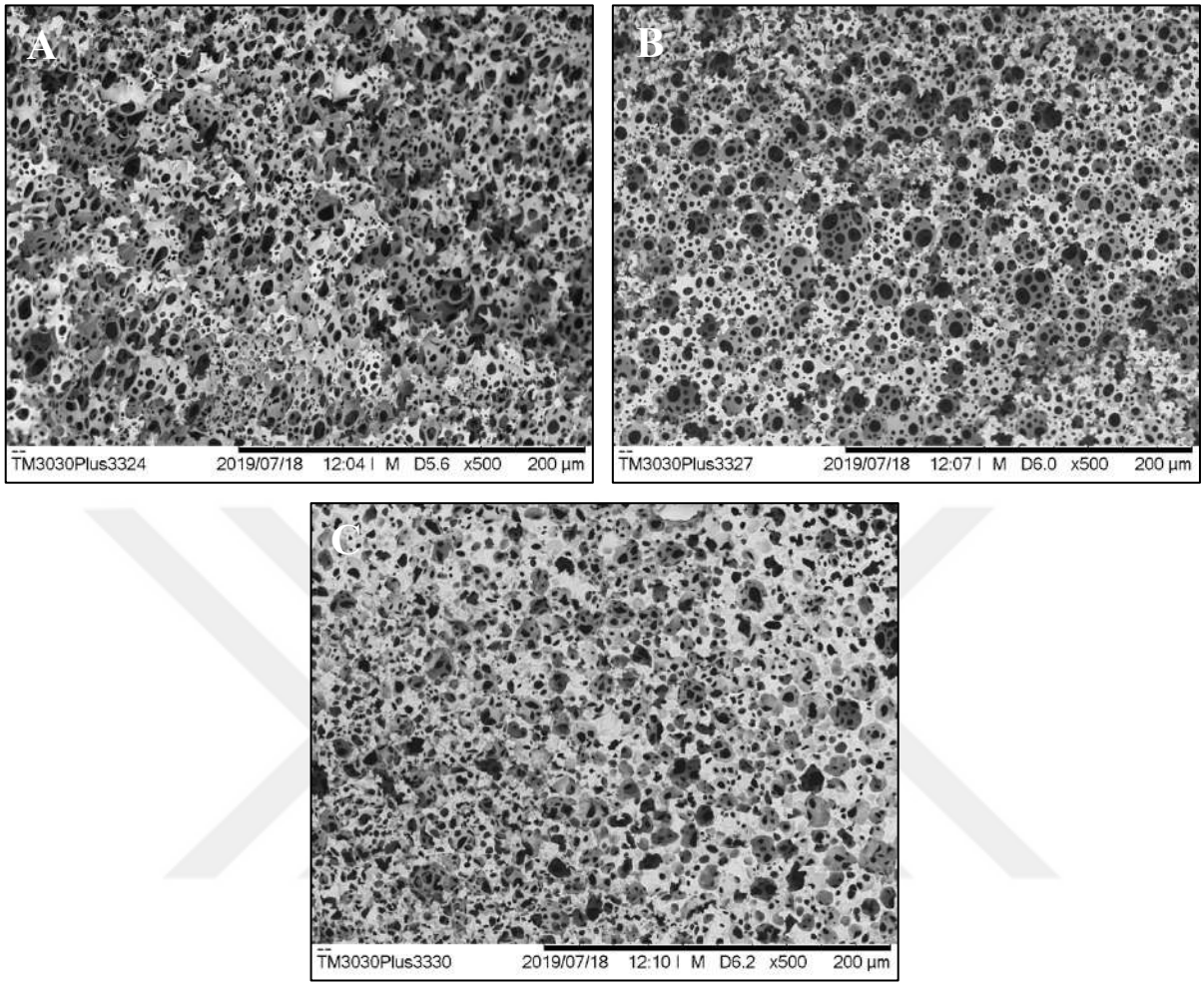

Figure 4. 9. *SEM Images of* 1:*8 Water Ratio and 300 rpm Speed of Mixing Microstereolithography PolyHIPE Samples; A-B: 0.01 printing speed, A: 40 mW power - B: 50 mW power and C: 0.02 printing speed, 80 mW power*

Figure 4. 9 indicates the SEM images of 1:8 water ratio and 300 rpm speed of mixing samples which are 0.01 mm s^{-1} printing speed and 40 mW-50 mW powers samples and 0.02 mm s^{-1} printing speed and 80 mW power sample, presented in A, B and C images, respectively. 0.01 mm s^{-1} printing speed and 40 mW-50 mW powers samples (A and B) have more net porous structure than 0.02 mm s^{-1} printing speed and 80 mW power sample (C). Furthermore, the highest porosity and interconnectivity belong to the B image that is 0.01 mm s^{-1} printing speed and 50 mW power sample.

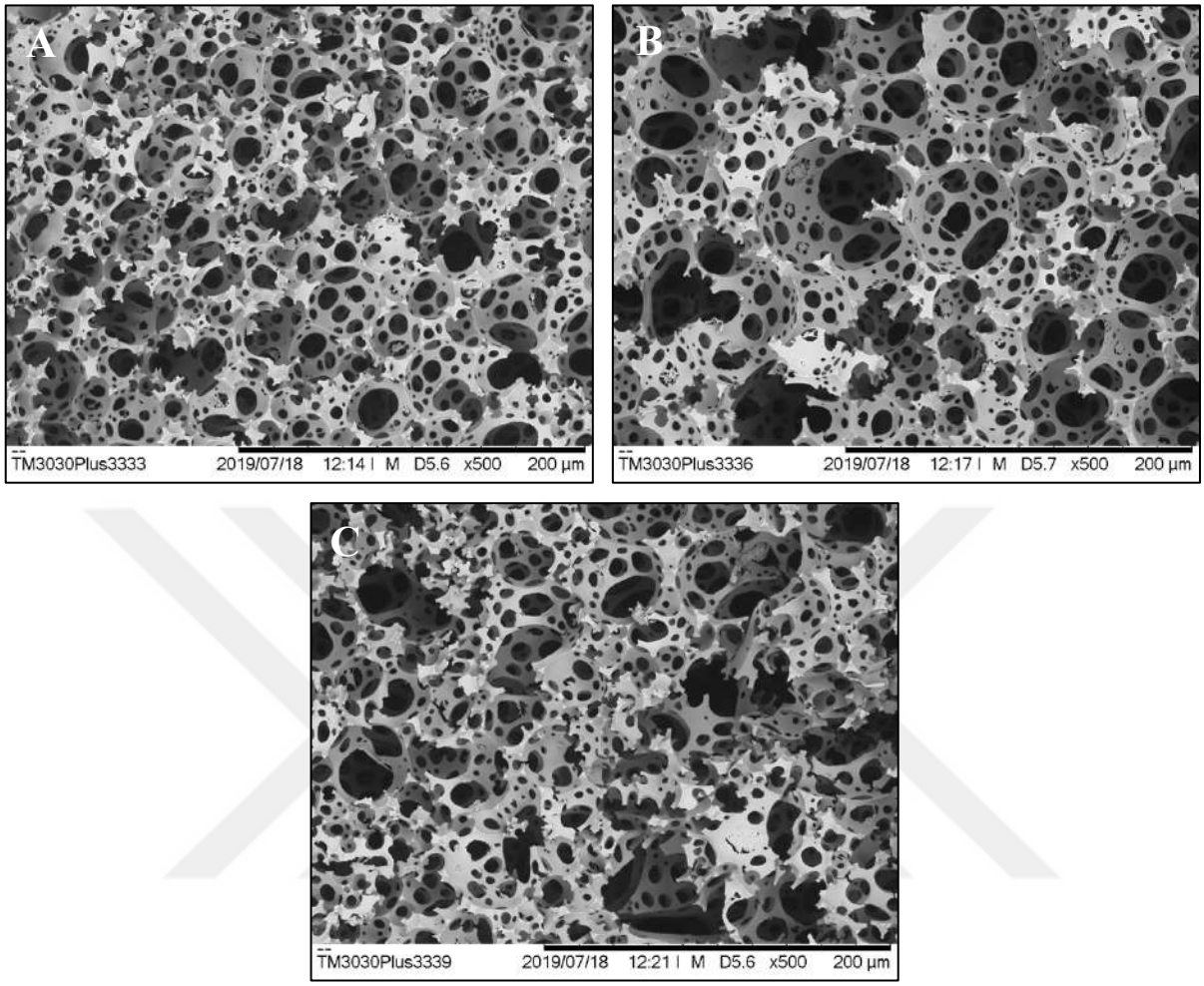

Figure 4. 10. *SEM Images of 1:12 Water Ratio and 100 rpm Speed of Mixing Microstereolithography PolyHIPE Samples; A-B: 0.01 printing speed, A: 40 mW power - B: 80 mW power and C: 0.02 printing speed, 80 mW power*

The SEM images of 1:12 water ratio and 100 rpm speed of mixing samples are presented in Figure 4. 10. While A and B images demonstrate the 0.01 mm s^{-1} printing speed and 40 mW-80 mW power samples, C image illustrates the 0.02 mm s^{-1} printing speed and 80 mW power sample. 0.01 mm s^{-1} printing speed and 40 mW power sample (A) has the most porous microstructure. Even though there is a significant difference in porosity between 0.01 mm s^{-1} printing speed and 40 mW power sample (A) and 0.01 mm s^{-1} printing speed and 80 mW power sample (B) images, their interconnectivities are almost the same. Moreover, 0.02 mm s^{-1} printing speed and 80 mW power sample has incomplete pores; however, it is better than the previous samples created with high printing speed and high power.

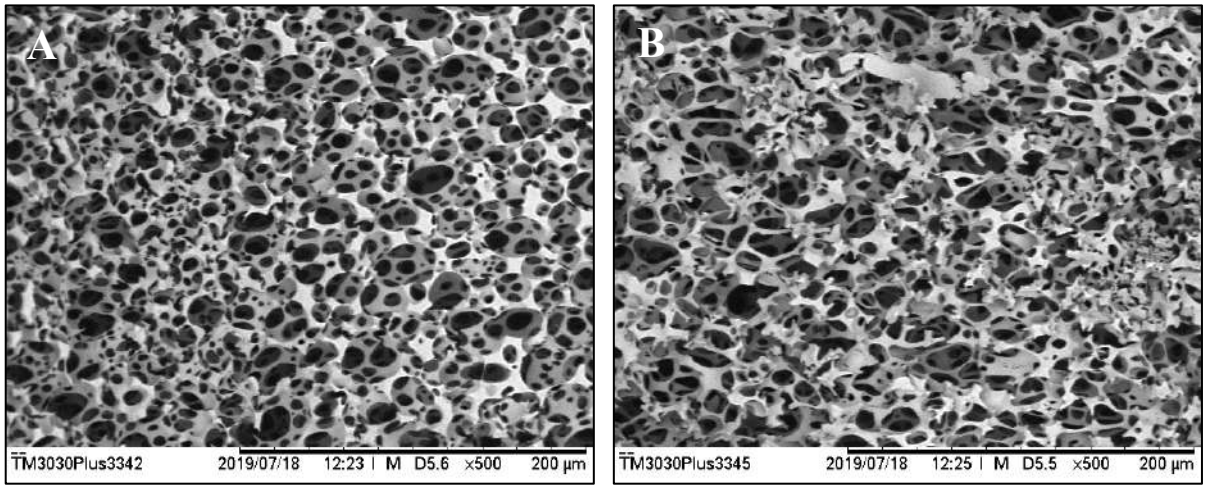

Figure 4. 11. *SEM Images of 1:12 Water Ratio and 300 rpm Speed of Mixing Microstereolithography PolyHIPE Samples; A-B: 0.04 printing speed, A: 60 mW power - B: 80 mW power*

Figure 4. 11 presents the SEM images of 1:12 water ratio and 300 rpm speed of mixing samples. 0.04 mm s^{-1} printing speed and 60 mW-80 mW power samples are shown in A and B, respectively. Both microstructures have unfinished pores; nevertheless, 0.04 mm s^{-1} printing speed and 60 mW power sample is clearer than the other. Also, they have a similar amount of porosity and interconnection. In other words, there is no remarkable difference between them in terms of porosity and interconnectivity.

Figure 4. 12 demonstrates the relationship between the pore size distribution and various variables such as water ratio, speed of mixing, printing speed, and power for microstereolithography samples as a graph. This graph is significant to determine the best printing conditions by combining with the SEM images of them. The minimum and maximum values of pore diameters will be given as rough values under the water ratio and speed of mixing categories, stating the exceptions.

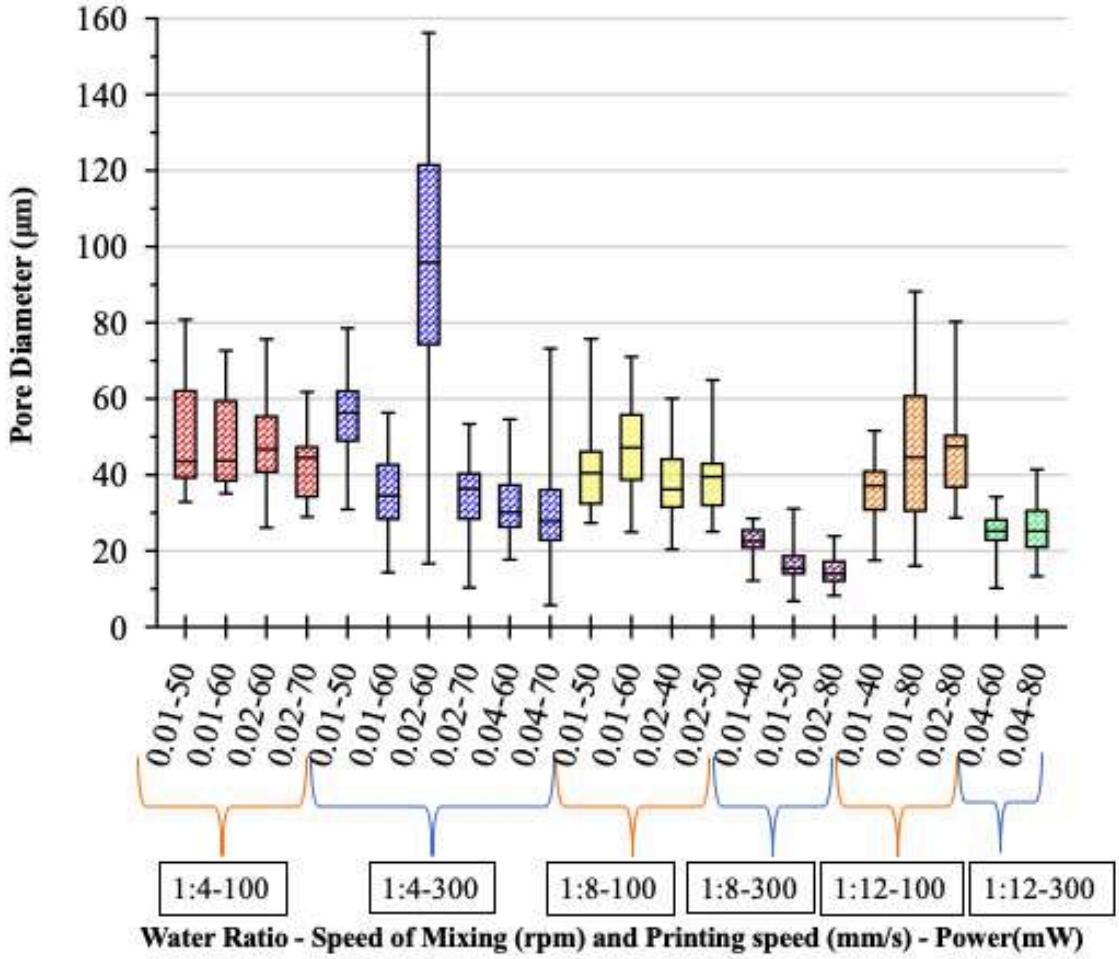

Figure 4. 12. *The graph of pore diameter (µm) and water ratio (1:4-1:8-1:12)-speed of mixing (100 rpm-300rpm) / printing speed (0.01 mm/s-0.02 mm/s-0.04 mm/s)-power (40 mW-50 mW-60 mW-70 mW-80 mW)*

For 1:4 water ratio and 100 rpm speed of mixing samples, there are four samples in this category. 0.01 mm s^{-1} and 0.02 mm s^{-1} are printing speeds, and 50 mW and 60 mW powers were chosen from the 0.01 mm s^{-1} printing speed and 60 mW and 70 mW powers were from 0.02 mm s^{-1} are printing speed. These four samples' the lowest pore diameters are between 60 µm and 80 µm and highest pore diameters are between 25 µm and 35 µm. Furthermore, the average pore diameter of these samples is roughly 45 ± 10 µm.

For 1:4 water ratio and 300 rpm speed of mixing samples, this category comprises of six samples. Printing speeds are 0.01 mm s^{-1}, 0.02 mm s^{-1}, and 0.04 mm s^{-1}, and while 50 mW

and 60 mW powers were examined for 0.01 mm s^{-1} printing speed, 60 mW and 70 mW powers were investigated for 0.02 mm s^{-1} and 0.04 mm s^{-1} printing speeds. Moreover, the lowest pore diameters are between 5 μm and 17 μm and highest pore diameters are between 18 μm and 78 μm for these samples, except the sample that has 0.02 mm s^{-1} printing speed and 60 mW power. Furthermore, the average pore diameter of these five samples is roughly 35 ± 10 μm. For the sample that have 0.02 mm s^{-1} printing speed and 60 mW power, while the smallest and highest pore diameters are 16.7 μm and 156.3 μm, the average of it is approximately 93.81 ± 34.29 μm.

For 1:8 water ratio and 100 rpm speed of mixing samples, four samples were investigated. In this category, 50 mW and 60 mW powers for 0.01 mm s^{-1} printing speed and 40 mW and 50 mW powers for 0.02 mm s^{-1} printing speed were examined. The minimum and maximum pore diameters are roughly 25 μm and 67 μm while the average value of pore diameter is 45 ± 10 μm for this category samples.

For 1:8 water ratio and 300 rpm speed of mixing samples, there are three samples in this category. Two of them have 0.01 mm s^{-1} printing speed and one of them has 0.02 mm s^{-1} printing speed. For 0.01 mm s^{-1} printing speed, 40 mW and 50 mW powers and 0.02 mm s^{-1} printing speed, 80 mW power were investigated. While the lowest values of pore diameter change from 6 μm to 12 μm and the alteration of the highest values are between 24 μm and 31 μm. Also, the average pore diameter is roughly 18 ± 4.2 μm.

For 1:12 water ratio and 100 rpm speed of mixing samples, three samples that have 0.01 mm s^{-1} and 0.02 mm s^{-1} printing speeds were examined. Two of these three samples have 40 mW and 80 mW for 0.01 mm s^{-1} printing speed and one of these has 80 mW for 0.01 mm s^{-1} printing speed. Their minimum and maximum pore diameters are between 16 μm and 85 μm. Also, the average pore diameter is about 40 ± 14 μm.

For 1:12 water ratio and 100 rpm speed of mixing samples, there are two samples that have 0.01 mm s^{-1} printing speed and 60 mW and 80 mW powers in this category. While the smallest and highest values of pore diameter are nearly between 10 μm and 40 μm, the average value is about 25 ± 6 μm.

Based on Figure 4. 12, to determine the pore size distribution 23 samples were examined. Among these samples, the lowest average pore diameter and the smallest gap between minimum and maximum values of pore diameters belong to 0.02 mm s^{-1} printing speed and 80 mW power in the category of 1:8 water ratio and 300 rpm speed of mixing samples.

4.4. Analysis of Kudo 3D Printer Samples

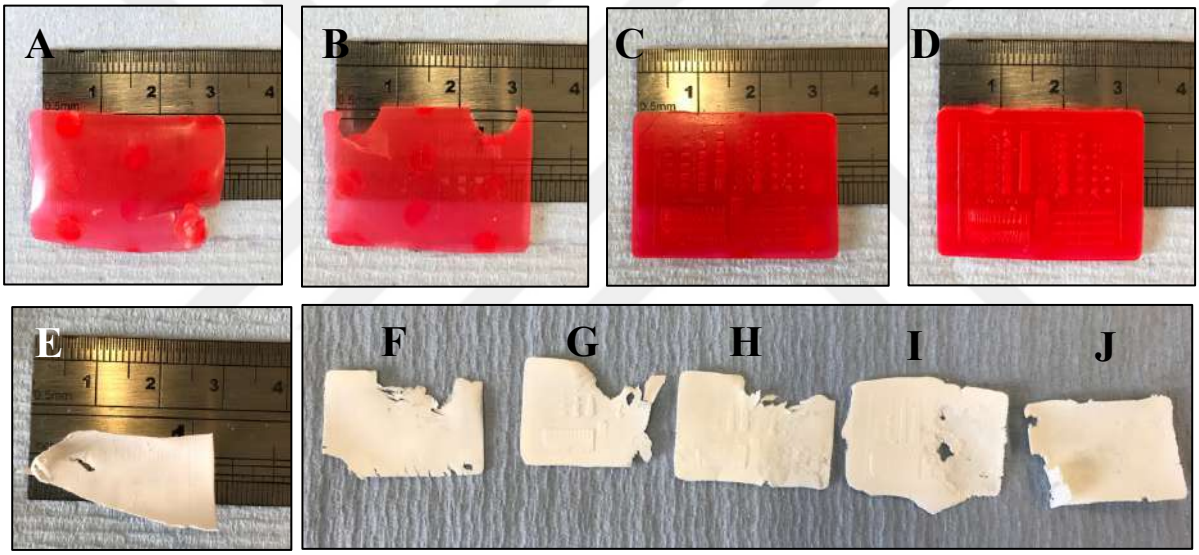

Figure 4. 13. *Calibration files created via Kudo 3D printer by using resin (A-B-C-D) and HIPEs (E-F-G-H-I-J)*

Figure 4. 13 demonstrates creating calibration files by the Kudo 3D printer. While A-B-C-D were formed with resin, E-F-G-H-I-J were fabricated with HIPEs. The difference between these samples is that different exposure times were applied for various layers in every sample. The calibration file consists of 54 layers and each layer has 0.030 mm thickness.

For A sample, the exposure times of the first layer, the second part layers (from 2 to 34), and third part layers (from 35 to 54) are 35 s, 20 s 15 s while for B sample, they are 25 s, 15 s, and 15 s for the same layers with A, respectively. Also, for D sample 30 s, 20 s, and 15 s has been used for the same layers. For C sample, layers have been separated as 1, from 2 to

32, and from 33 to 54 and exposure times are 30 s, 20 s, and 12 s. According to images, C and D samples are pretty good in terms of net shape and resolution; however, A and B images could not occur because of insufficient exposure time of the first layer.

Even though different exposure times for different layers were tried, any success could not be obtained for the fabrication of HIPEs calibration files.

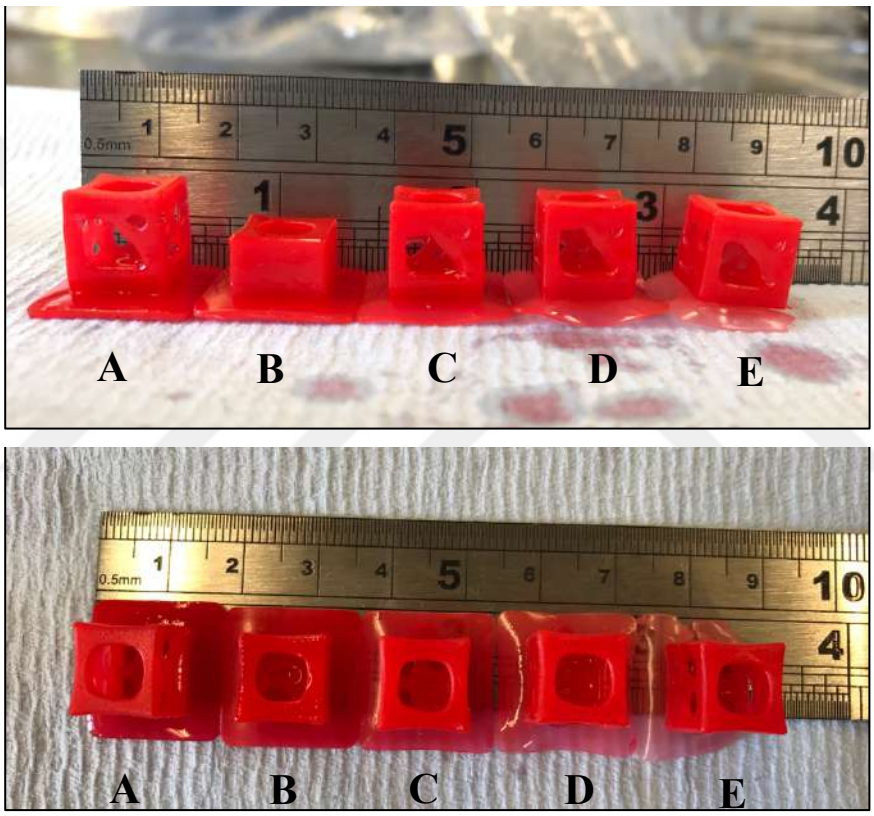

Figure 4. 14*. Cube-shaped resin scaffolds via Kudo 3D printer*

Figure 4. 14 presents cube-shaped resin scaffolds that were fabricated by using Kudo 3D printer. The thickness of one layer of these cube-shaped resin scaffolds is 0.030 mm, except B. 0.050 mm slice thickness were applied for the B sample. Even though all samples are well-shaped, the basement of D and E samples were not be formed very well. This might be related to the insufficient amount of the resin in the tank or the wrong adjustment of the building stage. Since the exposure time of the first layer is the same for all samples (A-B-C-D-E). The reason for the manufacturing of five samples is to observe the effect of different

exposure times on the producibility of details in the object. Nevertheless, any remarkable difference about that has not been determined.

Figure 4. 15 indicates the different sizes of cube-shaped resin scaffolds. According to these two images (A and B), as objects become smaller, details cannot be created. This is valid for samples whose dimensions are $0.5 \times 0.5 \times 0.5$ mm and smaller than it.

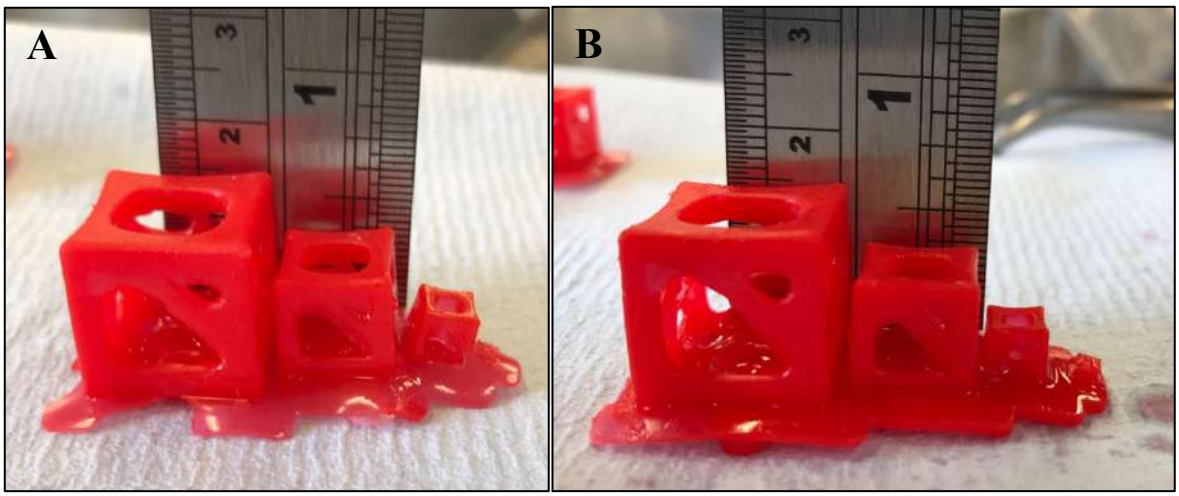

Figure 4. 15. *Different sizes of cube-shaped resin scaffolds via Kudo 3D printer*

Figure 4. 16 illustrates complex-shaped resin scaffolds. While A shows the big ($2 \times 2 \times 2$ cm) and single complex-shaped scaffold, B presents the different sizes of complex-shaped scaffolds. Although almost all details in the file could be created in a single sample (A), the same details could not be formed as objects are getting smaller (B).

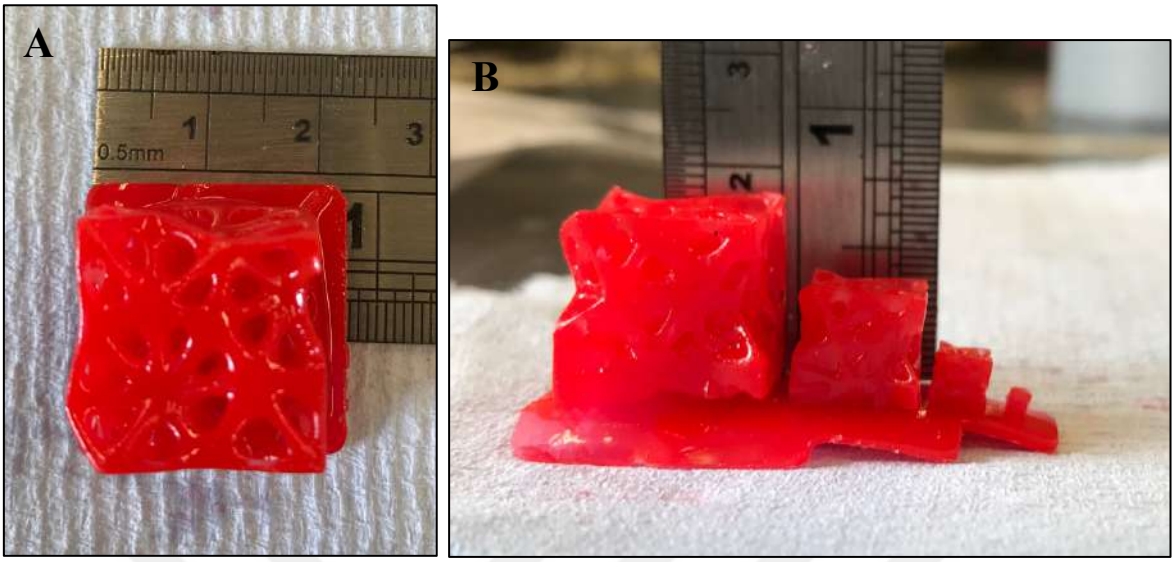

Figure 4. 16. *Single complex-shaped scaffold (A) and different sizes of complex-shaped resin scaffolds (B) via Kudo 3D printer*

Figure 4. 17 presents the different polyHIPE scaffold samples. These are various trials done in order to obtain well-shaped polyHIPE scaffolds. Image A shows the first sample, it could not be created due to the wrong adjustment of the building stage. Then, second trying (B) has achieved success by using the same exposure times for the same layers with the first sample (A). C image demonstrates the different sizes of cube-shaped polyHIPE scaffolds, and for smaller objects, the printing quality has been decreased.

D-E-F images indicate the big ($2.2 \times 2.2 \times 2.2$ cm) cube-shaped scaffold. D and E samples have the same conditions in terms of the exposure time but the difference is that the square-shaped silicon template was used in the tank to reduce the used amount of HIPEs for D sample. For E and F samples, silicon template was not used. Silicon allows manufacturing more net shape scaffolds (D). Moreover, lower lift and down speeds were utilized for the E sample. Therefore, better printing quality has been obtained.

G and H images present the small ($1.1 \times 1.1 \times 1.1$ cm) cube-shaped scaffold and they were produced with silicon template (H) and without it (G). Also, the exposure times are the same for both. As a result, H sample has better quality than G sample. For I sample, very high exposure times were used to observe the influences of it. This high exposure times caused extreme curing, so the object could not be formed clearly and its details.

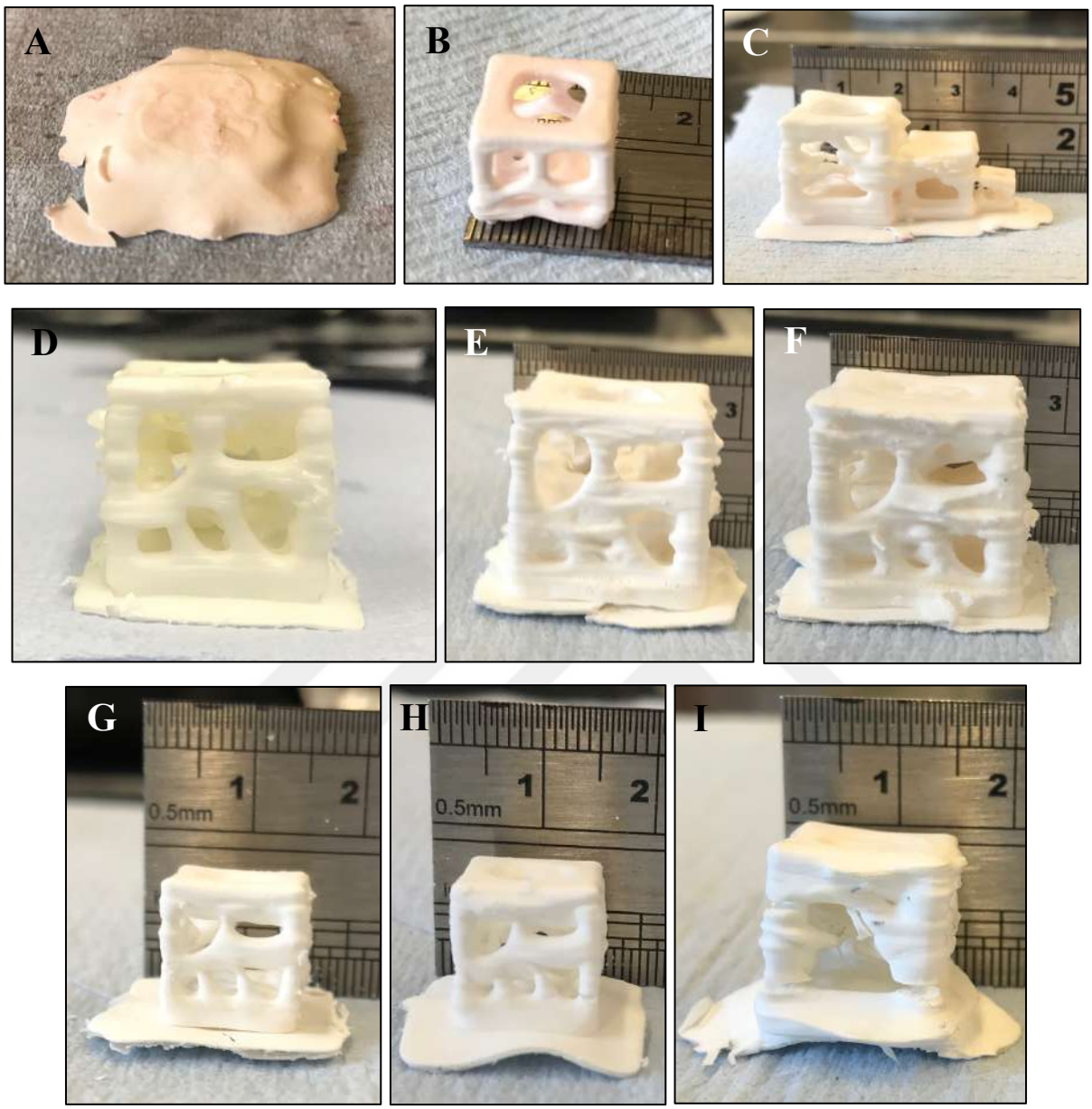

Figure 4. 17. *Cube-shaped polyHIPE scaffolds via Kudo 3D printer; A: the first sample tried to produce from PolyHIPE in Kudo 3D printer, B: Cube- shaped simple bone structure in 1.1×1.1×1.1 cm dimensions, C: Different sizes of cube-shaped polyHIPE scaffolds, D-E-F: cube- shaped simple bone structure in dimensions of 2.2×2.2×2.2 cm, G-H-I: : Cube- shaped simple bone structure in 1.1×1.1×1.1 cm dimensions with various production conditions in terms of exposure time and using silicon template*

4.4.1. Effect of Light Absorber on Porosity

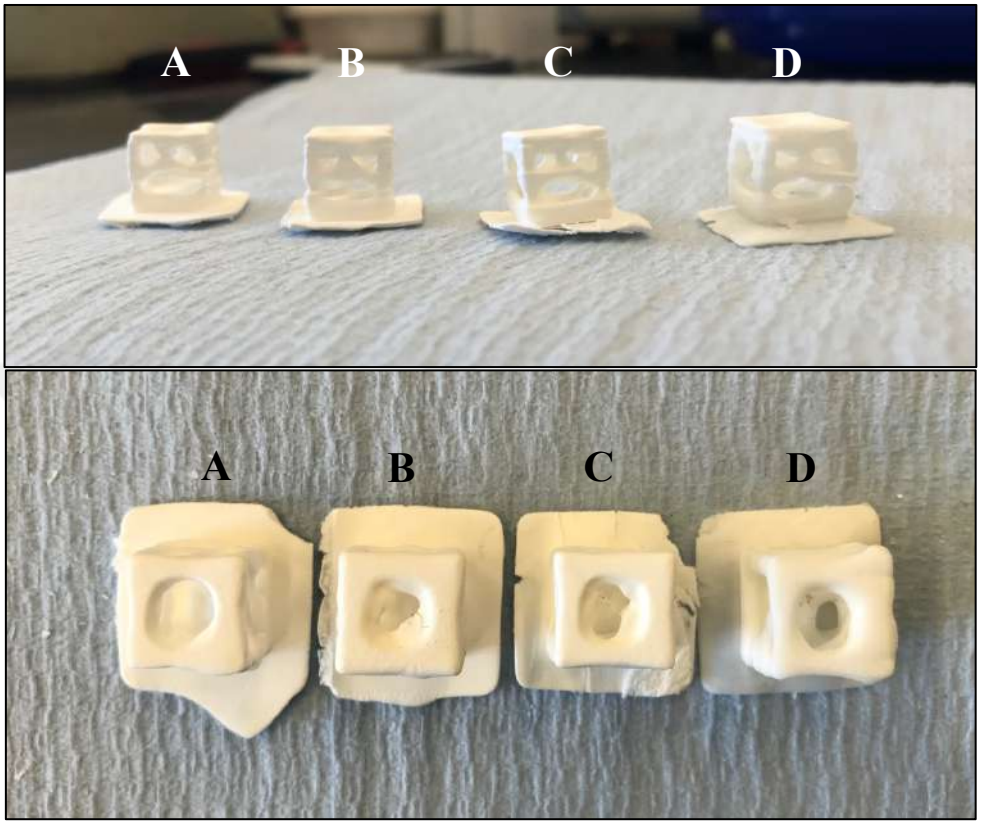

Figure 4. 18. *The polyHIPE samples of cube- shaped simple bone structure in 1.1×1.1×1.1 cm dimensions containing different amounts of light absorber; A:0%, B:1%, C:2%, and D:4%*

Figure 4. 18 illustrates the samples containing various amounts of the light absorber. A-B-C-D includes 0%, 1%, 2%, and 4%, respectively. The amount of the light absorber did not affect the occurrence of the object, remarkably. However, 4% of light absorber caused a reduction in printing quality. Small gaps occurred in the thin parts of the sample since the cross-linkage did not complete in some parts.

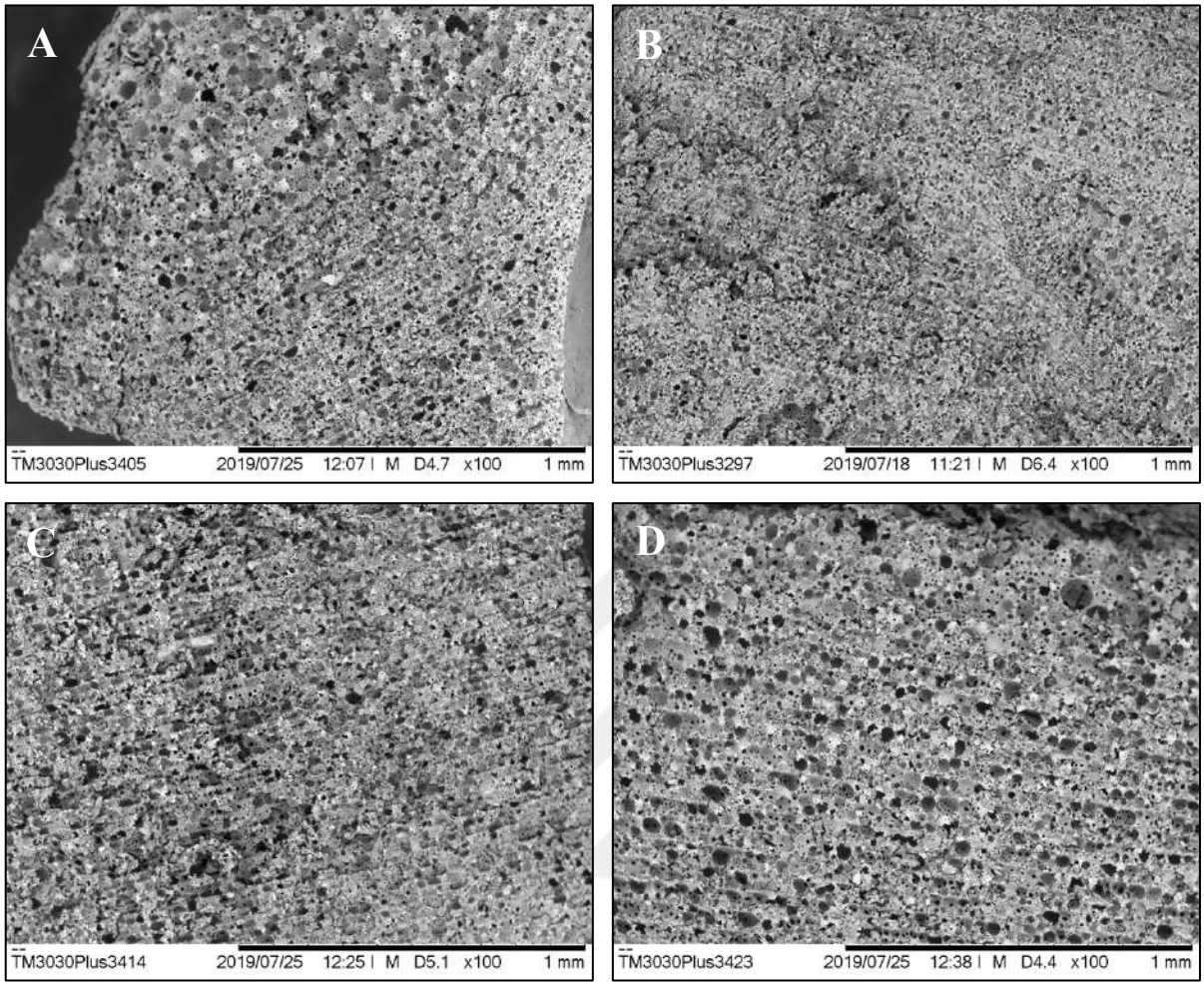

Figure 4. 19. *SEM images of Kudo 3D printer polyHIPE samples magnified 100 times; A: 0% light absorber, B: 1% light absorber, C: 2% light absorber, and D: 4% light absorber*

Figure 4. 19 presents the SEM images of printed polyHIPE samples via Kudo 3D printer magnified 100 times. A-B-C-D images show various amounts of light absorber that is 0%, 1%, 2%, and 4%, respectively. Based on SEM images, they have different pore quantities. Additionally, printing layers can be noticed easily due to layer-by-layer production. The layers in Figure 4. 19-D are clearer than the other three samples.

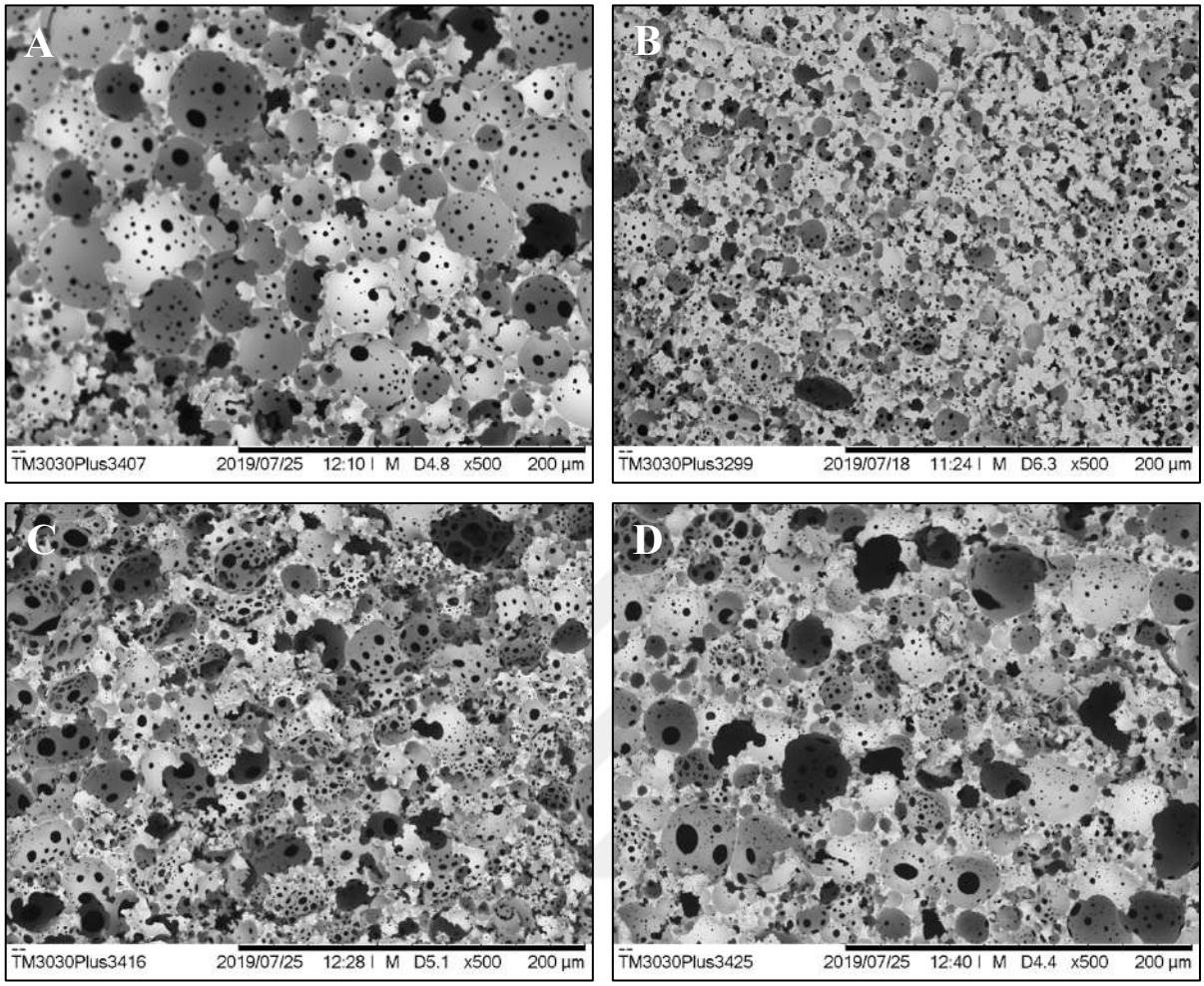

Figure 4. 20. *SEM images of Kudo 3D printer polyHIPE samples magnified 500 times; A: 0% light absorber, B: 1% light absorber, C: 2% light absorber, and D: 4% light absorber*

Figure 4. 20 illustrates the SEM images of printed polyHIPE samples via Kudo 3D printer magnified 500 times. The effect of light absorber on porosity can be observed from this figure. While the porosity has been increased from 0% light absorber (A) to 1% light absorber (B), it has been decreased from 1% light absorber (B) to 4% light absorber (C-D). 1% light absorber sample has the highest porosity whereas 0% light absorber sample has the lowest. The other effect of light absorber on porosity is the quality of pores. This means that pores in samples which were formed without light absorber are clearer than samples including light absorber.

In addition to these, the small voids in the pores are almost the same for all four images. Any increase or decrease have not been observed in the small voids. For this reason, the

interconnectivity is nearly the same for various amounts of light absorber samples. In other words, the amount of light absorber does not affect the degree of interconnectivity.

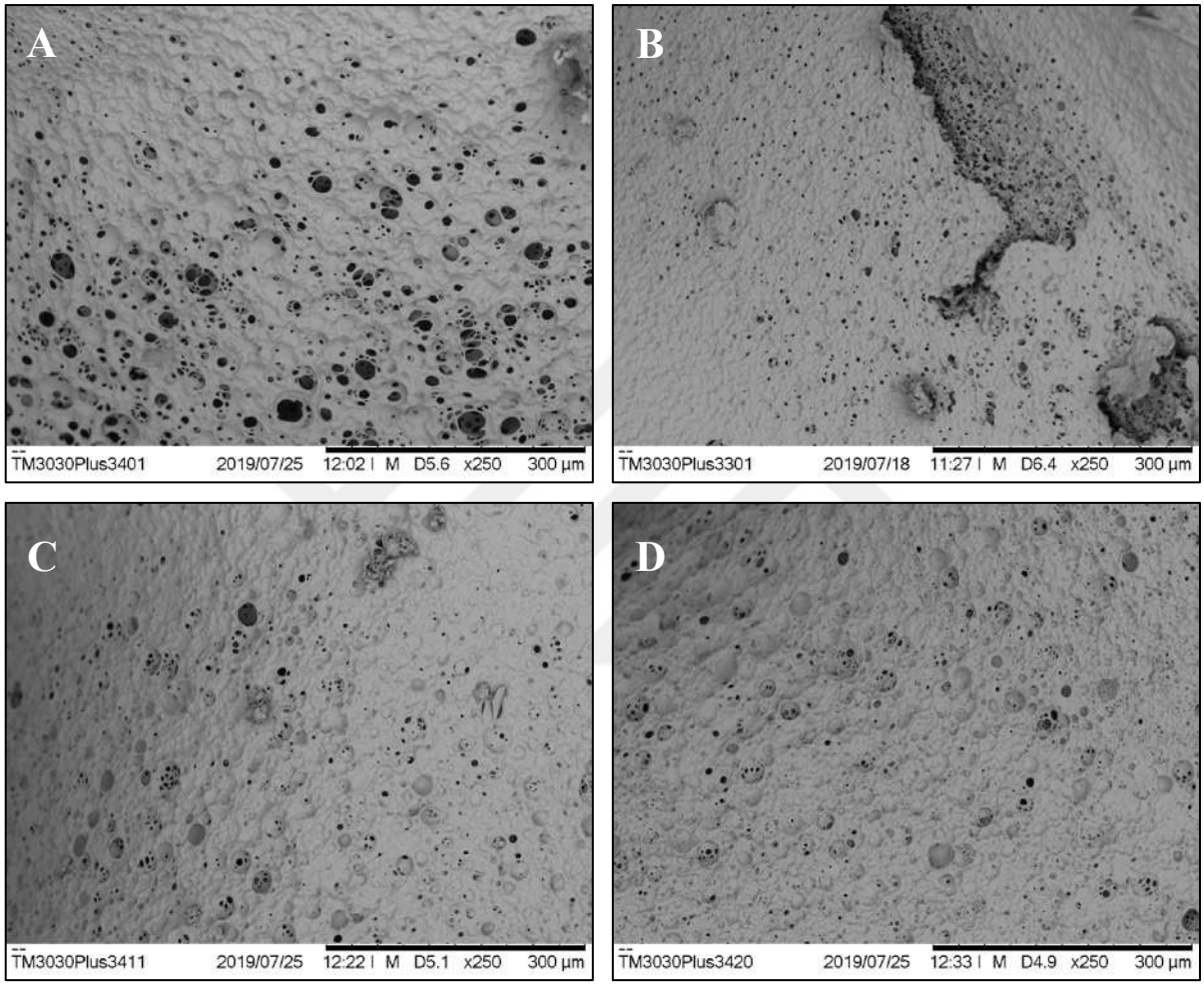

Figure 4. 21. *SEM images of Kudo 3D Printer polyHIPE samples taken from the surface; A: 0% light absorber, B: 1% light absorber, C: 2% light absorber, and D: 4% light absorber*

Kudo 3D Printer samples with different amounts of light absorber have been investigated in terms of surface porosity (Figure 4. 21). Based on the related figure, surface porosity reduces with the increasing amount of light absorber. 0% light absorber polyHIPE has the highest surface porosity while 1% light absorber polyHIPE has lower surface porosity than 0% light absorber polyHIPE. On the other hand, 2% and 4% light absorber polyHIPEs that have lower surface porosity than others have a similar quantity of the surface porosity with each other.

The size of pores on the surface has a similar relationship with the amount of surface porosity. It means the size of pores decreases with the rising light absorber amount. 0% light absorber polyHIPE has the largest pores on its surface while the others have smaller than it.

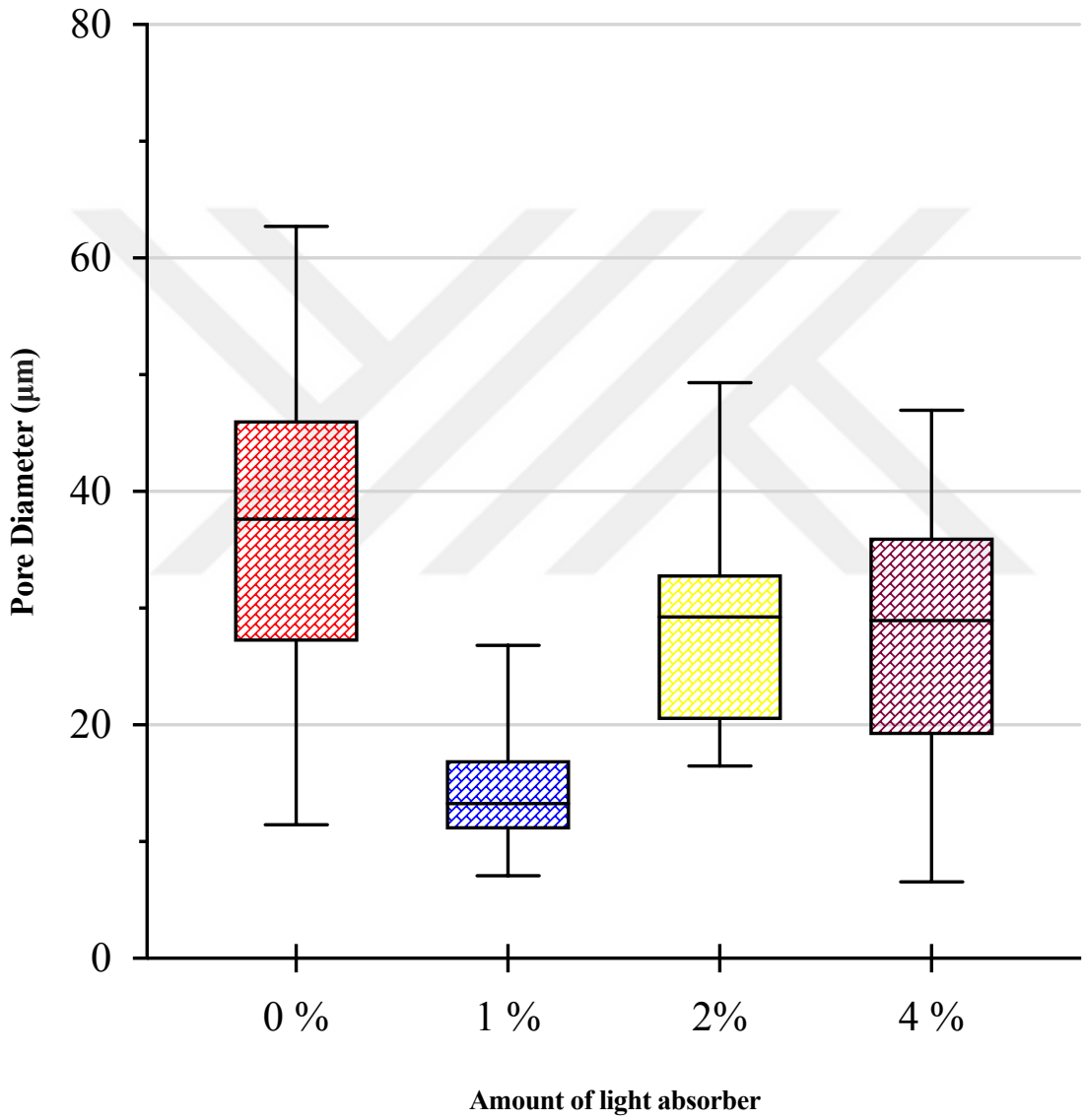

***Figure 4. 22**. The graph of pore diameter (µm) of polyHIPE samples containing various amounts of light absorber and different amounts of light absorber;0%, 1%, 2%, and 4%*

The relationship between pore diameter and amount of light absorber are presented in Figure 4. 22. According to the related graph, the pore size distribution altered with the

changing light absorber. For 0% light absorber sample, the smallest pore diameter is 11.5 μm and the largest pore size is 62.7 μm, respectively. Moreover, the minimum and maximum values of pore diameter are determined as 7.1 μm and 26.8 μm for 1% light absorber sample. When the 2% light absorber sample was examined in that graph, the lowest and highest pore diameters are determined as 16.5 μm and 49.3 μm. Finally, 4% light absorber sample, 6.6 μm and 46.9 μm are the smallest and highest pore diameters.

0% light absorber sample has the largest gap between minimum and maximum pore diameters whereas the smallest range of pore diameter is in the 1% light absorber. Other samples, 2% and 4% light absorbers, have the larger gaps between minimum and maximum of pore diameter, relatively. Also, their average pore diameter values are highly close to each other, and it is roughly 28.5 ± 9.5 μm. On the other hand, the average pore diameter value of the 0% light absorber sample is about 37.35 ± 12.82 μm whereas this average is almost 14.37 ± 4.65 μm for the 1% light absorber sample.

4.4.2. Effect of The Different Dimensions on Porosity

The fabrication of samples with different dimensions affect the printing quality. This can be observed in

Figure 4. ***23***. According to the figure, as samples are getting bigger the printing quality is affected negatively. The smallest shape has the highest quality in terms of the producible of all details in the shape. As samples are getting larger, HIPEs starts to accumulate in the thin and small parts of the sample. Thus, the net-shape polyHIPE cannot be formed.

Figure 4. 24 illustrates the SEM images of printed polyHIPE samples by using Kudo 3D printer magnified 100 times. A-B-C-D-E-F images demonstrate the different dimensions of the cube-shaped samples which are 1.1 cm, 1.3 cm, 1.5 cm, 1.8 cm, 2 cm, and 2.2 cm, respectively. Based on these six SEM images, they seem to have similar pore quantities. Additionally, printing layers can be observed in the images, especially D is clearer than the other five images in terms of the determination of layers.

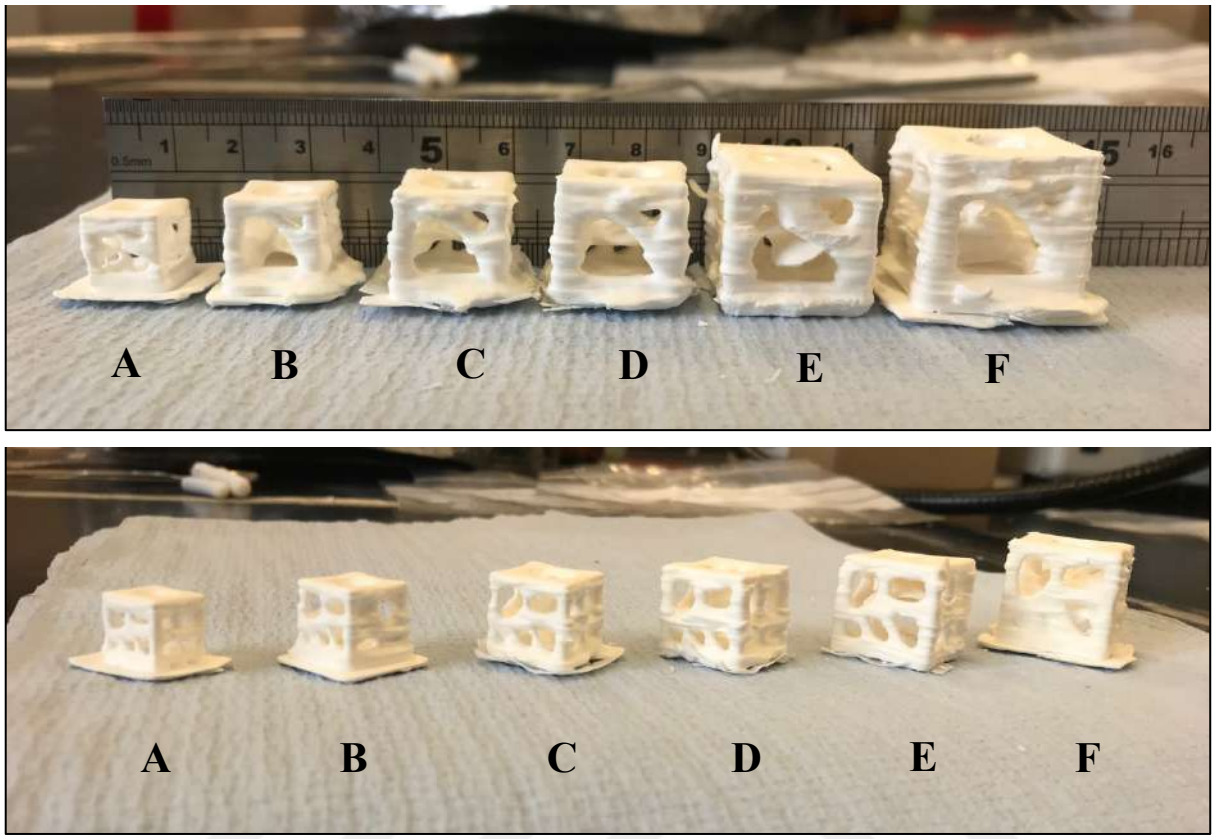

Figure 4. 23. *Different dimensions of printed cube-shaped polyHIPE samples via Kudo 3D printer; A: 1.1×1.1×1.1 cm, B:1.3×1.3×1.3 cm, C:1.5×1.5×1.5 cm, D:1.8×1.8×1.8 cm, E:2×2×2 cm, and F:2.2×2.2×2.2 cm*

Magnifying 500 times SEM images of the polyHIPE samples that have different dimensions have been demonstrated in Figure 4. 25. A-B-C-D-E-F shows the various dimensions; 1.1 cm, 1.3 cm, 1.5 cm, 1.8 cm, 2 cm, and 2.2 cm, respectively. There is no exact relationship between the dimensions of the samples and the amount of porosity. While the most porous structures belong to the smallest sample (A) and the second biggest sample (E), the second small sample has the least porous structure (B). C image that is the third smallest sample has the second most pore quantity. Finally, the largest sample (F) and the third-largest sample (D) has the lowest and the second-lowest pore amount, respectively.

Furthermore, any difference in the small voids in the pores have not been observed for all six different samples. The interconnectivity is almost the same for various dimensions of samples. It means the change in the sizes of the samples does not affect the degree of interconnectivity.

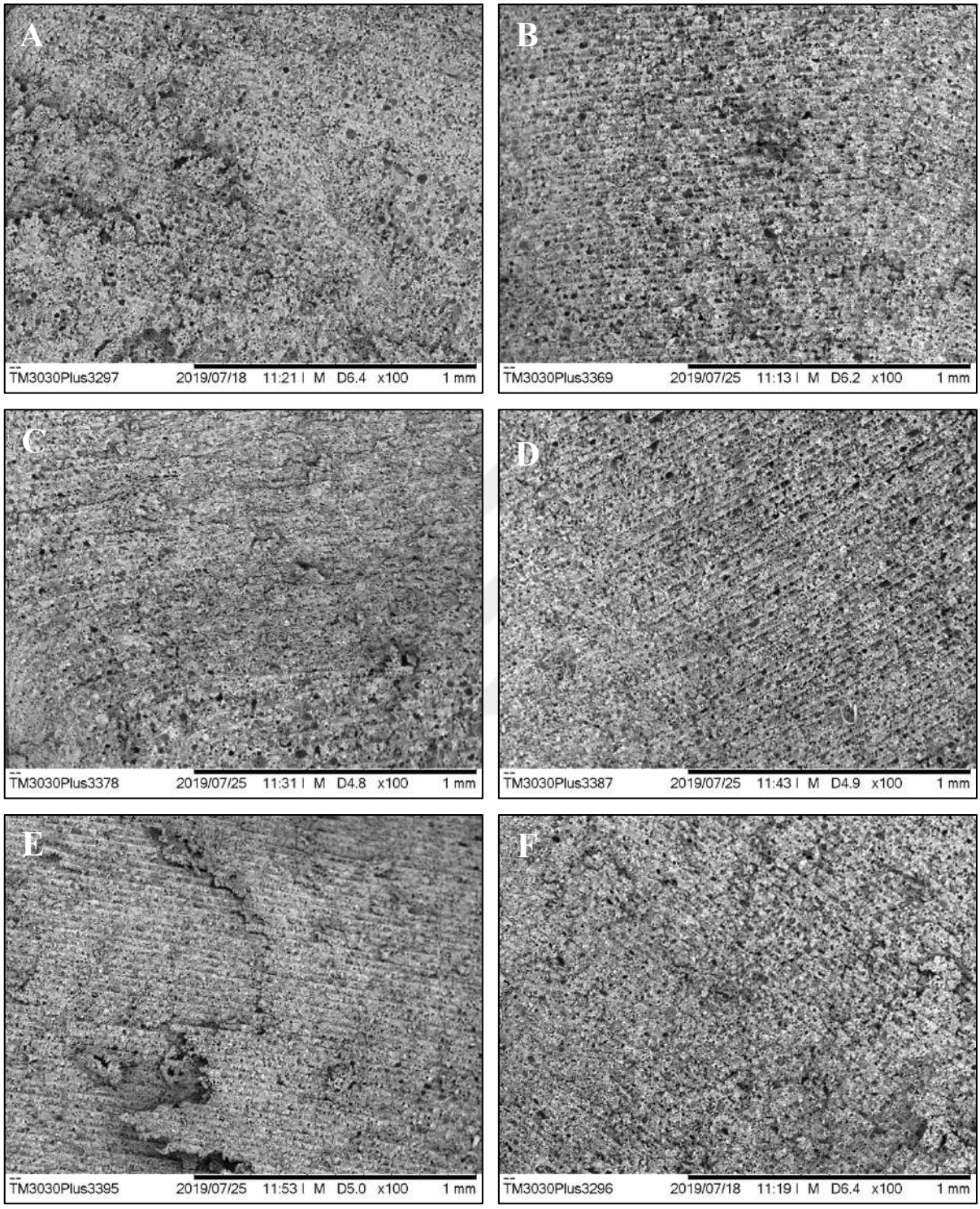

Figure 4. 24. *SEM images of Kudo 3D Printer polyHIPE samples magnified 100 times; A: 1.1×1.1×1.1 cm, B:1.3×1.3×1.3 cm, C:1.5×1.5×1.5 cm, D:1.8×1.8×1.8 cm, E:2×2×2 cm, and F:2.2×2.2×2.2 cm*

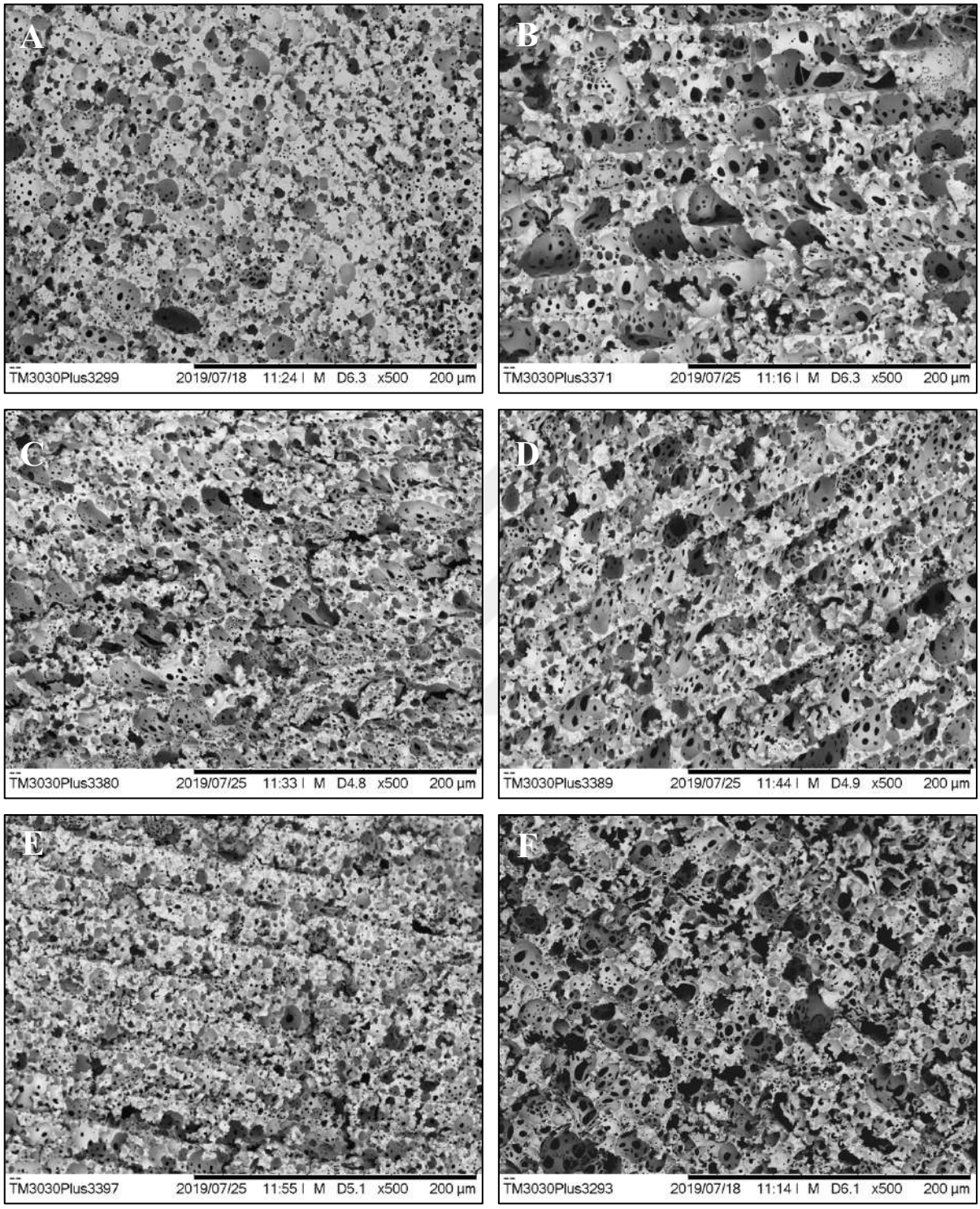

Figure 4. 25. *SEM images of Kudo 3D Printer polyHIPE samples magnified 500 times; A: 1.1×1.1×1.1 cm, B:1.3×1.3×1.3 cm, C:1.5×1.5×1.5 cm, D:1.8×1.8×1.8 cm, E:2×2×2 cm, and F:2.2×2.2×2.2 cm*

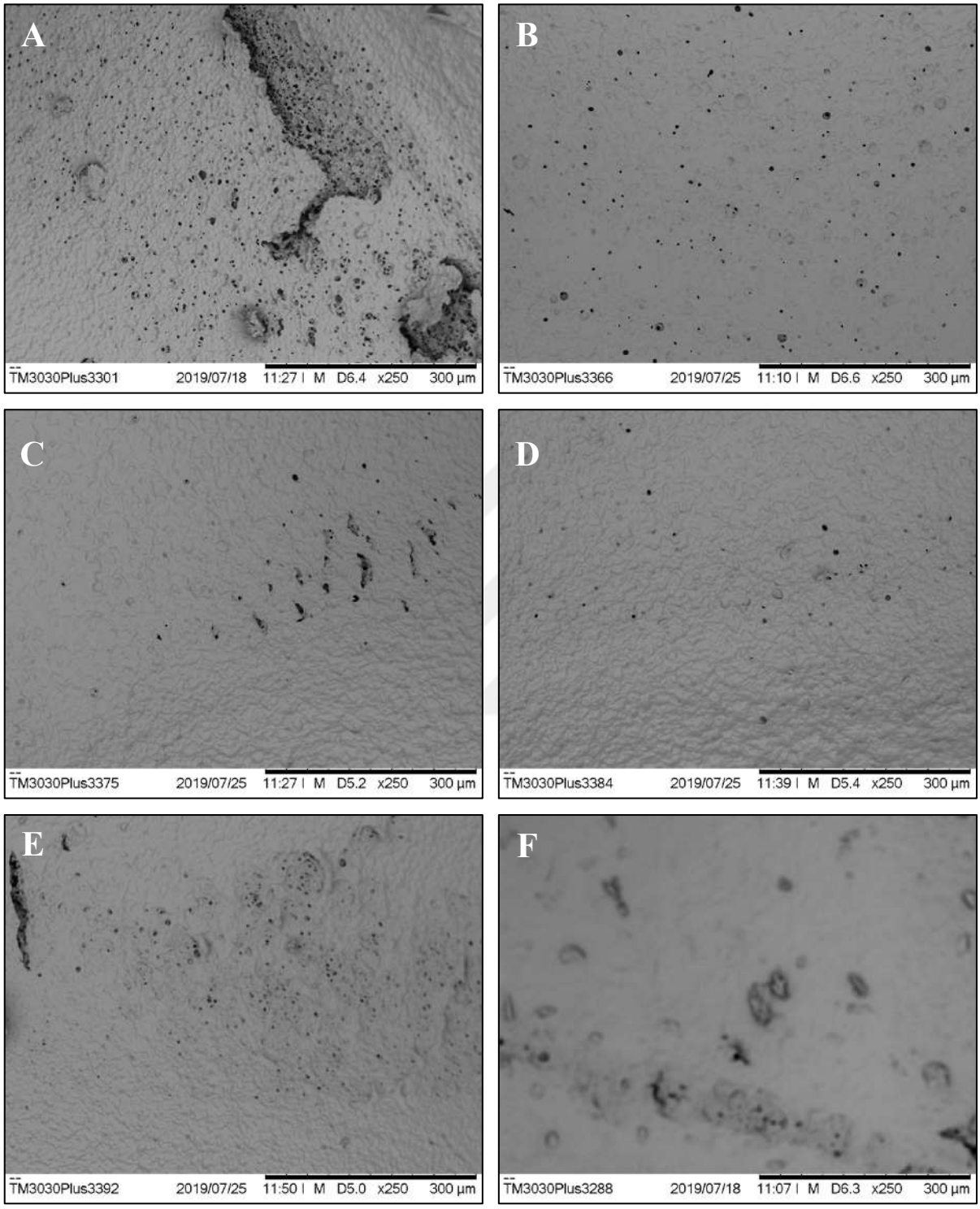

Figure 4. 26. *SEM images of Kudo 3D Printer polyHIPE samples taken from the surface; A: 1.1×1.1×1.1 cm, B:1.3×1.3×1.3 cm, C:1.5×1.5×1.5 cm, D:1.8×1.8×1.8 cm, E:2×2×2 cm, and F:2.2×2.2×2.2 cm*

Figure 4. 26 demonstrates the surface porosity of six different sizes of Kudo 3D samples. When this figure was examined, it can be determined that the highest amount of surface porosity is in image A, the smallest sample. Even though the lowest quantity of the surface porosity belongs to the largest sample (F), there is no direct relation between the amount of surface porosity and the sizes of samples. For instance, the second largest (E) and the second smallest (B) samples have almost the same quantity of surface porosity that is the second-highest. Also, the other two samples (C and D) has the second smallest amount of surface porosity.

Moreover, the size of pores on the surface is the largest on the smallest sample's surface and the others which are similar to each other are smaller than it.

To determine the change of the pore size distribution with the different dimensions of samples, a graph has been presented in Figure 4. 27. Based on this graph, the minimum and maximum values of pore diameter are determined as 7.1 μm and 26.8 μm for the smallest sample. Moreover, the lowest and the highest pore diameters of the second smallest sample are 10.1 μm and 39.4 μm. For the third smallest sample, 6.9 μm and 32.2 μm are the smallest and largest pore sizes. When the three biggest samples are examined, for the biggest sample, the smallest and highest pore size values are 7.9 μm and 47.7 μm. Additionally, 3.6 μm and 20.2 μm are the minimum and maximum sizes of pore diameters for the second-largest sample. Finally, for the third-largest sample, the lowest and highest pore diameters are 8.1 μm and 37.2 μm.

The biggest sample has the largest range of the minimum and maximum values of pore diameters while the smallest one is the second largest sample. The gap between minimum and maximum pore diameters for other samples alters between the smallest and largest. There is no correlation between the pore size distribution and the dimensions of samples. In addition to these, the average pore diameters are approximately 14.37 ± 4.65 μm, 24.35 ± 8.35 μm, 15.78 ± 7.14 μm, 19.04 ± 7.02 μm, 10.30 ± 3.70 μm, and 19.97 ± 8.65 μm from the smallest sample to largest, respectively.

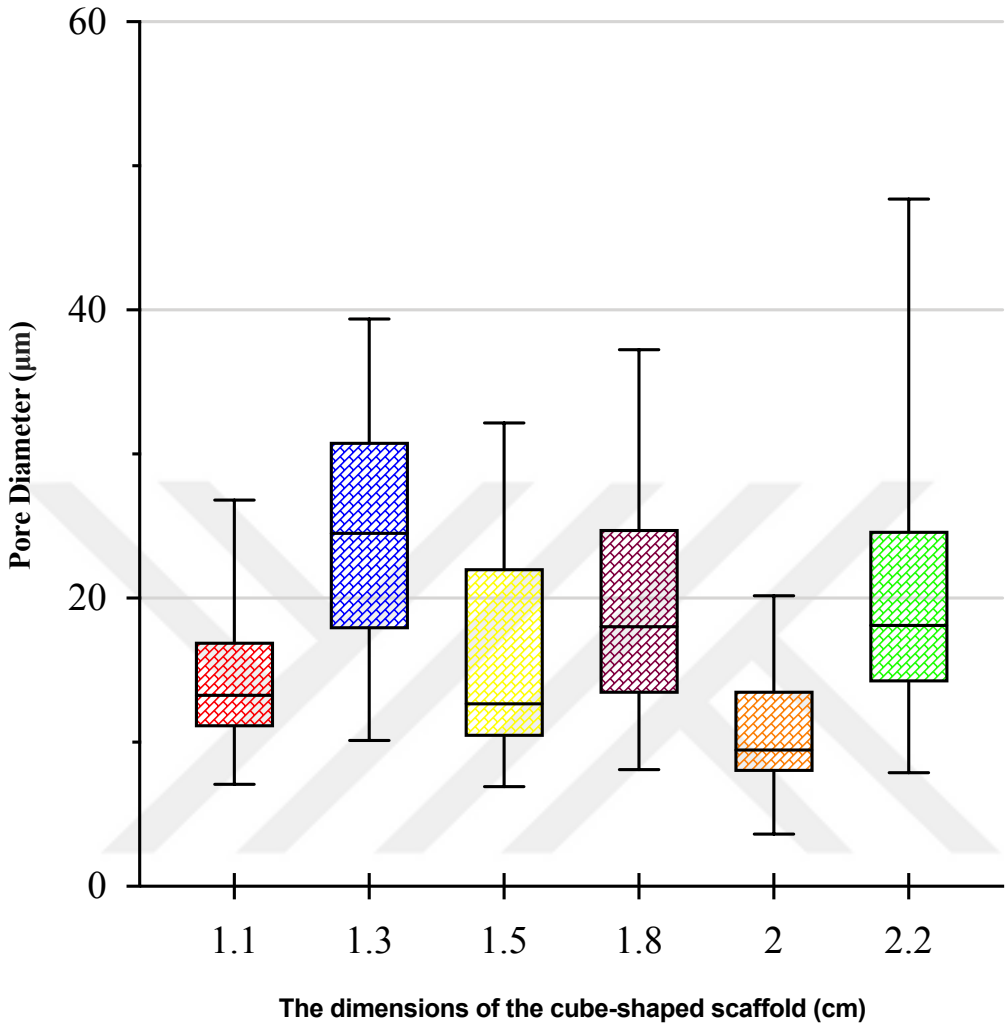

Figure 4. 27. *The graph of pore diameter (µm) of polyHIPE samples having various dimensions and different dimensions of the cube-shaped polyHIPE scaffold; 1.1 cm, 1.3 cm, 1.5 cm, 1.8 cm, 2 cm, and 2.2 cm*

4.4.3. Effect of Waiting Period of the HIPEs Before Printing on Porosity

The samples created through printing via Kudo 3D printer with different waiting periods are demonstrated in Figure 4. 28. Image A shows 1-day sample while image B illustrates the 7 days sample. Based on this figure, there is no alteration in the printing quality with the changing waiting period.

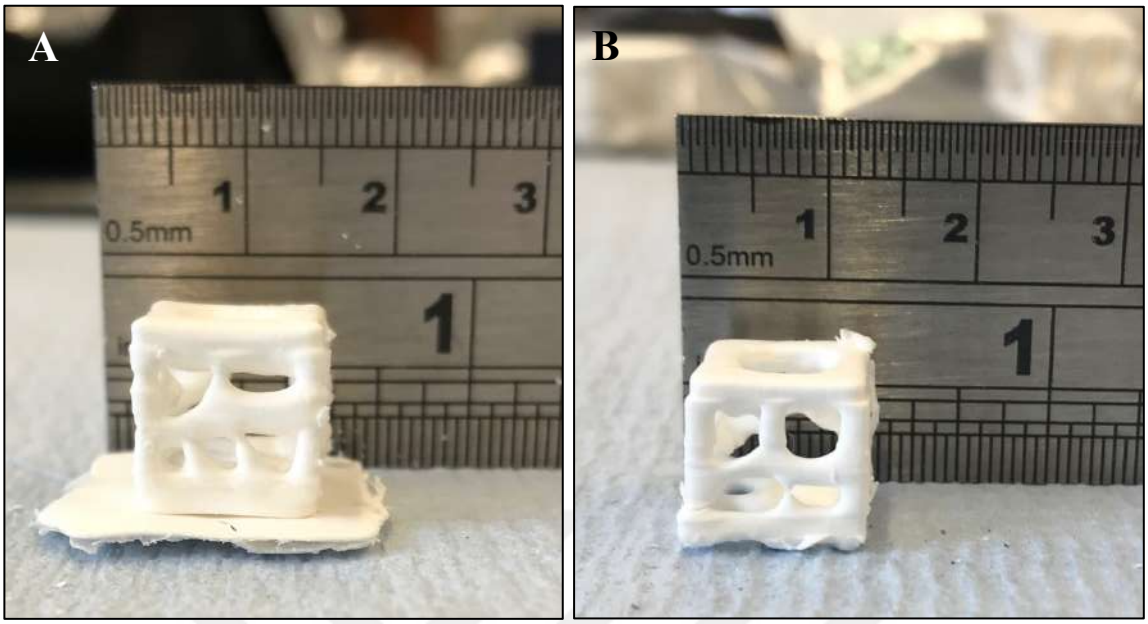

Figure 4. 28. *The cube-shaped simple bone structure polyHIPE samples (1.1×1.1×1.1 cm) produced from different waiting periods of HIPEs before printing; A: 1 day and B: 7 days*

Figure 4. 29 illustrates the SEM images of these two samples formed from the HIPEs that have different waiting periods. A-C-E presents the microstructure of the 1 day while B-D-F demonstrates the 7 days sample. A and B are images magnified 100 times whereas C and D have x500 magnification of the same cross-sections. According to these four images, 1-day and 7-days samples have about the same amount of porosity. Nonetheless, 7-days sample has larger pores than the 1-day sample. Moreover, an alteration has been observed in the interconnectivity. The quantity of the small voids has been increased with the rising waiting period. Therefore, the interconnectivity of the 7 days sample is higher than the 1-day sample. In addition to these, E and F images were taken for the determination of the surface porosity. 1-day sample is highly porous; however, 7 days sample has almost no porosity on its surface.

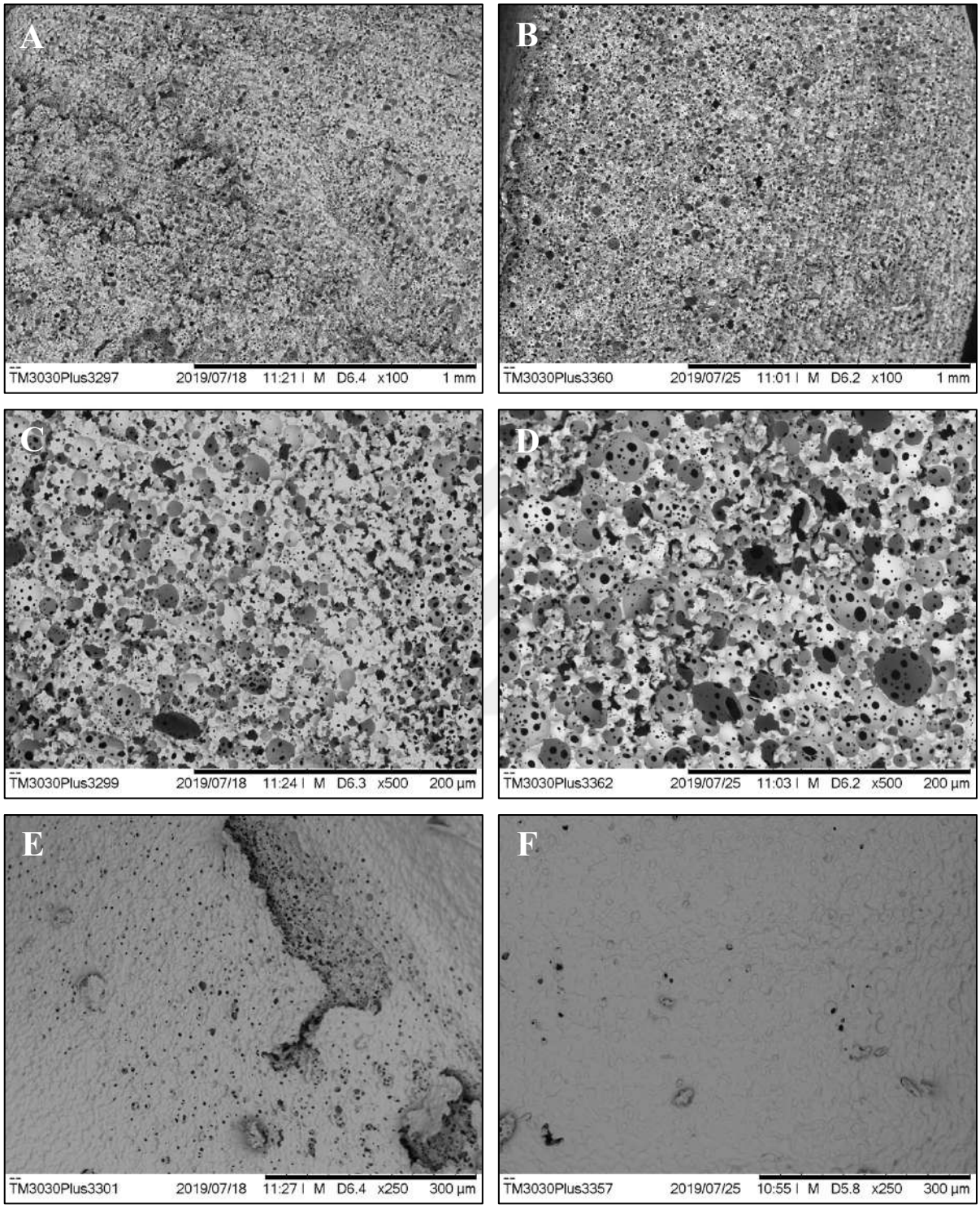

Figure 4. 29. *SEM images of Kudo 3D Printer polyHIPE samples; A-C-E: 1 day (x100-x500-x250 magnifications and A-C: cross-section, E: surface) and B-D-F: 7 days (x100-x500-x250 magnifications and B-D: cross-section, F: surface)*

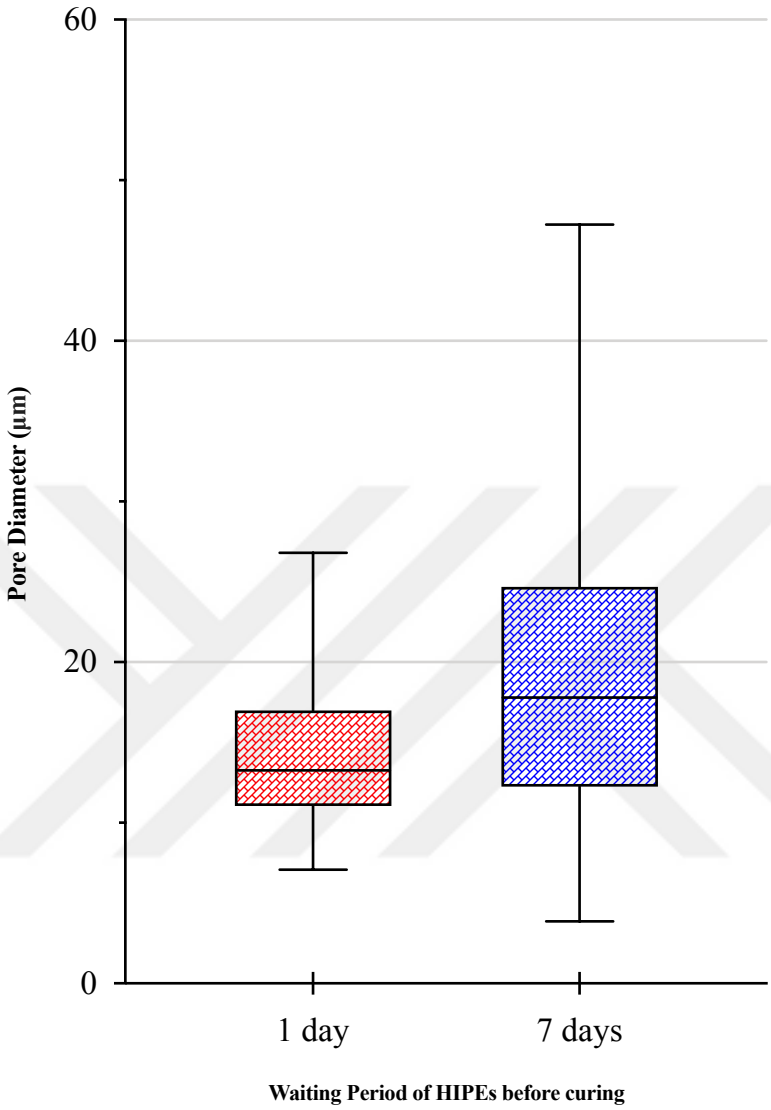

Figure 4. 30. *The graph of pore diameter (µm) of polyHIPE samples produced HIPEs having different waiting periods and waiting period of HIPEs before printing (1 day-7 days)*

Figure 4. 30 demonstrates the relationship between pore diameter and the waiting period of HIPEs before printing. The pore size distribution has been altered remarkably, especially in terms of the gap between the minimum and maximum pore diameters. The range of pore diameters and the average value of pore diameters increases with the rising waiting period.

The smallest and the largest values of pore diameters are 7.1 µm and 26.8 µm for 1-day sample while for 7-days sample, the minimum and maximum pore diameters are 3.9 µm and

47.2 μm, respectively. Moreover, the average pore diameters for 1-day and 7-days samples are determined as 14.37 ± 4.65 μm and 19.38 ± 9.40 μm.

4.5. Resolution

The samples which are produced in order to determine resolution are presented in Figure 4. 31. A illustrates the microstereolithography set-up samples and B shows Kudo 3D printer samples.

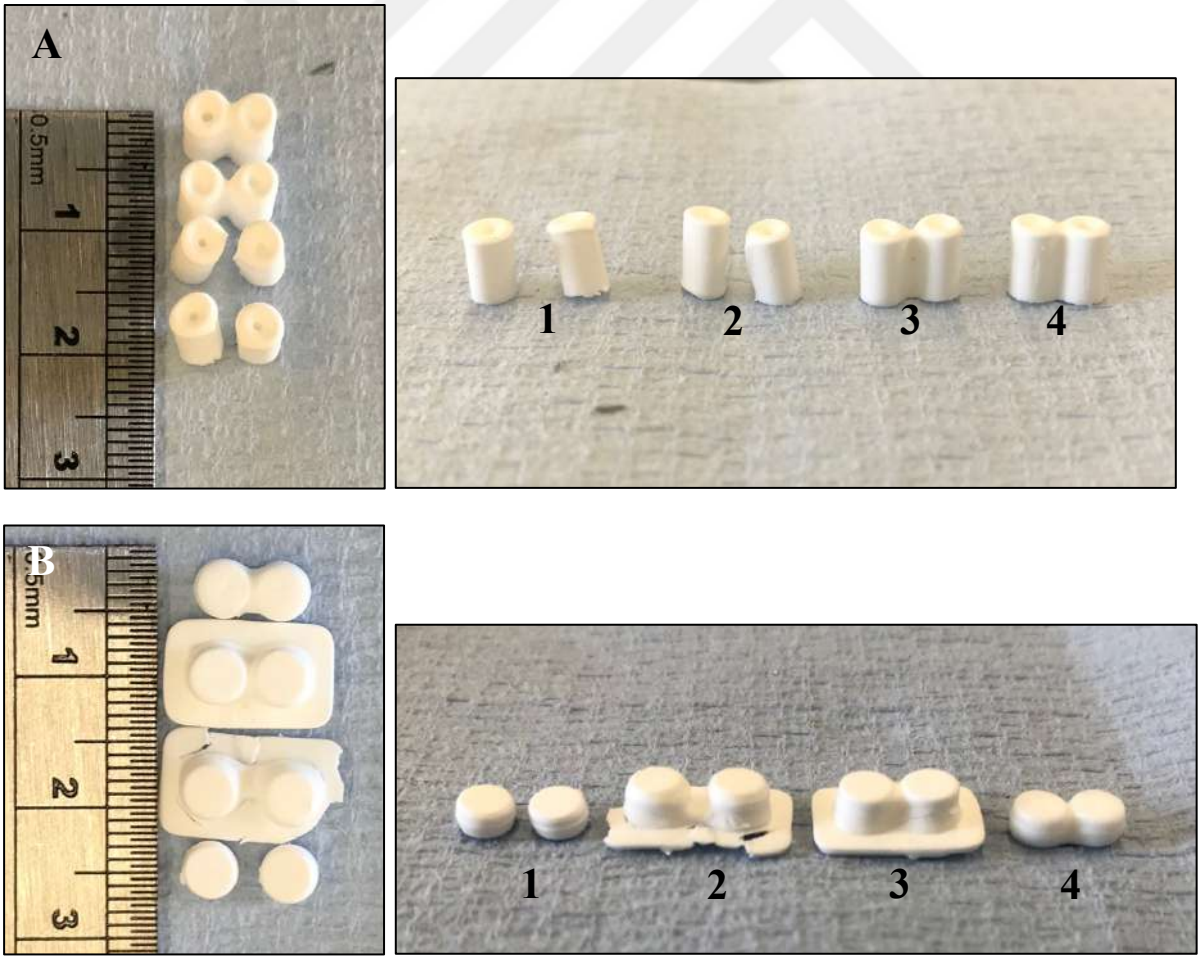

Figure 4. 31. *The polyHIPE samples produced to observe resolution; A: Microstereolithography set-up sample, B: Kudo 3D printer samples*

For microstereolithography set-up samples, two tubes were produced with spaces that are 0.43 cm, 0.40 cm, 0.32 cm, and 0.20 cm for sample 1, sample 2, sample 3, and sample 4, respectively. Two tubes have merged with each other in sample 3 and sample 4.

For Kudo 3D samples, spaces between cylinders for sample 1, sample 2, sample 3, and sample 4 are 0.43 cm, 0.25 cm, 0.10 cm, and 0.06 cm, respectively. Two cylinders have been started to merge in sample 2 and they have totally merged in sample 3 and sample 4. When compared to microstereolithography set-up samples, Kudo 3D samples have better resolution as they might be manufactured by locating closer each other.

CHAPTER 5: DISCUSSION

This dissertation aimed to investigate 3D printing of porous materials and the usage of HIPEs as ink for light-based additive manufacturing techniques. Based on this aim, a range of scaffolds was created using a commercial 3D printer, Kudo 3D Titan2 Printer. Moreover, the number of tubes were formed utilizing house-style laser set-up, microstereolithography set-up. In addition to these, a few samples were fabricated using commercial benchtop UV curing instrument. As well as the production of porous structures, HIPEs were examined in terms of stability.

HIPEs are greatly stable inks; therefore, they are suitable to store for days. Nonetheless, their stability decreases after a month, visibly. This reduction in stability is not a challenge for lab-based works but vitally important for large-scale production in factories. The industry must be careful while stocking HIPEs. Otherwise, a decrease in production quality will happen. Additionally, water ratio and stirring speed used during the preparation of HIPEs influence the stability. The higher water ratio and stirring speed ensure the more stable HIPEs. This is likely related to the viscosity of HIPEs since higher water ratio and mixing speed enhance to synthesis more viscous HIPEs. These outcomes indicate the similarity with the study of Luo et al. [62]. They found that higher internal phase volume causes higher viscosity, and as viscosity becomes higher, HIPEs become more stable.

This present dissertation further assesses porosity, the degree of interconnectivity, and surface porosity of porous materials produced by Kudo 3D printer depending on the waiting period of HIPEs before curing or printing, dimensions of samples, and the amount of light absorber.

Firstly, it should be mentioned that the porosity was retained during the Kudo 3D printing layer by layer. The porosity is mostly affected by the amount of light absorber. Even though the light absorber quantity does not influence remarkably the printing quality of objects, it highly affects the amount of porosity, homogeneity of pore sizes, and the pore size distribution. Homogeneity is determined by the gap between minimum and maximum pore sizes. As this gap is getting smaller, pores become more homogenous. After adding 1% light

absorber, porosity increases but as the addition of light absorber continue, porosity decreases. This might be related to the negative effect of light absorber on cross-linking. Moreover, the pore size distribution is affected in the same way. 1% light absorber ensures to create the most homogenous pores in terms of the similarity of pore sizes and the smallest pores (averagely 14.37 ± 4.65 μm). Higher amounts than 1 % cause a rise in the pore size distribution and a reduction in the homogeneity of pores. On the other hand, interconnectivity is not affected by the light absorber, which is similar for all light absorber quantities.

Furthermore, the effect of manufacturing of different sizes of samples on porosity is that there is not any relationship between various dimensions and porosity. Although the printing quality decreases as samples become larger, any direct proportion has not been established between the size and porosity. Therefore, the pore size distribution and homogeneity of pores do not alter depending on the samples' dimensions. Also, this independence from the sizes of samples is valid for interconnectivity as well. Interconnectivity is almost the same for all samples with various dimensions.

In addition to these, the waiting period of HIPEs before printing affects the porosity. As the increasing waiting period causes the decreasing stability of HIPEs even if this reduction in stability is not observed via the stability test. While the printing quality and the amount of porosity do not change with the waiting period, the size of pores rises and homogeneity of pores reduces with increasing waiting period. This can be also found literature, Luo et al. [62] and Wang et al [53] stated that pore size decreases as stability of emulsion increases. Robinson et al. [61] also mentioned that the pore size can be modified by changing the emulsions' stability. 1-day polyHIPE scaffold has the smaller pores (averagely 14.37 ± 4.65 μm) than 7 days polyHIPE scaffold (the average of pore size is 19.38 ± 9.40 μm) and it is highly homogeneous when compared to 7 days sample. On the other hand, the interconnectivity increases with the rising waiting period. In this part, the effect of the waiting period on the samples fabricated by UV curing machine should be explained. For these samples, another variable is the water ratio, so it must be considered while explaining the outcomes of the waiting period on porosity. While the porosity and the degree of interconnectivity of lower water ratio samples (1:4 and 1:8 water ratios) increases with increasing waiting time, it is exactly opposite for higher water ratio samples (1:12 water ratio). Porosity and interconnectivity of higher water ratio polyHIPEs decrease with

increasing waiting period. Furthermore, the waiting period does not influence noticeably the pore sizes and homogeneity for lower water ratios whereas the sizes of pores (averagely 17.76 ± 5.56 μm for 1-day sample) rises and homogeneity of pores decreases with increasing the waiting period for higher water ratio samples. It means that increasing waiting period affect the porosity negatively in terms of obtaining smaller and homogeneous pores for higher water ratio samples while this effectuating is positive for lower water ratio samples.

Secondly, surface porosity is mainly influenced by the addition of light absorber. As adding light absorber, surface porosity decreases, and then it becomes stable. Nonetheless, this is contrary to the literature as Sherborne et al. [24] found that the addition of light absorber enhances the surface porosity. Furthermore, the sizes of pores on the surface reduce with the increasing amount of light absorber. Moreover, dimensions of samples do not result in any impact on surface porosity. The final examination on surface porosity is the waiting period. Increasing waiting period causes a reduction on surface porosity. Although 1-day sample is highly porous on its surface, 7-days sample has almost no porosity on the surface of it.

This dissertation also explores the optimum printing conditions for microstereolithography set-up since there are many parameters affecting the final feature. The hierarchically porous structures might be obtained combining emulsion templating and microstereolithography technique, which is significant [57]. Therefore, the analysing of parameters in detail is highly important. Related parameters are water ratio, speed of mixing, printing speed and printing power. To investigate porous structures of microstereolithography set-up products, 6 different HIPEs were prepared combining 1:4, 1:8, and 1:12 water ratios and 100 and 300 rpm speeds of mixing. Then, for every different HIPE, 15 samples were produced applying 0.01 mm s^{-1}, 0.02 mm s^{-1}, and 0.04 mm s^{-1} and 40 mW, 50 mW, 60 mW, 70 mW, and 80 mW powers. Afterwards, two different criteria which are printing quality and the quality of the porous structure of samples was used for analyzation. Firstly, the best-printed samples were determined and a few samples were chosen among them. Secondly, their SEM images were taken to examine porous microstructures in terms of the size of pores, pore size distribution, and the degree of interconnectivity. The sample that meets the two criteria at the same time has the optimum conditions.

Based on this analysis, 0.01 mm s^{-1} printing speed and 50 mW power are optimum conditions for 1:4 water ratio and 100 rpm speed of mixing. This sample has more porous but it is not the more interconnected sample. For 1:4 water ratio and 300 rpm speed of mixing, 0.02 mm s^{-1} printing speed and 50 mW, 60 mW powers samples have the more amount of porosity and the degree of interconnectivity. Moreover, 0.02 mm s^{-1} printing speed and 50 mW, 60 mW powers samples are more porous and interconnected samples for 1:8 water ratio and 100 rpm speed of mixing while 0.01 mm s^{-1} printing speed and 50 mW power sample have the best porous microstructure in terms of pore quantity and interconnectivity among 1:8 water ratio and 300 rpm speed of mixing samples. Additionally, for 1:12 water ratio and 100 rpm speed of mixing, the most porous sample is 0.01 mm s^{-1} printing speed and 40 mW power sample while for 1:12 water ratio and 100 rpm speed of mixing, that is similar for two samples; 0.02 mm s^{-1} printing speed and 60 mW, 80 mW powers samples. To summarize, when compared these best samples among each other, it can be determined that 1:8 water ratio, 300 rpm speed of mixing, 0.01 mm s^{-1} printing speed and 50 mW power are the optimum parameters which give the average 16.39 ± 4.79 μm pore diameter. This value shows the similarity with the study of Owen et al. [57], the pore size was 20-30 μm.

In addition to these analyses, high printing speeds and powers cause unclear, incomplete, and damaged pores. This is possibly related to having insufficient time due to high printing speed. Since the fast speed of printing may cause the deformation of the water droplets or HIPEs are cured partially and then the water droplet is moved. The other finding is that the degree of interconnectivity depends on water ratio. As water ratio becomes higher, the degree of interconnectivity increases. Also, the closer printing powers like 40 mW and 50 mW gives a similar amount of porosity and the degree of interconnectivity if they have the same printing speed.

Another issue needed to examine is the resolution of printed polyHIPEs. The determination of resolution is related to the producibility of as far as closer objects to each other and very small objects. In this project, two-tubes/cylinders were manufactured in 4 different closeness using microstereolithography set-up and Kudo 3D printer. Kudo 3D printer enables fabricating closer cylinders whereas two tubes have been merged each other earlier in microstereolithography set-up. Although having 3.2 cm between tubes it could not be manufactured without merging in microstereolithography set-up; however, the cylinders

produced using Kudo 3D printer have started to merge in 0.25 cm space. It means that Kudo 3D printer provides higher resolution and enhance the fabrication of closer objects.

Nevertheless, the major limitation of this dissertation is that only one HIPE composition was utilized for all experiments. When the composition of HIPE is altered, all these findings could become different.

CHAPTER 6: CONCLUSION

To conclude, the stability of HIPEs depends on internal phase volume and stirring speed as higher water ratio and mixing speed cause higher viscosity and higher viscosity enhance the stability. Another consequence is that the porosity is retained during the printing layer-by-layer via Kudo 3D printer. Porosity depends on the amount of light absorber. When the incorporation of the light absorber is smaller than 1%, porosity and the homogeneity of pores increase and getting smaller pores. On the other hand, this trend is contrary to above 1% light absorber. While larger pores are obtained, pore amounts and homogeneity decreases. Moreover, rising waiting period results in getting bigger pore sizes and decreasing pore homogeneity due to increasing instability. In addition to these, the addition of light absorber increasing waiting period reduces the surface porosity. Interconnectivity is related to internal phase volume, increasing water ratio enhances the occurrence of more interconnected structures. Additionally, the sizes of printed polyHIPEs do not affect the porous microstructure depending on the dimensions.

The optimizing printing parameters are 1:8 water ratio, 300 rpm speed of mixing, 0.01 mm s^{-1} printing speed and 50 mW power for the fabrication of polyHIPEs via microstereolithography. This optimum condition provides the quality-printed polyHIPE with an average 16.39 ± 4.79 μm pore diameter. Furthermore, high printing speeds and powers cause a reduction in pore quality.

Finally, Kudo 3D printer allows manufacturing polyHIPEs with higher resolution than microstereolithography set-up.

Recommendations for further work:

- To observe the effects of the waiting period, the number of samples would be increased. This will probably give more reliable results. 14-days, 21-days, 28-days, and 35-days waiting periods can be used as well as 1-day and 7-days before printing of HIPEs.

- Viscosity of HIPEs could be measured to determine HIPEs that ensure the best porosity and printing quality.
- In this project, only porous structures of polyHIPEs were examined. To develop polyHIPEs for other applications such as sound absorption, acoustic properties would be investigated. Additionally, the other required properties could be examined as well as acoustic properties for other applications mentioned in the literature review section.

REFERENCES

[1] N. Sears, P. Dhavalikar, M. Whitely, and E. Cosgriff-Hernandez, *Fabrication of biomimetic bone grafts with multi-material 3D printing*, *Biofabrication*, 2017, **9**, 1-11.

[2] X. Zhou and C. J. Liu, *Three-dimensional Printing for Catalytic Applications: Current Status and Perspectives*, *Adv. Funct. Mater.*,2017, **27**, 1–13.

[3] B. Wendel, D. Rietzel, F. Kühnlein, R. Feulner, G. Hülder, and E. Schmachtenberg, *Additive processing of polymers*, *Macromol. Mater. Eng.*, 2008, **293**, 799–809.

[4] Z. C. Eckel, C. Zhou, J. H. Martin, A. J. Jacobsen, W. B. Carter, and T. A. Schaedler, *Additive manufacturing of polymer-derived ceramics, Science (80-.).*,2016, **351**, 58–62.

[5] N. Vanderesse, I. Ky, F. Quevedo González, N. Nuño, and P. Bocher, *Image analysis characterization of periodic porous materials produced by additive manufacturing*, *Mater. Des.*, 2016, **92**, 767–778.

[6] M. Subramanian, *Chapter 1: Introduction*, in 'Basics of Polymers:Fabrication and Processing Technology', 2015, Momentum Press, New York, pp1–2.

[7] M. Subramanian, *Chapter 4Polymer Materials and TheirTechnology:*, in 'Basics of Polymers:Fabrication and Processing Technology', 2015, Momentum Press, New York, pp21–36.

[8] D. Ozdil and H. M. Aydin, *Polymers for medical and tissue engineering applications*, J. Chem. Technol. Biotechnol., 2014, **89**,1793–1810.

[9] J. Jagur-Grodzinski, *Polymers for tissue engineering, medical devices, and regenerative medicine. Concise general review of recent studies*, Polym. Adv. Technol., 2006, **27**, 560–568.

[10] F. Yang, G. Zhao, C. Zhou, and D. Lin, *Phase change materials (PCM) based cold source for selective freezing 3D printing of porous materials*, Int. J. Adv. Manuf. Technol., 2018, **95**, 2145–2155.

[11] M. V. Twigg and J. T. Richardson, "*Fundamentals and applications of structured ceramic foam catalysts*," Ind. Eng. Chem. Res.,2007, **46**, 4166–4177.

[12] P. Sepulveda and J. G. Binner, *Processing of cellular ceramics by foaming and in situ polymerisation of organic monomers*, J. Eur. Ceram. Soc., 1999, **19**, 2059–2066.

[13] C. Zhou, P. Wang, and W. Li, *Fabrication of functionally graded porous polymer via supercritical CO 2 foaming*, Compos. Part B Eng., 2011, **42**, 318–325.

[14] J. Cao, C. R. Rambo, and H. Sieber, *Preparation of porous Al2O3-ceramics by biotemplating of wood,* J. Porous Mater., 2004, **11**, 163–172.

[15] N. Gama, A. Ferreira, and A. Barros-Timmons, *3D printed cork/polyurethane composite foams*, Mater. Des., 2019, **179**, 1-9.

[16] J. Gardan, *Additive manufacturing technologies: State of the art and trends*, Addit. Manuf. Handb. Prod. Dev. Def. Ind., 2017, **54**, 149–168.

[17] R. Janusziewicz, D. Shirvanyants, N. Ermoshkin, R. Janusziewicz, A. R. Johnson, D. Kelly, K. Chen, R. Pinschmidt, J. P. Rolland, A. Ermoshkin, E. T. Samulski and J. M. DeSimone, *Continuous liquid interface production of 3D objects*, Science, 2015, **347**, 1349–1352.

[18] M. M. Savalani and R. A. Harris, *Layer manufacturing for in vivo devices,* Proc. Inst. Mech. Eng. Part H J. Eng. Med., 2006, **220**, 505–520.

[19] M. N. Cooke, J. P. Fisher, D. Dean, C. Rimnac, and A. G. Mikos, *Use of Stereolithography to Manufacture Critical-Sized 3D Biodegradable Scaffolds for Bone Ingrowth,* J. Biomed. Mater. Res. - Part B Appl. Biomater., 2003, **64**, 65–69.

[20] F. P. W. Melchels, J. Feijen, and D. W. Grijpma, *A poly(d,l-lactide) resin for the preparation of tissue engineering scaffolds by stereolithography*, Biomaterials, 2009, **30**, 3801–3809.

[21] N. Sears, P. Dhavalikar, M. Whitely, and E. Cosgriff-Hernandez, *Fabrication of biomimetic bone grafts with multi-material 3D printing*, Biofabrication, 2017, **9**, DOI: 10.1088/1758-5090/aa7077.

[22] S. A. Skoog, P. L. Goering, and R. J. Narayan, *Stereolithography in tissue engineering*, J. Mater. Sci. Mater. Med., 2014, **25**, 845–856.

[23] M. B. Mawale, A. M. Kuthe, and S. W. Dahake, *Additive layered manufacturing: State-of-the-art applications in product innovation*, Concurr. Eng. Res. Appl., 2016, **24**, 94–102.

[24] C. Sherborne, R. Owen, G. C. Reilly, and F. Claeyssens, *Light-based additive manufacturing of PolyHIPEs: Controlling the surface porosity for 3D cell culture applications,*" Mater. Des., 2018, **156**, 494–503.

[25] T. Nakamoto, K. Yamaguchi, and A. P. Abraha, *Consideration on the producing of high aspect ratio micro parts using UV sensitive photopolymer*, MHS'96 Proceedings of the Seventh International Symposium on Micro Machine and Human Science, 2002, 53–58, DOI: 10.1109/MHS.1996.563401.

[26] A. Bertsch, S. Zissi, J. Y. Jézéquel, S. Corbel, and J. C. André, *Microstereophotolithography using a liquid crystal display as dynamic mask-generator,* Microsyst. Technol., 1997, **3**, 42–47.

[27] E. J. Mott, M. Busso, X. Luo, C. Dolder, M. O. Wang, J. P. Fisher, and D. Dean, *Digital micromirror device (DMD)-based 3D printing of poly(propylene fumarate) scaffolds*, Mater. Sci. Eng. C, 2016, **61**, 301–311.

[28] R. J. Narayan, A. Doraiswamy, D. B. Chrisey, and B. N. Chichkov, *Medical prototyping using two photon polymerization*, Mater. Today, 2010, **13**, 42–48.

[29] S. Pashneh-Tala, , R. Owen, H. Bahmaee, S. Rekštytė, M. Malinauskas, and F. Claeyssens, *Synthesis, Characterization and 3D Micro-Structuring via 2-Photon Polymerization of Poly(glycerol sebacate)-Methacrylate–An Elastomeric Degradable Polymer*, Front. Phys., 2018, **6**, 2-17, DOI: 10.3389/fphy.2018.00041.

[30] M. Bieda, F. Bouchard, and A. F. Lasagni, *Two-photon polymerization of a branched hollow fiber structure with predefined circular pores,* J. Photochem. Photobiol. A Chem., 2016, **319–320**, 1–7.

[31] T. a. Schaedler, A. J. Jacobsen, A. Torrents, A. E. Sorensen, J. Lian, J. R. Greer, L. Valdevit and W. B. Carter, "*Ultralight Metallic Microlattices*," Science, 2011, **334**, 962–965.

[32] B. Dhandayuthapani, Y. Yoshida, T. Maekawa, and D. S. Kumar, *Polymeric Scaffolds in Tissue Engineering Application: A Review*, Int. J. Polym. Sci., 2011, DOI: 10.1155/2011/290602.

[33] M. S. Shoichet, *Polymer scaffolds for biomaterials applications*, Macromolecules, 2010, **43**, 581–591.

[34] J. L. Robinson, R. S. Moglia, M. C. Stuebben, M. A.P. McEnery, and E. Cosgriff-Hernandez, *Injectable Polymerized High Internal Phase Emulsions with Rapid in Situ Curing*, Biomacromolecules, 2014, **15,** 1103-1112.

[35] W. Zhu, X. Ma, M. Gou, D. Mei, K. Zhang, and S. Chen, *3D printing of functional biomaterials for tissue engineering*, Curr. Opin. Biotechnol., 2016, **40**, 103–112.

[36] Z. Liu, J. Zhan, M. Fard, and J. L. Davy, *Acoustic properties of a porous polycarbonate material produced by additive manufacturing*, Mater. Lett., 2016, **181,** 296–299.

[37] Z. Liu, J. Zhan, M. Fard, and J. L. Davy, *Acoustic properties of multilayer sound absorbers with a 3D printed micro-perforated panel*, Appl. Acoust., 2017, **121**, 25–32.

[38] D. C. Akiwate, M. D. Date, B. Venkatesham, and S. Suryakumar, *Acoustic properties of additive manufactured narrow tube periodic structures*, Appl. Acoust., 2018, **136,** 123–131.

[39] F. Setaki, M. Tenpierik, M. Turrin, and A.Timmeren, *Acoustic absorbers by additive manufacturing*, Build. Environ., 2014, **72**, 188–200.

[40] P. Glé, E. Gourdon, and L. Arnaud, *Acoustical properties of materials made of vegetable particles with several scales of porosity,* Appl. Acoust., **72**, 249–259.

[41] F. Asdrubali, S. Schiavoni, and K. V. Horoshenkov, *A review of sustainable materials for acoustic applications,* Build. Acoust., 2012, **19**, 283–312.

[42] C. N. Wang and J. H. Torng, *Experimental study of the absorption characteristics of some porous fibrous materials,* Appl. Acoust., 2001, **62**, 447–459.

[43] S. Ersoy and H. Küçük, *Investigation of industrial tea-leaf-fibre waste material for its sound absorption properties*, Appl. Acoust., 2009, **70**, 215–220.

[44] H. Koruk and G. Genc, *Investigation of the acoustic properties of bio luffa fiber and composite materials*, Mater. Lett., 2015, **157**, 166–168.

[45] C. Parra-Cabrera, C. Achille, S. Kuhn, and R. Ameloot, *3D printing in chemical engineering and catalytic technology: Structured catalysts, mixers and reactors*, Chem. Soc. Rev., 2018, **47**, 209–230.

[46] J. Seo, D. I. Kushner, and M. A. Hickner, *3D Printing of Micropatterned Anion Exchange Membranes*, ACS Appl. Mater. Interfaces, 2016, **8**, 16656–16663.

[47] N. V. Gama, A. Ferreira, and A. Barros-Timmons, *Polyurethane foams: Past, present, and future*, Materials (Basel)., 2018, **11**, 1-35.

[48] N. V. Gama, R. Silva, M. Costa, A. Barros-Timmons, and A. Ferreira, *Statistical evaluation of the effect of formulation on the properties of crude glycerol polyurethane foams*, Polym. Test., 2016, **56**, 200–206.

[49] N. Gama, C. Amaral, T. Silva, R. Vicente, J. Coutinho, A. Barros-Timmons, and A. Ferreira, *Thermal energy storage and mechanical performance of crude glycerol polyurethane composite foams containing phase change materials and expandable graphite,* Materials (Basel)., 2018, **11**, DOI: 10.3390/ma11101896.

[50] T. A. Schaedler and W. B. Carter, *Architected Cellular Materials*, Annu. Rev. Mater. Res., 2016, **46**, 187–210.

[51] H. Yazdani Sarvestani, A. H. Akbarzadeh, A. Mirbolghasemi, and K. Hermenean, *3D printed meta-sandwich structures: Failure mechanism, energy absorption and multi-hit capability,* Mater. Des., 2018, **160**, 179–193.

[52] C. Ge, L. Priyadarshini, D. Cormier, L. Pan, and J. Tuber, *A preliminary study of cushion properties of a 3D printed thermoplastic polyurethane Kelvin foam*, Packag. Technol. Sci., 2018, **31**, 361–368.

[53] A. J. Wang, T. Paterson, R. Owen, C. Sherborne, J. Dugan, J. Li and F. Claeyssens, *Photocurable high internal phase emulsions (HIPEs) containing hydroxyapatite for additive manufacture of tissue engineering scaffolds with multi-scale porosity,* Mater. Sci. Eng. C,2016, **67**, 51–58.

[54] N. A. Sears, P. S. Dhavalikar, and E. M. Cosgriff-Hernandez, *Emulsion Inks for 3D Printing of High Porosity Materials*, Macromol. Rapid Commun., 2016, **37**, 1369–1374.

[55] D. W. Johnson, C. Sherborne, M. P. Didsbury, C. Pateman, N. R. Cameron, and F. Claeyssens, *Macrostructuring of Emulsion-templated Porous Polymers by 3D Laser Patterning*, Adv. Mater., 2013, **25**, 3177–3177.

[56] T. E. Paterson, G. Gigliobianco, C. Sherborne, N. H. Green, J. M. Dugan, S. MacNeil, G. C. Reilly and F. Claeyssens, *Porous microspheres support mesenchymal progenitor cell ingrowth and stimulate angiogenesis,* APL Bioeng., 2018, **2**, DOI: 10.1063/1.5008556.

[57] T. Paterson, N. H. Green, R. Owen, F. Claeyssens, C. Sherborne, and G. C. Reilly, *Emulsion templated scaffolds with tunable mechanical properties for bone tissue engineering*, J. Mech. Behav. Biomed. Mater., 2015, **54**, 159–172.

[58] J. L. Robinson, R. S. Moglia, M. C. Stuebben, M. A. P. McEnery, and E. Cosgriff-Hernandez, *Achieving Interconnected Pore Architecture in Injectable PolyHIPEs for Bone Tissue Engineering,* Tissue Eng. Part A, 2013, **20**, 1103–1112.

[59] X. Mu, T. Bertron, C. Dunn, H. Qiao, J. Wu, Z. Zhao, C. Saldana, and H. J. Qi, *Porous polymeric materials by 3D printing of photocurable resin*, Mater. Horizons, 2017, **4**, 442–449.

[60] A. Martins, S. Chung, A. J. Pedro, R. A. Sousa, A. P. Marques, R. L. Reis, and N. M. Neves, *Hierarchical starch-based fibrous scaffold for bone tissue engineering applications*, Ann. Am. Thorac. Soc., 2010, **12**, 181–204.

[61] J. L. Robinson, M. A. P. McEnery, H. Pearce, M. E. Whitely, D. J. Munoz-Pinto, M. S. Hahn, H. Li, N. A. Sears, and E.Cosgriff-Hernandez "*Osteoinductive PolyHIPE Foams as Injectable Bone Grafts*," Tissue Eng. Part A, 2016, **22**, 403–414.

[62] W. Luo, S. Zhang, P. Li, R. Xu, Y. Zhang, L. Liang, C. D. Wood, Q. Lu, and B. Tan, "*Surfactant-free CO2-in-water emulsion-templated poly (vinyl alcohol) (PVA) hydrogels*," Polymer (Guildf)., 2015, **61**, 183–191.